

A NEW CARBON NANOPARTICLE-POLYMER  
COMPOSITE FOR CELL IMPRINT  
LITHOGRAPHY

VIGNESWARAN NARAYANAMURTHY

UMP

Doctor of Philosophy

UNIVERSITI MALAYSIA PAHANG

## UNIVERSITI MALAYSIA PAHANG

### DECLARATION OF THESIS AND COPYRIGHT

Author's Full Name : Mr. Vigneswaran Narayanamurthy

Date of Birth : 15th March 1989

Title : A new carbon nanoparticle-polymer composite for cell imprint lithography

Academic Session : Semester 2 2016/2017

I declare that this thesis is classified as:

- CONFIDENTIAL (Contains confidential information under the Official Secret Act 1997)\*
- RESTRICTED (Contains restricted information as specified by the organization where research was done)\*
- OPEN ACCESS I agree that my thesis to be published as online open access (Full Text)

I acknowledge that Universiti Malaysia Pahang reserve the right as follows:

1. The Thesis is the Property of Universiti Malaysia Pahang
2. The Library of Universiti Malaysia Pahang has the right to make copies for the purpose of research only.
3. The Library has the right to make copies of the thesis for academic exchange.

Certified by:

\_\_\_\_\_  
(Student's Signature)

H3063257

\_\_\_\_\_  
New IC/Passport Number  
Date:

\_\_\_\_\_  
(Supervisor's Signature)

Dr. Fahmi Samsuri

\_\_\_\_\_  
Name of Supervisor  
Date:

NOTE : \* If the thesis is CONFIDENTIAL or RESTRICTED, please attach with the letter page 2 from the organization with the period and reasons for confidentiality or restriction.

### **SUPERVISOR'S DECLARATION**

I hereby declare that I have checked this thesis and in my opinion, this thesis is adequate in terms of scope and quality for the award of the degree of Doctor of Philosophy.

---

(Supervisor's Signature)

Full Name : Dr. Fahmi Samsuri

Position : Associate Professor

Date :



UMP

### **STUDENT'S DECLARATION**

I hereby declare that the work in this thesis is based on my original work except for quotations and citation which have been duly acknowledged. I also declare that it has not been previously or concurrently submitted for any other degree at Universiti Malaysia Pahang or any other institutions.

---

(Student's Signature)

Full Name : VIGNESWARAN NARAYANAMURTHY

ID Number : PEL13006

Date : 15 March 2016



UMP

A NEW CARBON NANOPARTICLE-POLYMER COMPOSITE FOR CELL  
IMPRINT LITHOGRAPHY



VIGNESWARAN NARAYANAMURTHY

Thesis submitted in fulfillment of the requirements  
for the award of the degree of  
Doctor of Philosophy

UMP

Faculty of Electrical & Electronics Engineering

UNIVERSITI MALAYSIA PAHANG

JUNE 2017

## DEDICATION



*I dedicate this thesis to my family members, Mom, Dad, Lakshmi, Balaji and Gopal. Also to my friends and teachers.*

## ACKNOWLEDGEMENTS

As the famous phrase in Sanskrit says “*Matha Pitha Guru Dheivam*”, first and foremost, I would like to thank my parents, teachers and almighty. I would like to thank almighty for providing peace and strength to overcome the hurdles during this journey. Big thanks to my family and friends for supporting throughout my journey.

I thank my supervisor Dr. Fahmi Samsuri (Mr. Cool) for his constant support and believing in me. I have learned a lot from him during my research journey. I would like to thank the Faculty of electrical and electronics engineering, UMP and the staff members for supporting throughout this journey. Special thanks to Mrs. Salmiah for providing timely help and support.

My gratitude to Dr. Hairul Aini Hamzah and Mrs. Madia Baizura for their support to this research. And also I thank all the staff members of the Basic medical science, Department of Medicine, IIUM, Kuantan for their support during cell culture. I thank Ms. Alaina Yuhainis for helping and assisting during cell culture.

My gratitude to Dr. T.V. Kumary and Mrs. Deepa K. Raj from Sree Chitra Tirunal Institute for Medical Sciences and Technology, Trivandrum for their help and support during *in-vitro* evaluation of the polymer.

My thanks to Dr. Khairudin Mohamed and Ms. Tze Pin Lee from Nanofabrication and Functional Materials Research Group, School of Mechanical Engineering, Universiti Sains Malaysia for their help and support in the fabrication of the biochip.

Many thanks to Dr. Ridhwan Abdul Wahab, Dr. Mohd Hamzah Mohd Nasir, and ICRACU staff members for their support during fluorescent imaging.

I thank technical staff Mr. Mohd. Maizam Bin Maideen (Department of medicine, IIUM, Kuantan) and Central laboratory staffs at UMP for SEM imaging.

I thank and acknowledge the reception of UMP Doctoral Scholarship Scheme (DSS) and UMP Post Graduate Research Grants Scheme for financial support. Many thanks to the staffs of Institute of postgraduate studies and International office for their commendable service.

## ABSTRAK

Ciri morfologi sel memainkan peranan yang penting dalam penyelidikan sel, penyampaian ubat, diagnostik, terapeutik dan aplikasi-aplikasi lain. Cetakan-bio adalah teknik litografi lembut digunakan untuk mendapatkan replika bentuk morfologi sel. Pendekatan proses baru pengestrakan ciri morfologi daripada teknik replika cetakan dilaporkan. Ciri morfologi seperti bentuk dan saiz sel serta nukleus, liang dalam membran sel boleh diimejkan dan bentuk yang sama boleh dikesan. Teknik ini membantu untuk menyiasat bentuk alur, liang atau mikrovilus di permukaan sel dan membantu dalam diagnosis yang lebih baik serta analisa di peringkat sel tunggal. Walau bagaimanapun teknik penetapan konvensional, pemotongan dan observasi di bawah mikroskop imbasan elektron (sem) atau mikroskop transmisi elektron (tem) memberikan pandangan lebih terperinci kerana proses tersebut memperkenalkan variasi dalam sampel disebabkan proses yang kompleks dan rumit yang terlibat. Cetakan-bio berdasarkan mikrofluidic juga memainkan peranan yang penting dalam aplikasi penyelidikan sel tunggal. Pengendalian dan penetapan kedudukan sel-sel tunggal di peringkat skala mikro merupakan keperluan penting untuk pelbagai aplikasi termasuk genomik, proteomik, secretomik, dan analisa disintegrasi sel. Saluran mikrofluidic (saluran lurus, saluran bercabang, dan saluran ular) dengan orientasi pelbagai perigi-mikro dikesan kebolehannya dalam memerangkap sel tunggal. Biochip berdasarkan mikrofluidic mampu memerangkap sel dalam keadaan menegak dengan susunan perigi-mikro heksagon. Perigi-mikro yang berdiameter 35 mikron adalah saiz yang mencukupi untuk membenarkan sel ditangkap melekat pada permukaan untuk kajian jangka masa pendek. Aliran proses untuk fabrikasi biochip diperjelaskan. Untuk penangkap sel tunggal (PST) keupayaan biochip mikrofluidic didapati bertambah baik dari saluran yang lurus, ke saluran bercabang, dan saluran ular. Untuk penangkap sel yang banyak (PSB) adalah dari susunan berkurangan daripada saluran yang lurus, ke saluran cawangan, dan saluran ular. Diantara tiga reka bentuk, saluran ular cetakan-bio menawarkan PST yang tinggi dengan mengurangkan PSB. Sel-sel kanser paru-paru manusia digunakan dalam uji kaji ini. Dapatan kajian menunjukkan pembangunan pendekatan karbon polimer-nanopartikel komposit untuk teknik pengimejan untuk sel-sel, yang boleh memberikan maklumat morfologi pada skala organel sel sub tunggal dalam terperinci adalah novel. Mikroskop elektron digunakan untuk imej replika. Teknik ini menangkap imej sel bersama-sama dengan sub selnya secara lengkap dan terperinci morfologi sel. Had teknik ini ialah, ia hanya menyediakan maklumat morfologi. Maka morfologi abnormal yang tidak dapat ditekup tidak boleh dianalisa. Teknik ini didapati dapat menganalisa sel-sel tunggal untuk dikaji berdasarkan morfologi, terutama untuk aplikasi penghantaran ubat dan untuk siasatan laluan molekul. Untuk prospektif masa depan, ciri-ciri morfologi yang diperoleh melalui teknik ini juga boleh digunakan untuk melatih rangkaian neural buatan untuk membuat keputusan sepenuhnya berdasarkan teknik ini.



## ABSTRACT

Morphological features of cells play a vital role in cell research, drug delivery, diagnostic, therapeutic and many other applications. Bioimprint is a soft lithography technique used to obtain the imprint replica of cell morphology. Herein report a new process approach of morphology feature extraction from the imprint replica technique. Morphological features like shape and size of cell, shape and size of nucleus, pores in the cell membrane can be imaged comparatively and the same can be detected. This technique helps to investigate the shape of grooves, pores, blebs or microvillus on the cellular surface and helps in better diagnosis and analysis at single cell level. However conventional method involving fixation, sectioning and viewing under scanning electron microscope (SEM) or transmission electron microscope (TEM) can provide cell's inside anatomy details, although the process introduces variations in samples due to complex and tedious process involved. Also microfluidics-based biochip plays a vital role in single cell research applications. Handling and positioning of single cells at the microscale level is an essential need for quite various applications including genomics, proteomics, secretomics, and lysis analysis. Characterized the effect of microfluidic channel (straight channel, branched channel, and serpent channel) with a microwell array orientation for single cell trapping. Demonstrated microfluidic-based biochips capable of vertical cell trapping with a hexagonal array of microwells. Microwells were of 35  $\mu\text{m}$  in diameter, a size sufficient to allow attachment of captured cells for short term study. Explained the process flow for the fabrication of the biochip. Single cell capture (SCC) capabilities of the microfluidic-biochips were found to be improving from the straight channel, branched channel, and serpent channel accordingly. Multiple cell capture (MCC) were in the order of decreasing from the straight channel, branch channel, and serpent channel. Among three designs investigated, serpent channel biochip offers high SCC with reduced MCC. Human lung cancer cells were used for characterization. The findings of this research is that developed a novel approach of carbon nanoparticle-polymer composite (CPC) for imaging technique for the cells, which can provide morphology information on single cell sub organelle scale in much detail. It is observed that 0.3 wt. % of load carbon nanoparticle (CNP) in carbon polymer mixture (CPM) were optimal for cell-imprint replica fabrication. The electrical resistance of the 3-CPC (0.3 wt. %) were reduced by 68 % when compared to N-CPC (0 wt. %). Electron microscopes were used to image the replica. Technique delivers cell image along with its complete sub cell scale level morphological details. The limitation of this technique is that, it only provides the morphology information. Thus abnormalities which do not designate on morphology cannot be diagnosed. This technique finds its application where single cells are to be analyzed and diagnosis for study based on morphology, especially for drug delivery applications and for investigations based on molecular pathways. As a future prospective, morphology features obtained through this technique can also be used to train the artificial neural network for decision making completely based on this technique.

## TABLE OF CONTENTS

<b>DECLARATION</b>	
<b>TITLE PAGE</b>	<b>i</b>
<b>DEDICATION</b>	<b>ii</b>
<b>ACKNOWLEDGEMENTS</b>	<b>iii</b>
<b>ABSTRAK</b>	<b>iv</b>
<b>ABSTRACT</b>	<b>v</b>
<b>TABLE OF CONTENTS</b>	<b>vi</b>
<b>LIST OF TABLES</b>	<b>xiii</b>
<b>LIST OF FIGURES</b>	<b>xiv</b>
<b>LIST OF SYMBOLS</b>	<b>xviii</b>
<b>LIST OF ABBREVIATION</b>	<b>xix</b>
<b>CHAPTER 1</b>	<b>1</b>
<b>INTRODUCTION</b>	<b>1</b>
1.1 Overview	1
1.2 Motivation and problem statement	3
1.3 Objectives	4
1.4 Scope of research	4
1.5 Thesis outline	5
<b>CHAPTER 2</b>	<b>7</b>

<b>CELL MORPHOLOGY AND IMPRINT FABRICATION</b>	<b>7</b>
2.1 Current scenario	7
2.2 Cell morphology for cancer diagnosis	7
2.3 Recent approaches in imprint lithography	9
2.3.1 Nanoimprint lithography methods	9
2.3.1.1 Thermoplastic nanoimprint lithography (T-NIL)	10
2.3.1.2 UV-nanoimprint lithography (UV-NIL)	11
2.3.1.3 Step and flash imprint lithography (SFIL)	12
2.3.1.4 Step and stamp imprint lithography (SSIL)	13
2.3.1.5 Laser assisted direct imprinting	14
2.3.2 Approaches for the fabrication of cell imprint replica	15
2.4 Cell imprint lithography for cell diagnosis at sub single cell scale level	16
2.5 Biomimetic smart culture substrates and microenvironments	20
2.6 Chapter summary	23
<b>CHAPTER 3</b>	<b>24</b>
<b>PASSIVE HYDRODYNAMIC MICROFLUIDIC BIOCHIP PLATFORM FOR SINGLE CELL ANALYSIS</b>	<b>24</b>
3.1 Overview	24
3.2 Microfluidic biochip platforms for single cell trapping	24
3.2.1 Techniques	27
3.2.2 Hydrodynamic trapping	29

3.3	Critical Review	51
3.4	Chapter summary	57
<b>CHAPTER 4</b>		<b>58</b>
<b>CARBON NANO PARTICLE-POLYMER COMPOSITE CELL IMPRINT LITHOGRAPHY</b>		<b>58</b>
4.1	Organization of this chapter	58
4.2	Cell culture and maintenance	61
4.3	Carbon-polymer composite preparation and imprinting	61
4.3.1	Carbon nanoparticle characterization	61
4.3.2	Carbon-polymer mixture preparation and optimization:	62
4.3.2.1	Carbon nanoparticle-triglyme ultrasonication	62
4.3.2.2	Carbon-polymer mixture	63
4.3.2.3	UV photo polymerization	63
4.3.3	Photopolymer effect and cell cytoskeleton study	63
4.3.3.1	Polymer-cell response	63
4.3.3.2	Bioimprinting effect to cells	64
4.3.4	Carbon polymer composite (CPC) electrical resistance measurement	64
4.4	Passive hydrodynamic microfluidic biochip platform	65
4.4.1	Biochip design	65
4.4.2	Biochip design simulation analysis	66
4.4.3	Biochip fabrication	66

4.4.4	Microfluidic biochip for single cell trapping and cell viability test	69
4.4.5	Single cell fluorescent measurements	69
4.5	Fabrication of cell imprinted carbon polymer composite (CI-CPC)	69
4.5.1	Fabrication of plain carbon polymer composite CPC	70
4.5.2	Fabrication of cell imprinted carbon polymer composite (CI-CPC)	70
4.5.3	Scanning electron microscope imaging	71
4.6	Cell imprinted carbon polymer composites (CI-CPC) for cell diagnosis	71
4.6.1	Bezoar extract preparation	71
4.6.2	Vincristine sulphate solution preparation	71
4.6.3	Experiments on A549	71
4.6.4	Experiments on MCF-7	72
4.6.5	Comparative interpretation on various imaging modalities	72
4.7	Cell morphology feature detection	73
4.8	<i>In-vitro</i> study of polymer composites for biomedical applications	75
4.8.1	Sample preparation	75
4.8.2	Cytotoxicity studies	75
4.8.2.1	Direct contact	76
4.8.2.2	Test on extract	76
4.8.3	Cytocompatibility studies	76
4.8.3.1	Cell adhesion	76
4.8.3.2	Live dead analysis	77

4.8.3.3	Cytoskeleton analysis	77
4.8.3.4	Cell adhesion with MTT assay	77
<b>CHAPTER 5</b>		<b>78</b>
<b>RESULTS AND DISCUSSIONS</b>		<b>78</b>
5.1	Carbon-polymer composite imprinting	78
5.1.1	Carbon nanoparticle characterization	78
5.1.2	Carbon-polymer mixture preparation and optimization	79
5.1.3	Photopolymer effect and cell cytoskeleton study	80
5.1.3.1	Polymer-cell response	80
5.1.3.2	Bioimprinting effect to cells	81
5.1.4	Carbon polymer composite (CPC) electrical resistivity measurement	83
5.2	Passive hydrodynamic microfluidic biochip platform	84
5.2.1	Microfluidic design simulation study	84
5.2.2	Microfluidic biochip for single cell trapping and design analysis	86
5.2.3	Cell viability	87
5.2.4	Single cell fluorescent measurements	87
5.3	Fabricated carbon polymer composite (CPC)	90
5.3.1	Fabricated plain carbon polymer composite	90
5.3.2	Fabricated cell imprinted carbon polymer composite (CI-CPC)	92
5.3.3	Cell morphology resolution comparison	94
5.4	Cell imprinted carbon polymer composite (CI-CPC) for cell diagnosis	96

5.4.1	A549 cell replica morphology analysis	96
5.4.2	MCF-7 cell replica morphology analysis	100
5.4.3	Interpretation on various imaging techniques	102
5.5	Cell morphology feature detection	104
5.6	<i>In-vitro</i> study of polymer composites for biomedical applications	107
5.6.1	Cytotoxicity studies	108
5.6.1.1	Direct contact	108
5.6.1.2	Test on extract	109
5.6.2	Cytocompatibility studies	110
5.6.2.1	Live dead analysis	111
5.6.2.2	Cytoskeleton analysis	111
5.6.2.3	Cell adhesion with MTT assay	112
5.7	Chapter summary	113
	<b>CHAPTER 6</b>	<b>114</b>
	<b>CONCLUSION AND FUTURE RECOMMENDATIONS</b>	<b>114</b>
6.1	Summary of the research	114
6.2	Research contributions	115
6.3	Future recommendations	116
	<b>REFERENCES</b>	<b>117</b>
	<b>APPENDIX A</b>	<b>133</b>
	<b>CELL CULTURE PROTOCOLS</b>	<b>133</b>

7.1	Cell culture techniques	133
7.2	Complete growth media preparation	133
7.3	Thawing cells	133
7.4	Changing media	134
7.5	Subculturing cells	134
7.6	Cryopreservation of cells	134
7.7	Measuring cell density using trypan blue exclusion assay method	135
7.8	Seeding of cells	135
<b>APPENDIX B</b>		<b>136</b>
<b>INTELLECTUAL PROPERTIES</b>		<b>136</b>
<b>GALLERY</b>		<b>140</b>

A large, semi-transparent watermark of the UMMP logo is centered on the page. The logo consists of a stylized 'U' shape formed by two overlapping triangles, one light blue and one light purple, with a yellow diamond in the center. The letters 'UMMP' are written in white, bold, sans-serif font across the bottom of the 'U' shape.

UMMP



## LIST OF TABLES

Table 2.1	Material and process used for cell imprint fabrication	15
Table 2.2	Key features of membrane vesicle populations	18
Table 3.1	Comparison of various microfluidic techniques for single-cell trapping	28
Table 3.2	Critical summary of contact-based hydrodynamic vertical trapping	53
Table 4.1	Boundary conditions of modelling	66
Table 5.1	Comparative interpretation of simulation and experimental results	89
Table 5.2	Comparative summarization of conventional and CIL approach	107



UMP

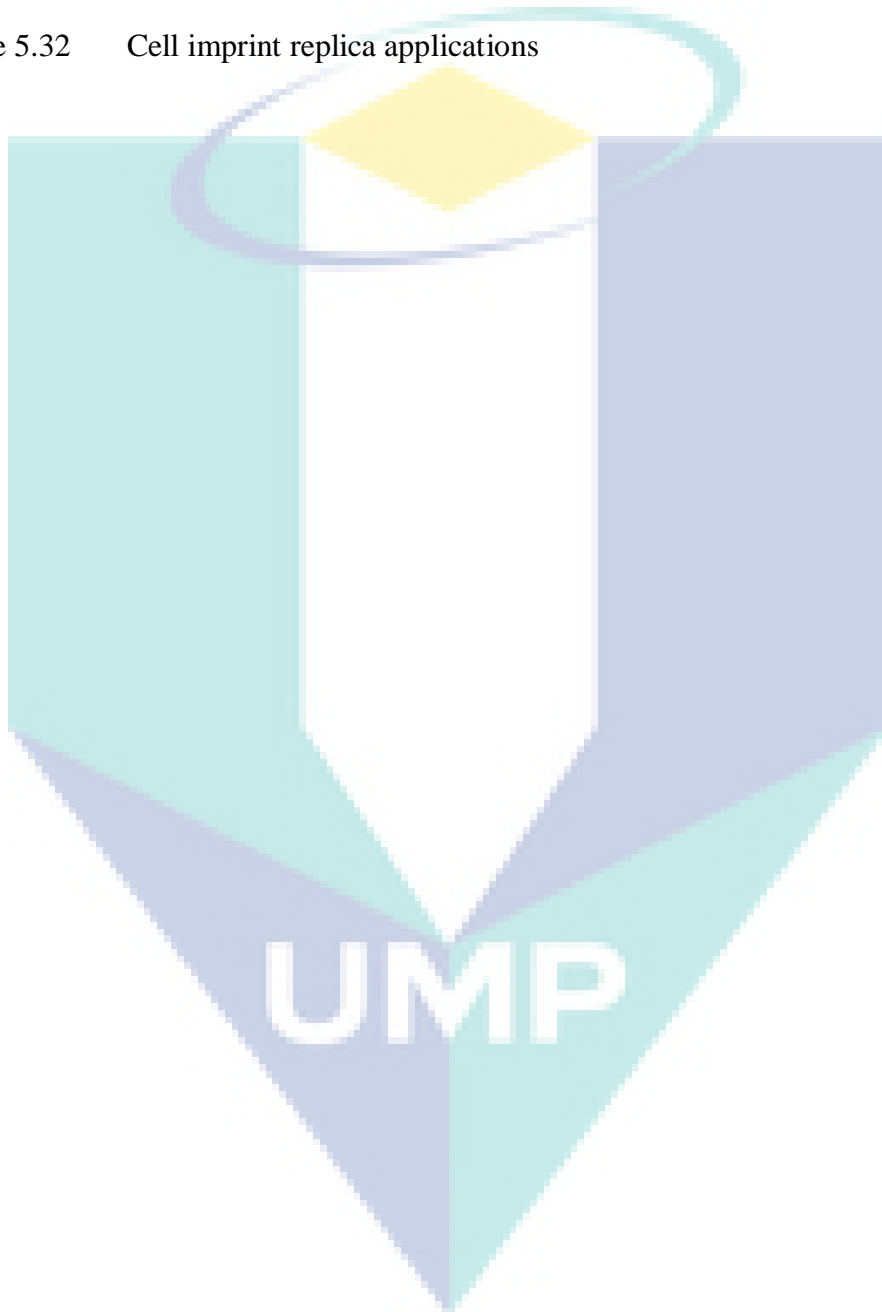
## LIST OF FIGURES

Figure 1.1	Deaths due to various cancers	2
Figure 1.2	Brief research flow	6
Figure 2.1	Different methods of NIL	9
Figure 2.2	System and image of T-NIL	10
Figure 2.3	AFM imprint images	11
Figure 2.4	Step and flash imprinting process	12
Figure 2.5	Step and flash imprinting process	13
Figure 2.6	Step and Stamp Imprinting Process	14
Figure 2.7	LADI Process	15
Figure 2.8	Loading conductive filler wt. % vs conductivity	16
Figure 2.9	Schematic representation of the extracellular vesicles	17
Figure 2.10	Summary of some adaptive cellular responses	17
Figure 2.11	Size ranges of major types of membrane vesicles	18
Figure 2.12	Morphology of necrosis and apoptosis	19
Figure 2.13	Schematic representation of apoptosis process	19
Figure 2.14	Factors involved in cell culture substrates	20
Figure 2.15	Cell culture scaffold properties	21
Figure 2.16	Approaches in cell microenvironment	22
Figure 2.17	Matrix-cell interactions	22
Figure 3.1	Publications trend on single cell analysis	25
Figure 3.2	Applications of SCA	26
Figure 3.3	Diverse approaches for single cell trapping	28
Figure 3.4	Cell trapping correlation with micro well diameter	30
Figure 3.5	Cell trapping in array of traps	31

Figure 3.6	Non-contact trapping of cells using steady streaming micro eddies	32
Figure 3.7	Array of jail designs for cell trapping	33
Figure 3.8	Microfluidic cell array	34
Figure 3.9	Hydrodynamic cell traps	35
Figure 3.10	Cell trapping correlation with channel length	36
Figure 3.11	Hydrodynamic trap using stagnation point	37
Figure 3.12	Cell capture using pockets	38
Figure 3.13	Cell trapping correlation with different micro well diameter	39
Figure 3.14	Single micro particle trapping using different trap designs	40
Figure 3.15	Trapping using microchannel	41
Figure 3.16	Cell trapping using V shaped pockets	43
Figure 3.17	Single particle trajectory manipulation	44
Figure 3.18	Spheres being trapped in the array of traps	45
Figure 3.19	Microfluidic device showing cells being trapped	48
Figure 3.20	Microfluidics with TCMA and different fluid channels	50
Figure 3.21	Cell being trapped in a fluidic trap	51
Figure 4.1	Flow chart of research methodologies	59
Figure 4.2	Graphical representation of overall methodology used in the study	60
Figure 4.3	Flow chart for carbon photopolymer fabrication	62
Figure 4.4	Schematic illustration of resistivity measurement setup	65
Figure 4.5	Fabricated biochip and its operation	68
Figure 4.6	Imprinting process	70
Figure 4.7	Series of image processing steps for feature detection	73
Figure 5.1	CNP SEM characterization	78
Figure 5.2	CNP TEM Characterization	79

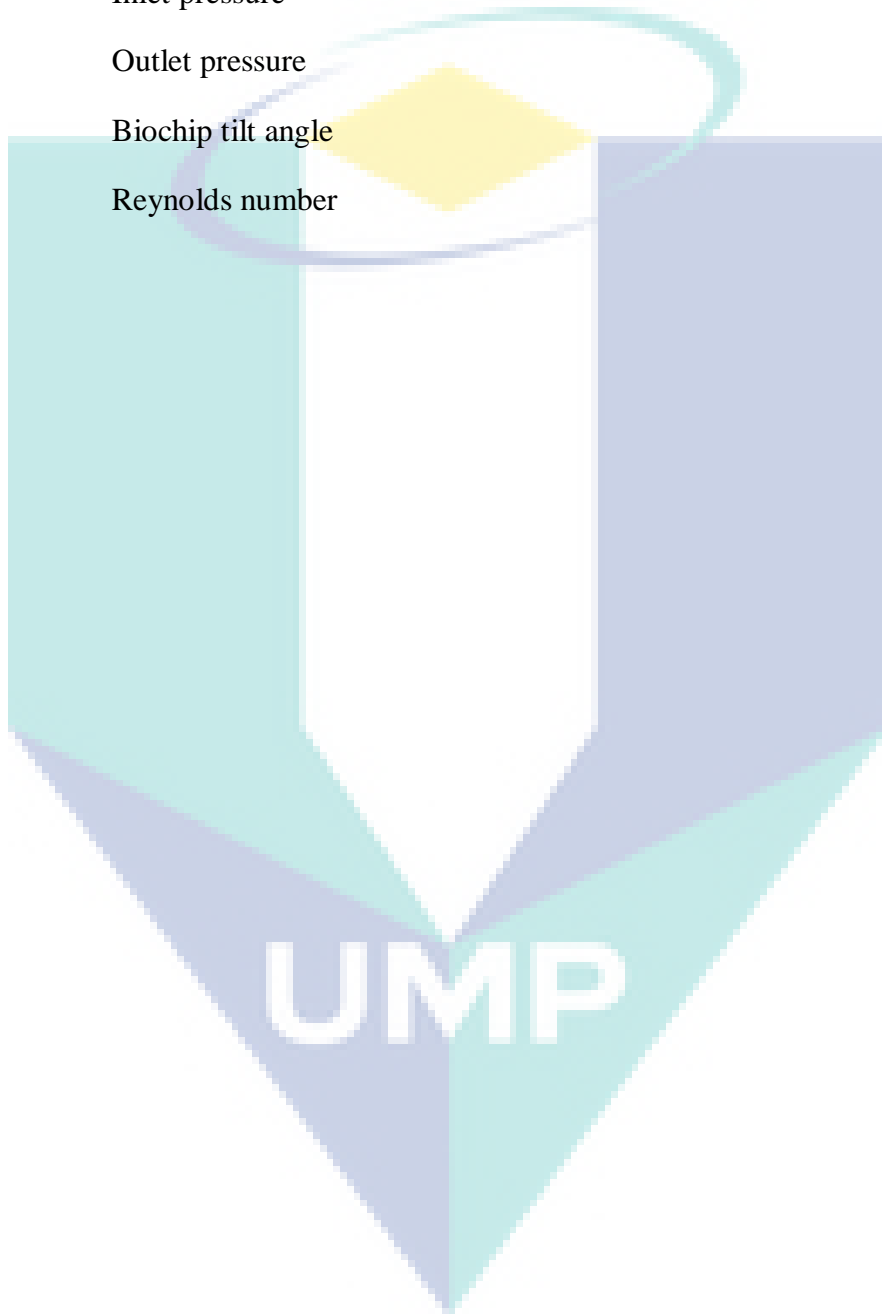
Figure 5.3	Filler wt % vs imprinting capability of the polymer	80
Figure 5.4	Polymer-Cell response	81
Figure 5.5	Bioimprinting effect to cells	82
Figure 5.6	Fluorescent imaging of bioimprinting effect to cells morphology	83
Figure 5.7	CNP load wt. % vs resistance of CPC	84
Figure 5.8	Microfluidic design simulation study	85
Figure 5.9	Single cell trapping in three biochips	86
Figure 5.10	Microfluidic biochip trapping capabilities	87
Figure 5.11	Cell viability and cytoskeleton study	88
Figure 5.12	CPC showing plain and smooth bottom surface after peeling off	91
Figure 5.13	CPC replica of fungi	91
Figure 5.14	HeLa CI-CPC replica	92
Figure 5.15	HGF-1 CI-CPC replica	93
Figure 5.16	HT-29 CI-CPC replica	94
Figure 5.17	Cell morphology resolution comparison	95
Figure 5.18	A549 VC treated CI-CPC replica	97
Figure 5.19	A549 BZ treated CI-CPC replica	98
Figure 5.20	A549 BZ treated CI-CPC replica (higher magnification)	99
Figure 5.21	A549 BZ treated CI-CPC cell membrane closer look	100
Figure 5.22	MCF-7 BZ treated CI-CPC replica	101
Figure 5.23	Interpretation with different imaging techniques	103
Figure 5.24	Cell morphology feature detection	105
Figure 5.25	Imprint replica for tissue engineering applications	108
Figure 5.26	Cell response to direct contact study	109
Figure 5.27	Cell responses for test on extract study	110

Figure 5.28	MTT assay for test on extract	110
Figure 5.29	Live dead Imaging	111
Figure 5.30	Cytoskeleton analysis (Actin –phalloidin imaging)	112
Figure 5.31	MTT assay for cell adhesion	112
Figure 5.32	Cell imprint replica applications	113

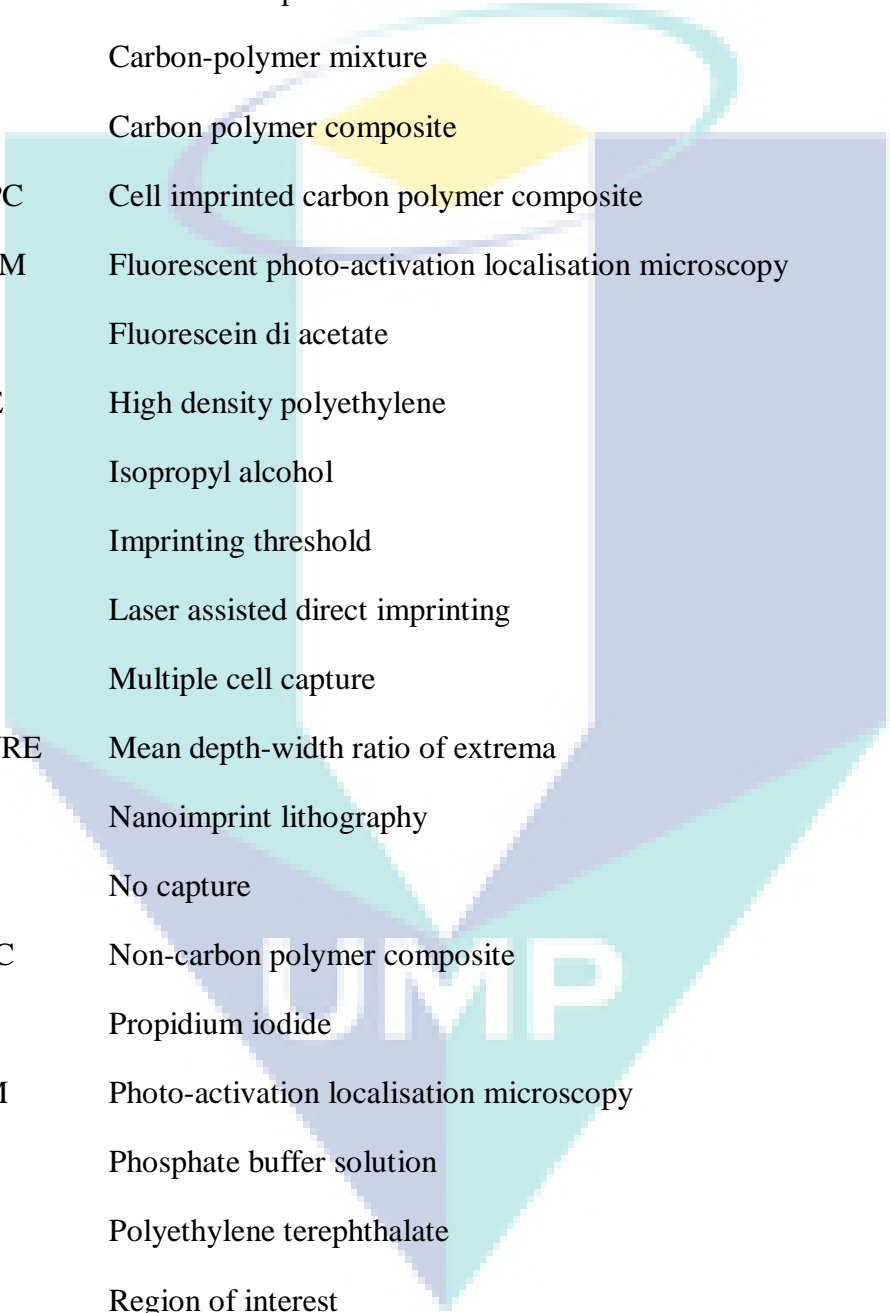


## LIST OF SYMBOLS

$U_i$	Inlet velocity
$U_o$	Outlet velocity
$P_i$	Inlet pressure
$P_o$	Outlet pressure
$\theta$	Biochip tilt angle
$Re$	Reynolds number

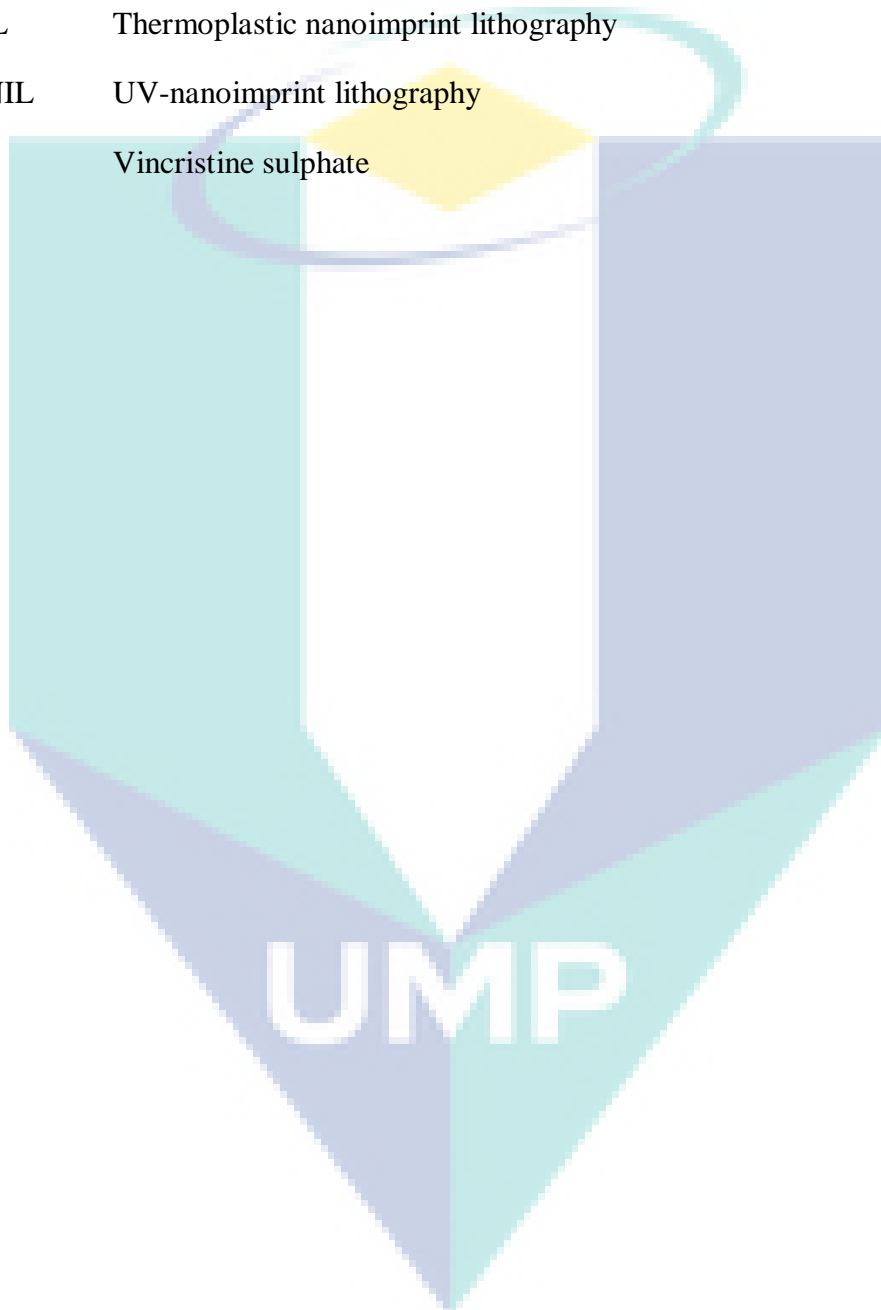


## LIST OF ABBREVIATION



BZ	Bezoar
CGM	Complete growth media
CNP	Carbon nano particle
CPM	Carbon-polymer mixture
CPC	Carbon polymer composite
CI-CPC	Cell imprinted carbon polymer composite
FPALM	Fluorescent photo-activation localisation microscopy
FDA	Fluorescein di acetate
HDPE	High density polyethylene
IPA	Isopropyl alcohol
IL	Imprinting threshold
LADI	Laser assisted direct imprinting
MCC	Multiple cell capture
MDWRE	Mean depth-width ratio of extrema
NIL	Nanoimprint lithography
NC	No capture
N-CPC	Non-carbon polymer composite
PI	Propidium iodide
PALM	Photo-activation localisation microscopy
PBS	Phosphate buffer solution
PET	Polyethylene terephthalate
ROI	Region of interest
SFIL	Step and flash imprint lithography
SSIL	Step and stamp imprint lithography
SCA	Single cell analysis

SCC	Single cell capture
SEM	Scanning electron microscope
TEM	Transmission electron microscope
TCMA	Truncated cone-shaped microcell array
T-NIL	Thermoplastic nanoimprint lithography
UV-NIL	UV-nanoimprint lithography
VC	Vincristine sulphate





## CHAPTER 1

### INTRODUCTION

#### 1.1 Overview

Cells are the smallest and fundamental unit of life. Cells replicate independently. Cells can be broadly classified into prokaryotes (single cellular) and eukaryotes (multicellular), the former do not contain a nucleus. Prokaryotes include bacteria and archaea. Eukaryotes include fungi, plant and animal. A eukaryote cell consists of a nucleus and other organelles. Cell organelles include mitochondria, nucleotides, endoplasmic reticulum, golgi apparatus nucleus which consists of chromatin, DNA and nucleolus enclosed by the nuclear envelope (Orgel, 1998, Maton et al., 1997, Becker et al., 2003). Any abnormalities can reveal more insights when investigated and studied at cellular scale level. This helps in better disease diagnosis and to provide correct treatment.

Cancer is a group of diseases in which cell growth is unregulated. Division and growth of cancer cells are uncontrollable which ultimately leads to tumors. Cancer cells may spread and affect other organs too. Cancers are of several types like adrenal cancer, anal cancer, bone cancer, breast cancer, cervical cancer, colon/rectum cancer, endometrial cancer, esophagus cancer, eye cancer, gallbladder cancer, kidney cancer, leukemia, liver cancer, lung cancer, lymphoma, nasopharyngeal cancer, non-hodgkin lymphoma, oral cavity and oropharyngeal cancer, osteosarcoma, ovarian cancer, pancreatic cancer, prostate cancer, salivary gland cancer, skin cancer, small intestine cancer, stomach cancer, testicular cancer, thymus cancer, thyroid cancer, vaginal cancer and vulvar cancer (American Cancer Society, 2015). From statistics shown in Figure 1.1, cancer and cancer related deaths are increasing day by day, though researcher and doctors are actively working on the solution for it (Zainal Ariffin and Nor Saleha, 2011, Ferlay et al., 2015, Bray et al., 2013).

## Various Cancer Deaths Worldwide

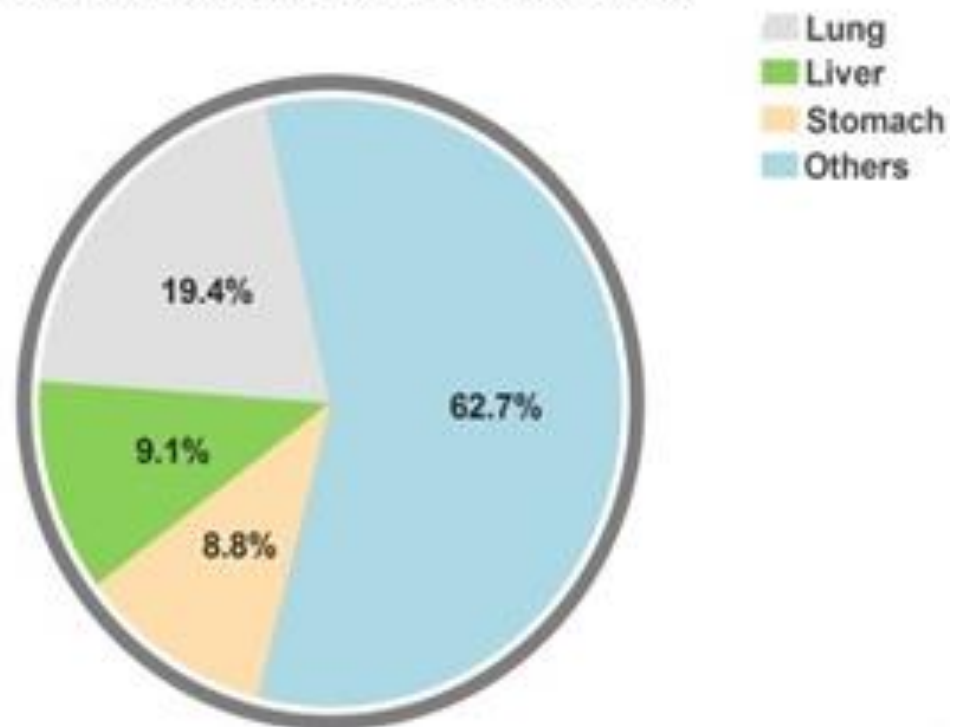


**Figure 1.1 Deaths due to various cancers**

Adapted from source: Zainal Ariffin and Nor Saleha (2011), Bray et al., (2013), Ferlay et al., (2015)

Based on world cancer report from the World Health Organization (WHO) (Stewart and Wild, 2016), it is clear that cancer is a leading cause of death worldwide, accounting for 8.2 million deaths in 2012. The most common causes of cancer death are cancers of lung (1.59 million deaths), liver (745 000 deaths), stomach (723 000 deaths), colorectal (694 000 deaths), breast (521 000 deaths) and esophageal cancer (400 000 deaths) (Stewart and Wild, 2016, Torre et al., 2015, Siegel et al., 2015, Siegel et al., 2016).

Report from National Cancer Registry Malaysia (Zainal Ariffin and Nor Saleha, 2011) mentioned that the cumulative cancer risks in peninsular Malaysia were up to 18% of 26,089 cancer patients, in which 54.7% were females and 45.3% were males. The statistics showed that the risk of getting cancer is very high that 1 in 4 Malaysian will have the potential of getting cancer in their lifetime.

## 1.2 Motivation and problem statement

The recent trend is to diagnose and analyze the high resolution single cell scale level for better investigations and treatments (Heath et al., 2016, Darmanis et al., 2016, Van Loo and Voet, 2014). Several researchers are working towards this perspective. Micro fluidics and lab on chips based techniques have also been designed, developed and reported for these purposes (Nock et al., 2010, Nock et al., 2011, Alkaisi et al., 2007, Wang and Bodovitz, 2010). Most of the conventional imaging techniques used to image cells involved light microscope, in which imaging source is light. Recently electron microscopes have been used to image cells in more detail, whose imaging source is an electron beam. The former has a higher wavelength when compared to the latter. Thus the latter method can provide high-resolution cell imaging (Williams and Carter, 1996).

Cells are composed of water, inorganic ions, and carbon-containing (organic) molecules. Water is the most abundant molecule in cells, accounting for 70% or more of the total cell mass. Also, cells are very delicate, thus pre-processing method are involved for electron microscope imaging. The traditional methods involved in imaging the cells include several tedious processes like its preparation, which involves fixation, processing (dehydration, clearing, and infiltration), embedding, sectioning, and staining (Bozzola and Russell, 1999). It was reported that this technique lacks precise and accurate morphological details due to artefacts introduced by tissue processing which leads to changes like shrinkage, washing out of particular cellular components, and alterations of the structures in the tissue (Kellenberger et al., 1992, Loqman et al., 2010).

Cell imprint replica using the imprinting technique can be done to lock the molecular process and can be imaged using high resolution imaging systems. Investigations on the surface morphologies of cancer cell at high resolution can reveal more information. High resolution topography images of cell membrane can provide some important features involving exosomes, micro vesicles, apoptotic bodies and many others. These minute features and pores, play major role in cell diagnosis, drug delivery, therapy and many more. These can be associated and also be correlated with many cell signaling events. High resolution cell topography images, when interpreted and compared along with the conventional analysis, can help in understanding the cell signaling in more detailed and precise manner than before.

### 1.3 Objectives

Broad objective of this research is to develop a nanoparticle photopolymer composite for cell imprint lithography assisted by passive microfluidic platforms for biomedical applications. For achieving this broad objective, following specific objectives have been conceived.

1. To develop and optimize the process of carbon polymer composite imprinting supporting cancer cell feature detection for diagnosis.
2. To design and develop passive microfluidic biochip to facilitate the single cell research investigation and for the fabrication of single cell imprint replica.
3. *In-vitro* evaluation of fabricated polymer for its use in tissue engineering applications.

### 1.4 Scope of research

In order to meet the outlined objective, the following scopes of research have been identified. Briefly research flow is shown in Figure 1.2. Research activities under first objectives are:

- Optimization of carbon polymer composite imprinting.
- High resolution imaging techniques to obtain the high resolution replica images.
- Cancer cell imprinting with and without stimulations.
- Cell imprint replicas consisting cell morphology for diagnosis.
- Replica images are analyzed for any abnormalities and its corresponding features detected.

As for second objective:

- Design, develop and fabrication of biochips at NFM, USM.
- Experimental evaluation of microfluidic biochip for single cell trapping.

As for third objective:

- *In-vitro* evaluation of the fabricated carbon polymer composites for enabling its use in tissue engineering applications.
- Cytotoxicity and cyto-compatibility test for its *In-Vitro* characterization.

## 1.5 Thesis outline

Thesis outline is as follows,

Chapter 1 describes about the recent statistics of cancer along with the current limitations of diagnosis and research investigations. This has brought the author to arrive at the objectives along with scopes for addressing the issues.

Chapter 2 provides the literatures about the cellular diagnosis based on morphology. Summarizing the issues associated with conventional approach, thereby how fabrication of cell imprint replica address the problem providing the solutions. Described the past literatures for the imprinting approaches involved.

Chapter 3 presents the past literatures on microfluidic techniques and the passive hydrodynamic based microfluidics for single cell trapping. For single cell replica fabrications, single cells need to be trapped initially for investigations.

Chapter 4 describes in detail about the methodologies involved in this study.

Chapter 5 presents the results and discussions of the study conducted.

Chapter 6 presents the conclusions of the study with future scope and directions of this research.

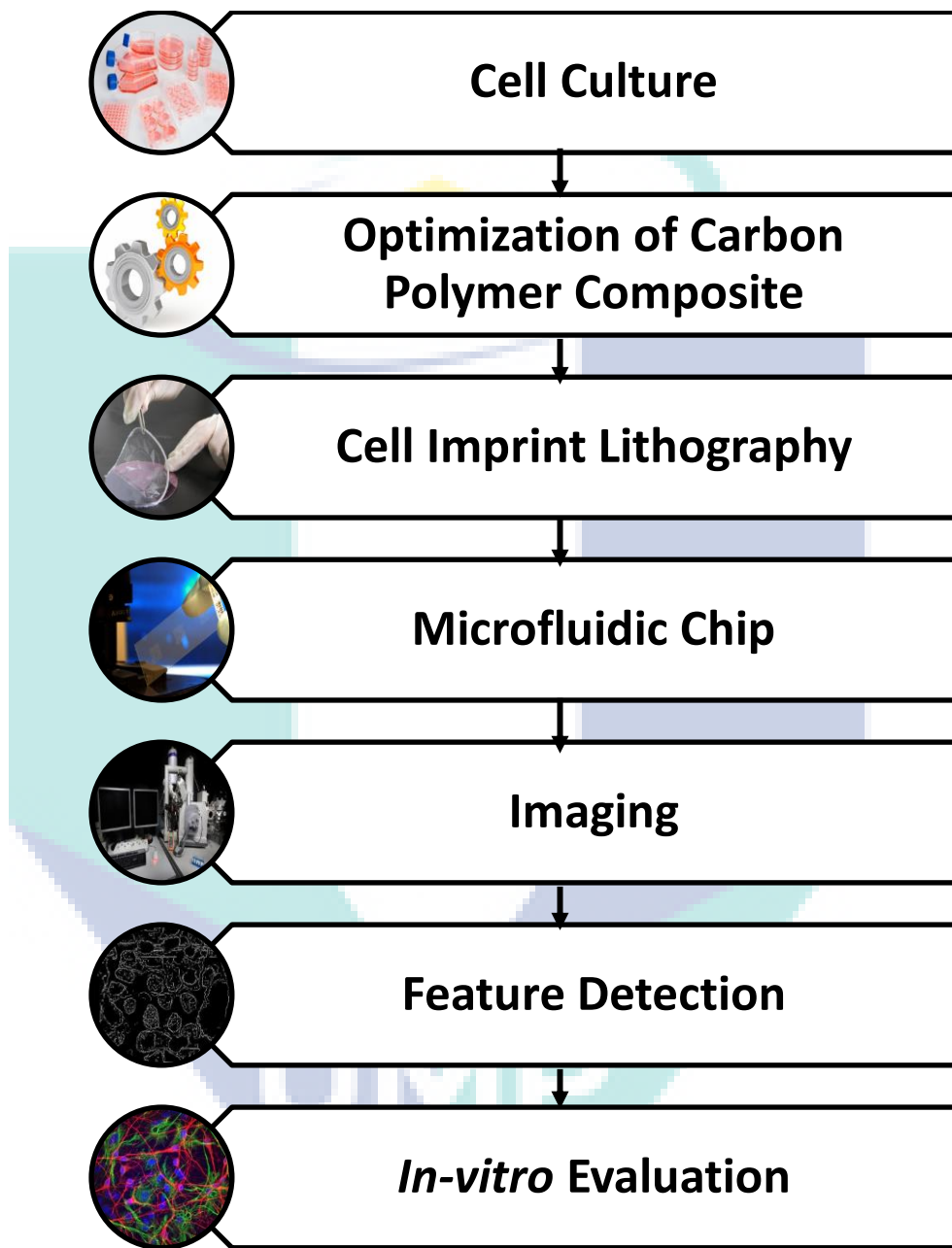


Figure 1.2 Brief research flow

## CHAPTER 2

### CELL MORPHOLOGY AND IMPRINT FABRICATION

#### 2.1 Current scenario

Various researches are going on throughout the world for better cancer diagnosis and treatment. Recent direction is to diagnose and analyze the cancer cells at the single cell scale level for better understanding of cell signaling at extracellular and for several applications like drug delivery, diagnosis, cancer research investigations and therapy.

#### 2.2 Cell morphology for cancer diagnosis

In cytology, the cell morphological features help to distinguish any abnormality in the cell, as there would be changes in morphology between normal cell and in the affected cell region (Rello et al., 2005). The diagnosis of a cell using morphological features and statistical features acts as the prominent method for the clinical applications. Cell morphological image processing method is a well suited approach to analyze a cell in much detail. Cell morphology features involved can be broadly classified into morphometric, densitometric, textural and structural features (Rodenacker and Bengtsson, 2003). Based on these features, cell morphology deviations that have occurred between normal and abnormal cell can be determined.

Some of the literatures that used cell morphology and the parameters involved in cancer cell diagnosis are presented below. By considering the morphological features, the size and shape of the cell can be determined. The radius and area are used to estimate the size of the cell and compactness, and smoothness is used to assess the shape of the cell (Street et al., 1993). The statistical features or the statistics computed on smoothness, major and minor axis and some other properties are used to detect the cell abnormality (Thiran and Macq, 1996, Wolberg et al., 1995). The variation in size and shape of the nuclei is considered as a major factor for the diagnosis of cancer (Thiran and Macq,

1996). Demonstrated that texture analysis techniques could provide valuable diagnostic decision support in a complex domain, such as colorectal tissue (Atlamazoglou et al., 2001). The Fourier transform analysis over the corneal endothelial cells to correlate the cell structure with the patient's age provided the cancer identification (Fitzke et al., 1997). Due to the limitations of the manual diagnosis, the automated screening test based on the computer aided visualization (Ageing, 2003) has been developed to increase the performance of the diagnosis.

An automated computational tool to improve the diagnostic performance have been developed and deployed to use in practice. Generally, the automated cell diagnosis system consists of three components such as pre-processing, feature extraction and classification of the state of the cancer cells. The pre-processing system mainly focuses on the noise removal in the obtained images. Filtering process was used to reduce the noise. Usually, the value of the pixel located in a selected neighborhood pixel is used to remove the random noise in the images (Baheerathan et al., 1999). After the noise removal task, segmentation of the nuclei and the cell boundary region were performed using both the region based approach and the boundary based approach. Clustering algorithm was dominantly used to segment the desired region in the image. To diagnose the changes in the normal cells, the two types of deviations, one at the cellular level and another at the tissue level were considered.

Wide ranges of researches were carried out in order to resolve the problems identified in the diagnosis of cells and its abnormality. Traditionally, the cell diagnosis based on morphology was performed by doing biopsy for the samples and followed by observations under the microscope, the abnormal cells were determined (Andrion et al., 1995, Ismail et al., 1989). Even though optical methods were adopted for the diagnosis and acts as a clinical screening tool, it also has its own limitations of exploring insights of the abnormality in much detail. But all these involve the study of cell at cluster level with not much detail of the cell at single cell sub organelle level. Conventionally used technique to visualize the insights of single cell sub organelle scale morphology details are scanning electron microscope (SEM) or transmission electron microscope (TEM), involving several tedious processes like fixation and processing. It was reported that processes involving artifacts were introduced leading to changes like alterations of the structure in the tissue and cell morphology shrinkage due to dehydration (Kellenberger et al., 1992, Loqman et al., 2010). Considering all the above discussed points and



drawbacks of the conventional methods, we investigated imprint lithography approach for cell morphology diagnosis research. In below sections, discussed in detail are the imprint lithography processes.

## 2.3 Recent approaches in imprint lithography

Nano patterning is more of great need nowadays. It is the process of patterning the surface at nano scale. Nanoimprint lithography (NIL) is a process of fabricating patterns of nanometer scales. NIL was successful because of its high resolution. It is a simple process with low cost and high throughput. Imprint lithography is a nano-patterning technique. This technique allows patterning features of size less than sub 100 nm. It facilitates various applications like bio molecule immobilisation at the nano-scale, scaffold for cell culture, high resolution cell replica imaging and for various other biomedical applications. (Truskett and Watts, 2006, Mendes et al., 2007, Lan and Ding, 2010, Gadegaard and McCloy, 2007, Li et al., 2011, Martino et al., 2012, Samsuri et al., 2011, Nock et al., 2011, Muys et al., 2006)

### 2.3.1 Nanoimprint lithography methods

Nanoimprint lithography methods are broadly classified and described in the following sections. Below in Figure 2.1 shows different approaches involved in NIL.

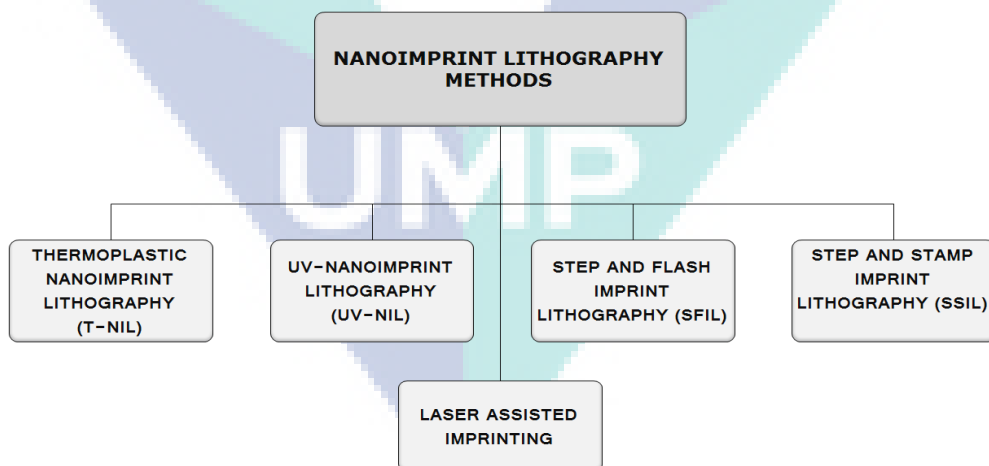


**Figure 2.1** Different methods of NIL

Image source: Vigneswaran et al. (2014)

### 2.3.1.1 Thermoplastic nanoimprint lithography (T-NIL)

Thermoplastic Nanoimprint lithography (T-NIL) is very old technique which is even now practiced because of its simple process, low cost and high throughput. Illustration of the system involved is showed in Figure 2.2. In this process a thermo cure resist is spin coated on the substrate. The property of thermo cure resist is that once it is heated above the glass transition, the polymer is of liquid state. After cooling it becomes hardened by crosslinking. Using this property of the resist, the mold of specific feature is pressed on to the resist upon heating above the glass transition temperature. After cooling, the pattern gets transferred to the resist from the mold and is separated from the resist. Features in the mold can be transferred to the substrate by using chemically reactive plasma to selectively remove the deposited material. Though this has several applications, but it cannot be used for the applications dealing with live cells. The process can damage the cells because of heating. The drawback of this technique is that it cannot be performed at room temperature and it requires high imprint pressures which cause inaccuracy in alignment (Lan and Ding, 2010).

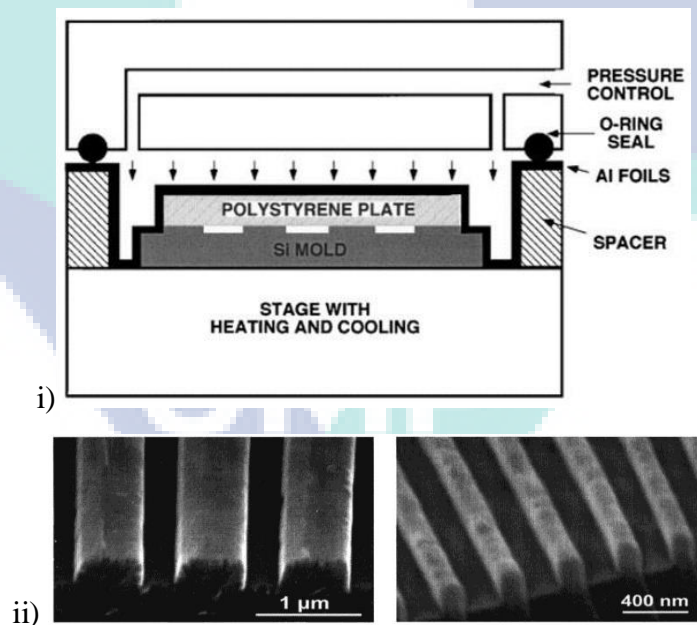


**Figure 2.2 System and image of T-NIL**

Image source: Hu et al., (2005). Image shows (i) Configuration of nanoimprint lithography system with tissue-culture polystyrene plates on top of the Si mold, (ii) Nanoimprinted structure in thick tissue-culture polystyrene: (a) gratings with 0.5  $\mu\text{m}$  half-pitch and 440 nm height and (b) gratings with 120 nm half-pitch and 290 nm height.

### 2.3.1.2 UV-nanoimprint lithography (UV-NIL)

The process of UV-NIL is almost same as like T-NIL, but the resin used is UV curable. The property of the UV curable resin is that initially it is in liquid state which is then hardened and cross-linked by exposing it to UV radiation. In this process, the mold is pressed onto the resin and then it is cured by UV radiation. Later mold is separated from the resin leaving back the features onto the resin which is then cleaned to remove any residuals. Positive aspects of this method are that it can be performed at room temperature and with low imprint pressure, so the alignment accuracy is better. Below Figure 2.3 shows the cancer cell replica obtained through the UV imprint technique (Truskett and Watts, 2006, Vratzov et al., 2003, Wendel et al., 1994). Image showing the AFM imprint images of Ishikawa endometrial cancer cells (Nock et al., 2010). Cell morphology details are clearly visible and patterned. Features like nucleus and cytoskeleton are visible. Cell morphology details at lower and higher magnification is showed.

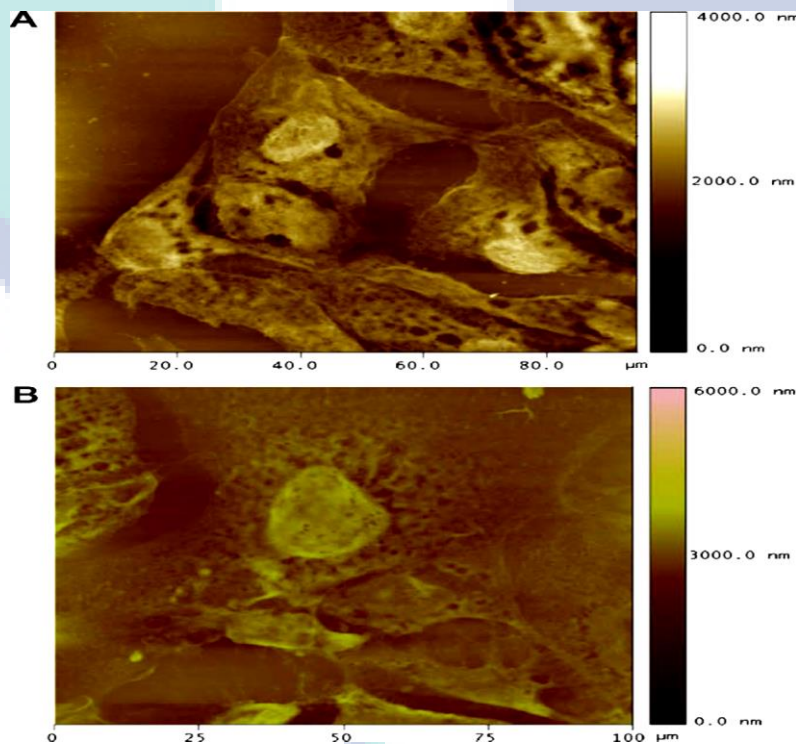


**Figure 2.3** AFM imprint images

Image source: Nock et al., (2010)

### 2.3.1.3 Step and flash imprint lithography (SFIL)

SFIL uses a low viscosity, photo-curable, organosilicon liquid. The template used in this is transparent, rigid so that it allows layer-to-layer alignment. High throughput, low cost, no projection optics and operation at room temperature is the main advantages of the SFIL. Repeated use per wafer decreases stamp lifetime. In Figure 2.5 the process is clearly explained. In this process, a template is created on a standard mask blank by using the patterned chromium as an etch mask to produce high-resolution relief images in the quartz. The etched template and a substrate that has been coated with an organic planarization layer are brought into close proximity. A low-viscosity, photopolymerizable formulation containing organosilicon precursors is introduced into the gap between the two surfaces. The template is then brought into contact with the substrate. The solution that is trapped in the relief structures of the template is photo polymerized by exposure through the backside of the quartz template. The template is separated from the substrate, leaving a UV-cured replica of the relief structure on the planarization layer. Features smaller than 60 nm in size have been reliably produced using this imprinting process. If the process is not carried out carefully, then it can produce defects in a propagating manner as shown in Figure 2.5 (Bailey et al., 2001, Bailey et al., 2002).

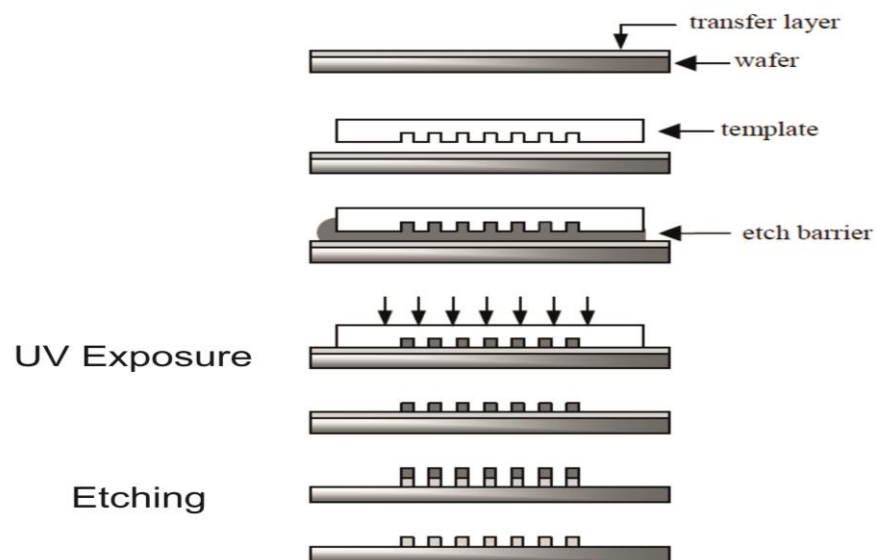


**Figure 2.4 Step and flash imprinting process**

Image source: Bailey et al., (2001). Image showing Step and Flash Imprinting Process,

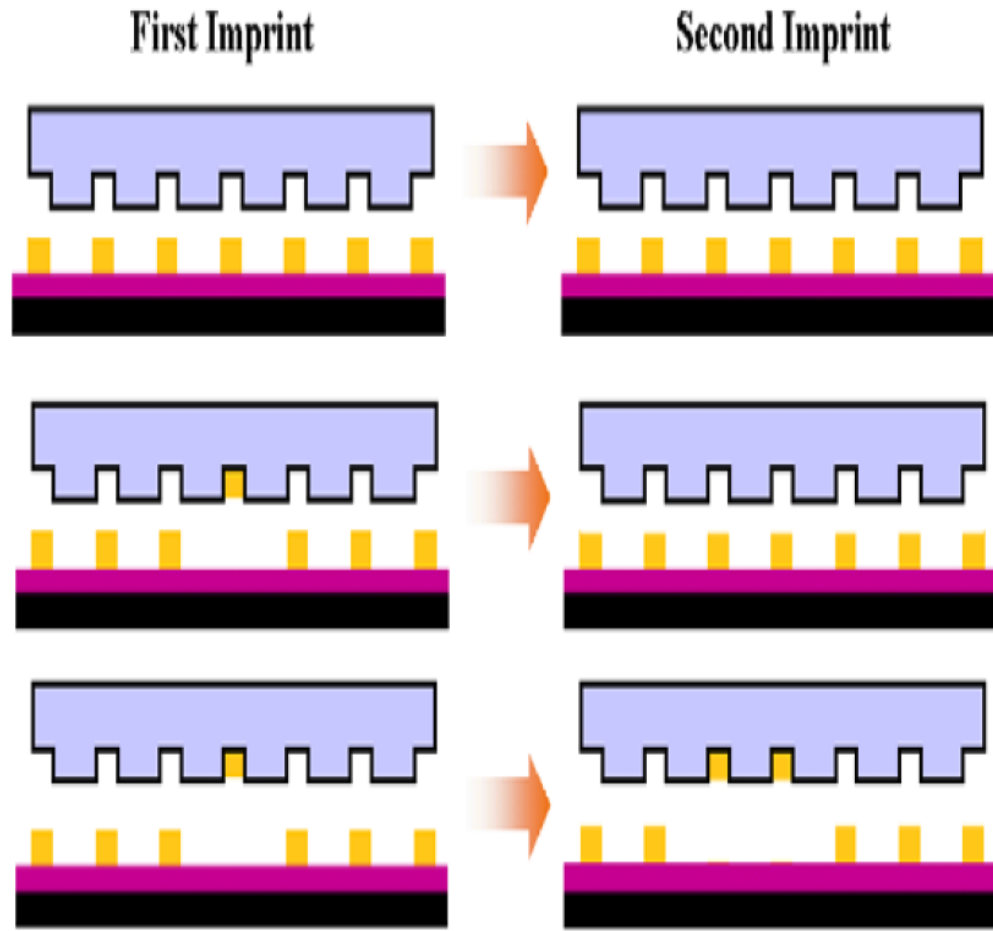


**Figure 2.5 Step and flash imprinting process**

Image source: Bailey et al., (2001). Image showing hypotheses for defect generation and propagation in SFIL Process.

#### 2.3.1.4 Step and stamp imprint lithography (SSIL)

In this technique, a stamp is pressed on to the polymer for creating the imprints. The stamp is lifted and pressed next to create more imprints. And the process is repeated to produce more of same imprints. Alignment of stamp to already existing features on the substrate makes it possible to use SSIL together with UV lithography for mix and match (Torres, 2003). Figure 2.6 shows the consecutive steps involved in the fabrication. The image shows the step by step process involved in SSIL.

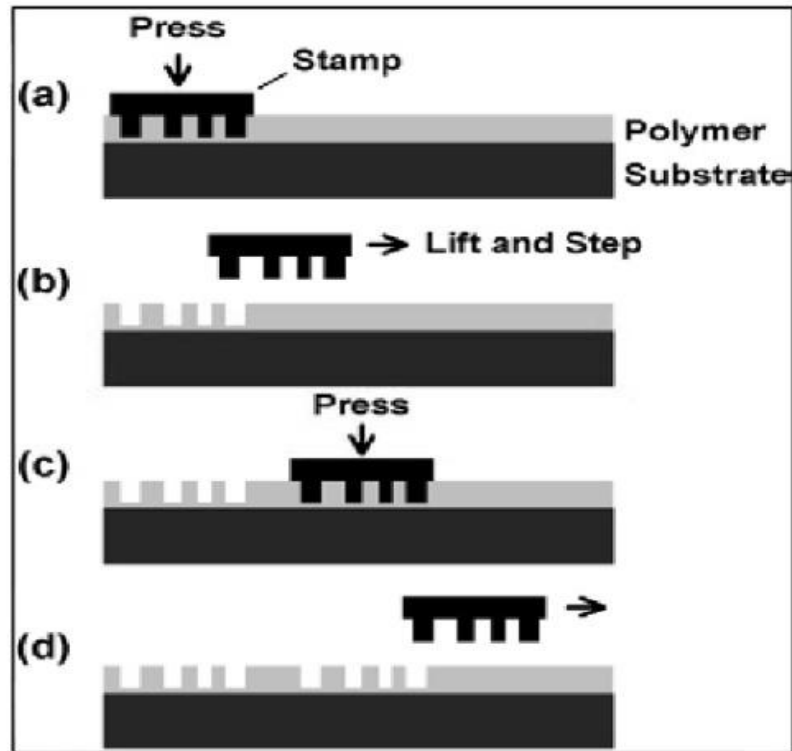


**Figure 2.6 Step and Stamp Imprinting Process**

Image source: Torres, (2003)

### 2.3.1.5 Laser assisted direct imprinting

In this method, imprints are made directly with the use of lasers. Process illustration of the method is shown in Figure 2.7. The quartz moulds were diced to fit within the excimer laser beam area, ensuring that all the silicon beneath the mould melts during (Laser Assisted Direct Imprinting) LADI. Then the pressure between the mould and silicon wafer were applied by sandwiching them between two large press plates. The mould is placed above the silicon wafer. Mould is made of fused quartz and hence transparent to the laser beam. Based on the reflectivity of the silicon, the process monitored. When silicon melts, it changes from a semiconductor to a metal, hence its surface reflectivity to visible light increases (Chou et al., 2002, Janes et al., 2013, Kim et al., 2012, Lee et al., 2012).

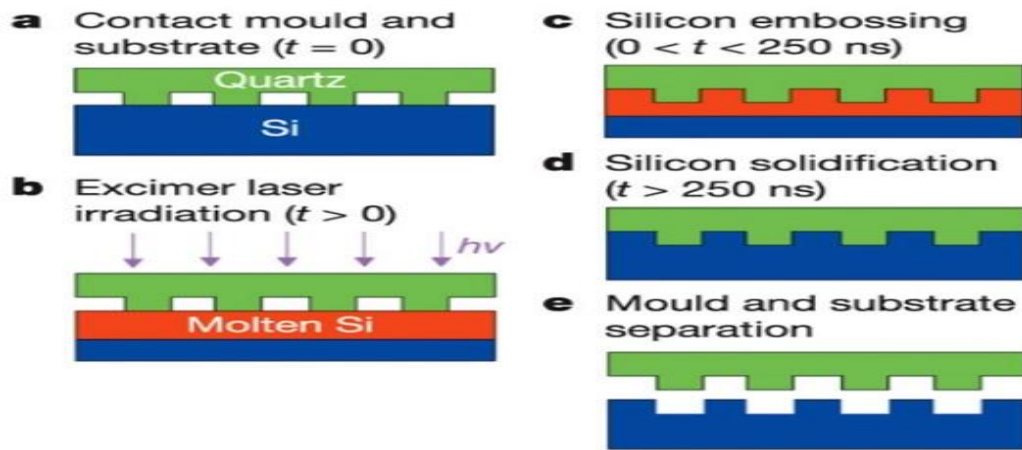


**Figure 2.7 LADI Process**

Image source: Chou et al., (2002). Image showing the series of steps involved in LADI process.

### 2.3.2 Approaches for the fabrication of cell imprint replica

When it comes to imprinting cells, the imprinting process should not damage the cells, as cells are delicate and needs to be handled carefully. From the literature search, material and method used for the fabrication of direct negative cell imprint replica are summarized in Table 2.1. Generally for polymer composites, it can be clearly seen from Figure 2.8, that after the percolation threshold ( $p_c$ ), resistivity dropped drastically.

**Table 2.1 Material and process used for cell imprint fabrication**

S.No.	Material	Process	Ref.
1	PDMS	Thermal Curing	(Muys et al., 2006a)
2	Photopolymer	UV curing	(Samsuri et al., 2010)
4	Poly(urethane acrylate) (PUA)	UV	(Lee et al., 2014)
5	Methylsilane and peroxide	CVD Process	(Pfluger et al., 2012)
6	Parylene	CVD Process	(Koppes et al., 2016)

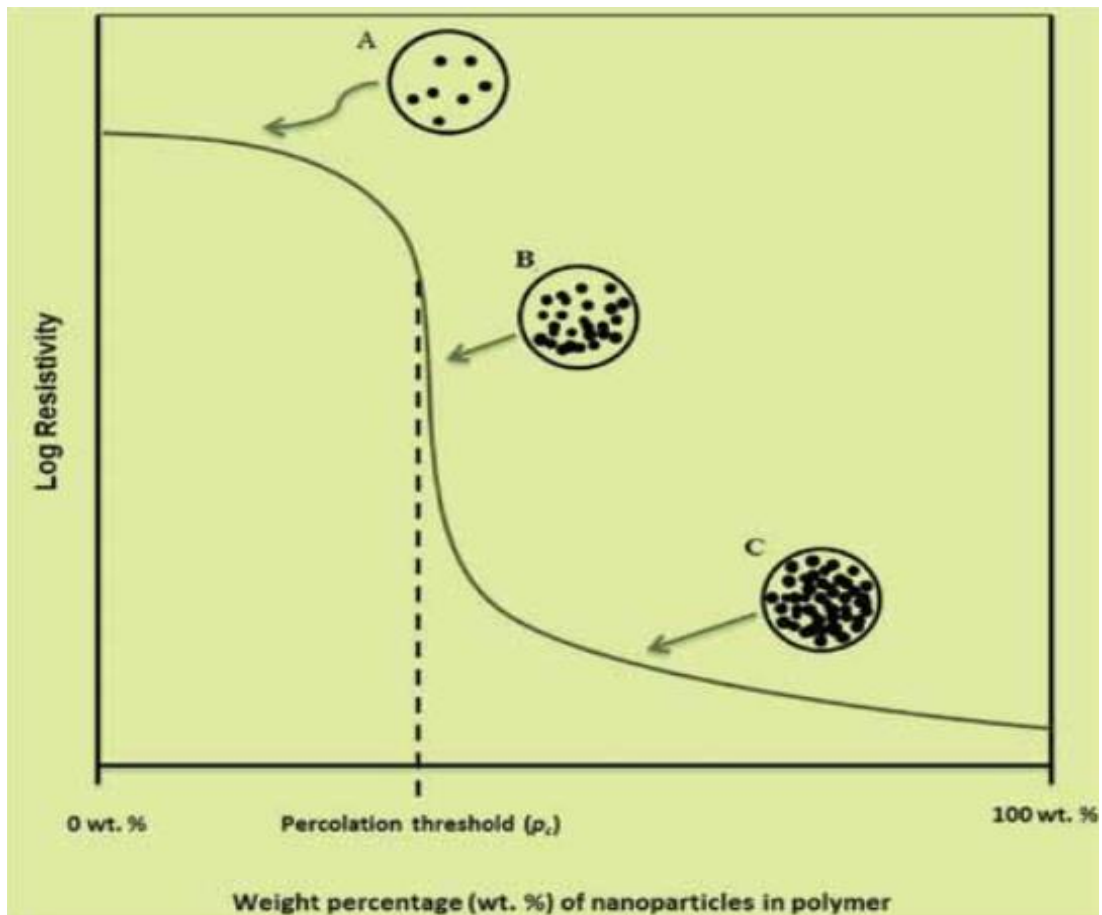


**Figure 2.8 Loading conductive filler wt. % vs conductivity**

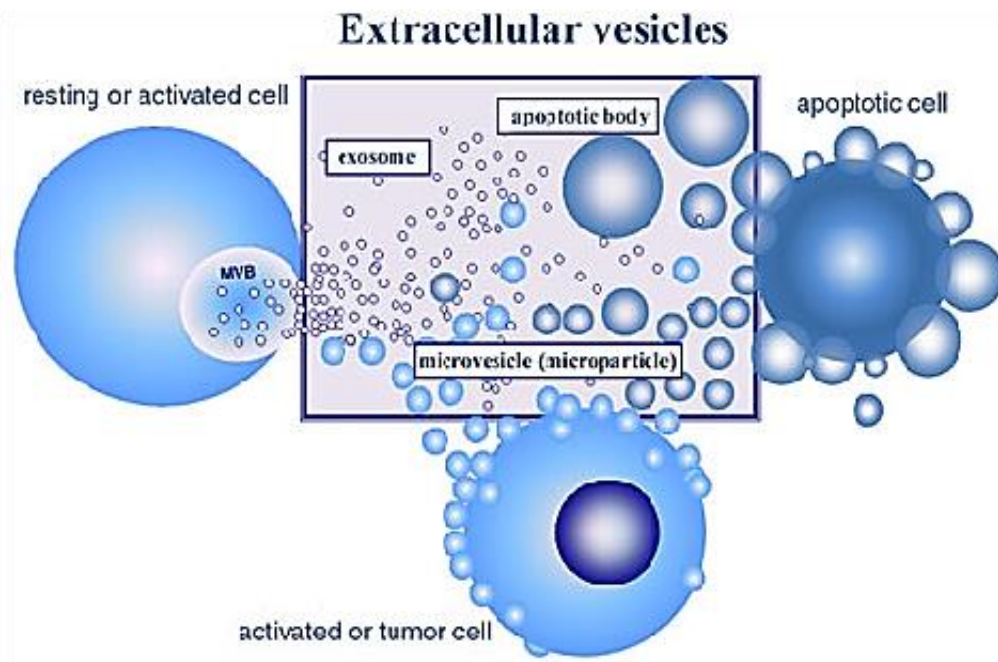
Image source: Khosla, (2012). Image shows the change in resistivity with respect to the loading of the filler wt. %.

UV-NIL has established itself as a promising alternative for imprinting cell when compared to other methods, as it can be performed at room temperature, rapid curing and low pressure conditions with better feature transfer which adds to its merits.

#### **2.4 Cell imprint lithography for cell diagnosis at sub single cell scale level**

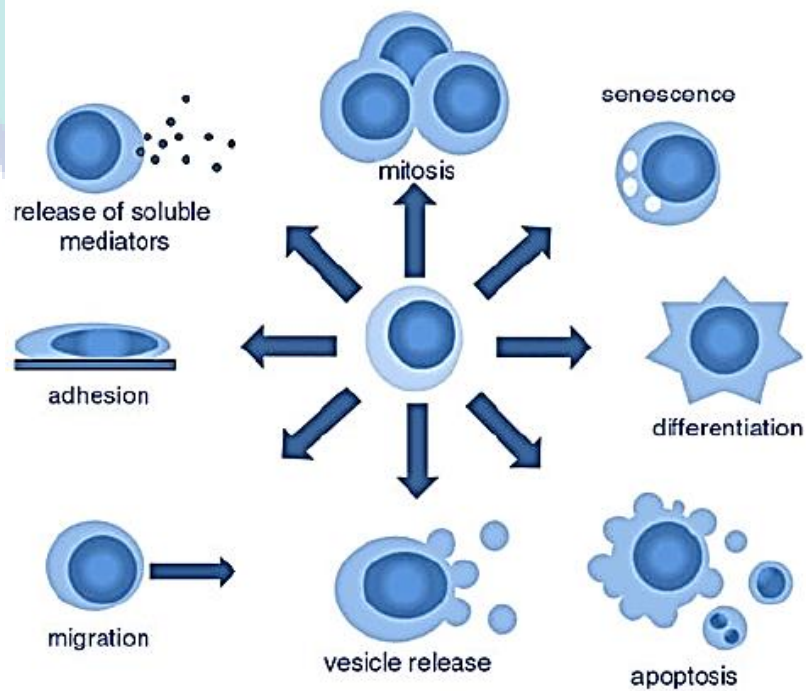
Subtle cell morphology features relating to cellular process are shown below in Figure 2.9, Figure 2.10 and Figure 2.11 (György et al., 2011). Some of the subtle cell morphology features include micro-vesicles, blebs, and apoptotic bodies. Key features of the membrane vesicle population are described with detail in Table 2.2 (György et al., 2011).





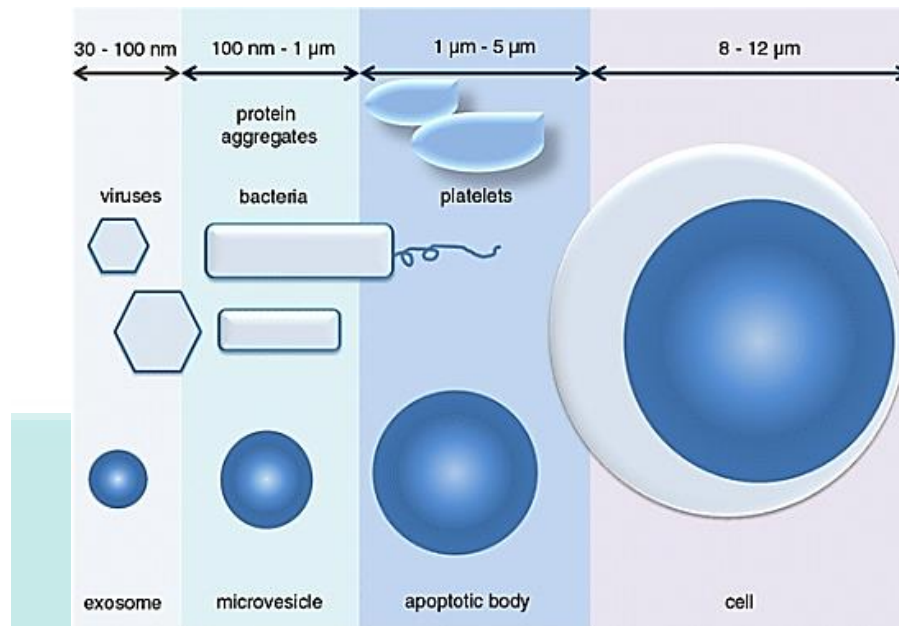
**Figure 2.9** Schematic representation of the extracellular vesicles

Image source: György et al., (2011)



**Figure 2.10** Summary of some adaptive cellular responses

Image source: György et al., (2011)



**Figure 2.11** Size ranges of major types of membrane vesicles

Image source: György et al., (2011)

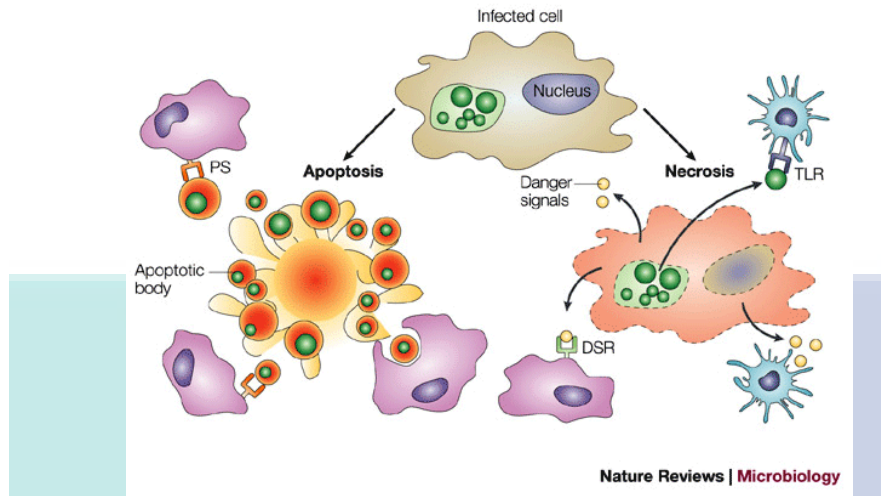
**Table 2.2** Key features of membrane vesicle populations

Source: György et al., (2011)

	Exosomes	Microvesicles	Apoptotic bodies
Size range	Approximately 50–100 nm	100–1,000 nm (~ 100–400 nm in blood plasma)	1–5 μm
Mechanism of generation	By exocytosis of MVBs	By budding/blebbing of the plasma membrane	By release from blebs of cells undergoing apoptosis
Isolation	Differential centrifugation and sucrose gradient ultracentrifugation 100,000–200,000g, vesicle density is 1.13–1.19 g/mL	Differential centrifugation 18,000–20,000g	Established protocols are essentially lacking; most studies use co-culture with apoptotic cells instead of isolating apoptotic bodies
Detection	TEM, western blotting, mass spectrometry, flow cytometry (bead coupled)	Flow cytometry, capture based assays	Flow cytometry
Best characterized cellular sources	Immune cells and tumors	Platelets, red blood cells and endothelial cells	Cell lines
Markers	Annexin V binding, CD63, CD81, CD9, LAMP1 and TSG101	Annexin V binding, tissue factor and cell-specific markers	Annexin V binding, DNA content

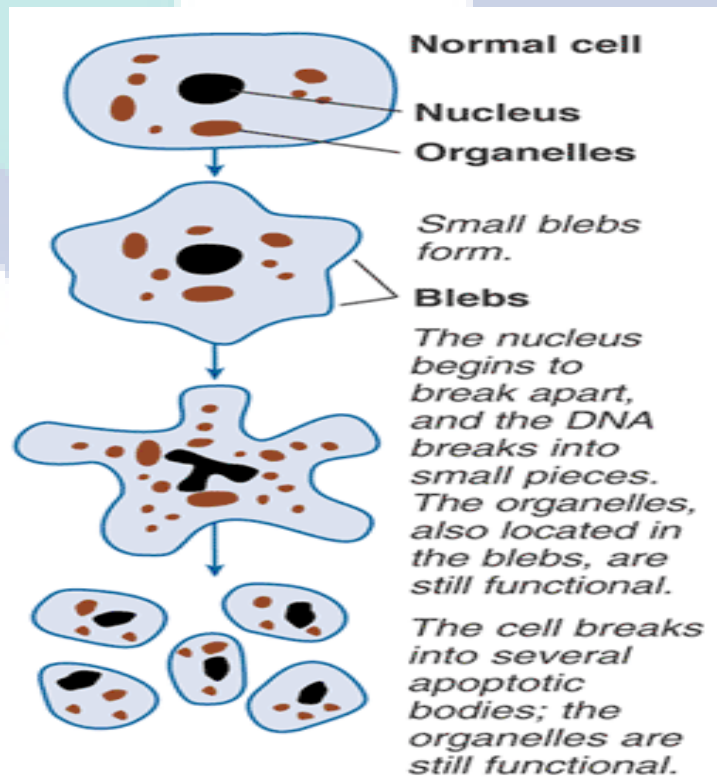
For decades, many previous investigations had demonstrated many types of cell death, including apoptosis, autophagy, paraptosis, oncosis or necrosis (Van Cruchten & Van den Broeck, 2002). Illustration of cell death process is showed in Figure 2.12 (Byrne and Ojcius, 2004). Figure 2.13 (Neuman, 2003) shows phases of apoptosis from early to

late apoptosis. Thus, precise differentiation in identifying types of death involving cell morphology is much needed for cancer therapy and drug delivery applications.



**Figure 2.12 Morphology of necrosis and apoptosis**

Image source: Byrne and Ojcius, (2004)



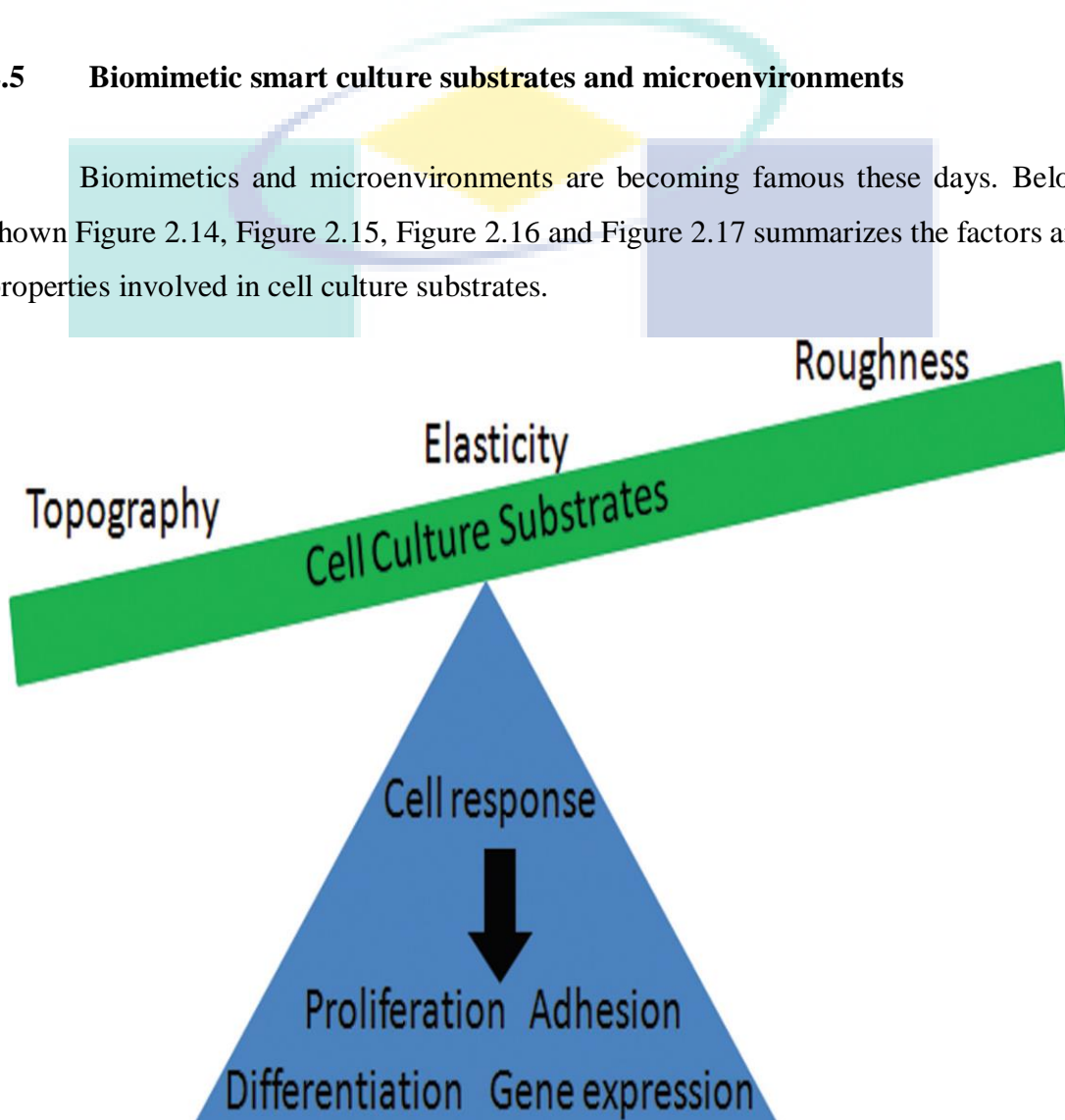
**Figure 2.13 Schematic representation of apoptosis process**

Image source: Neuman, (2003)

When these cellular process and morphological features are correlated with high resolution imaging along with conventional detection methods, they can pave way in better understanding of the complex process.

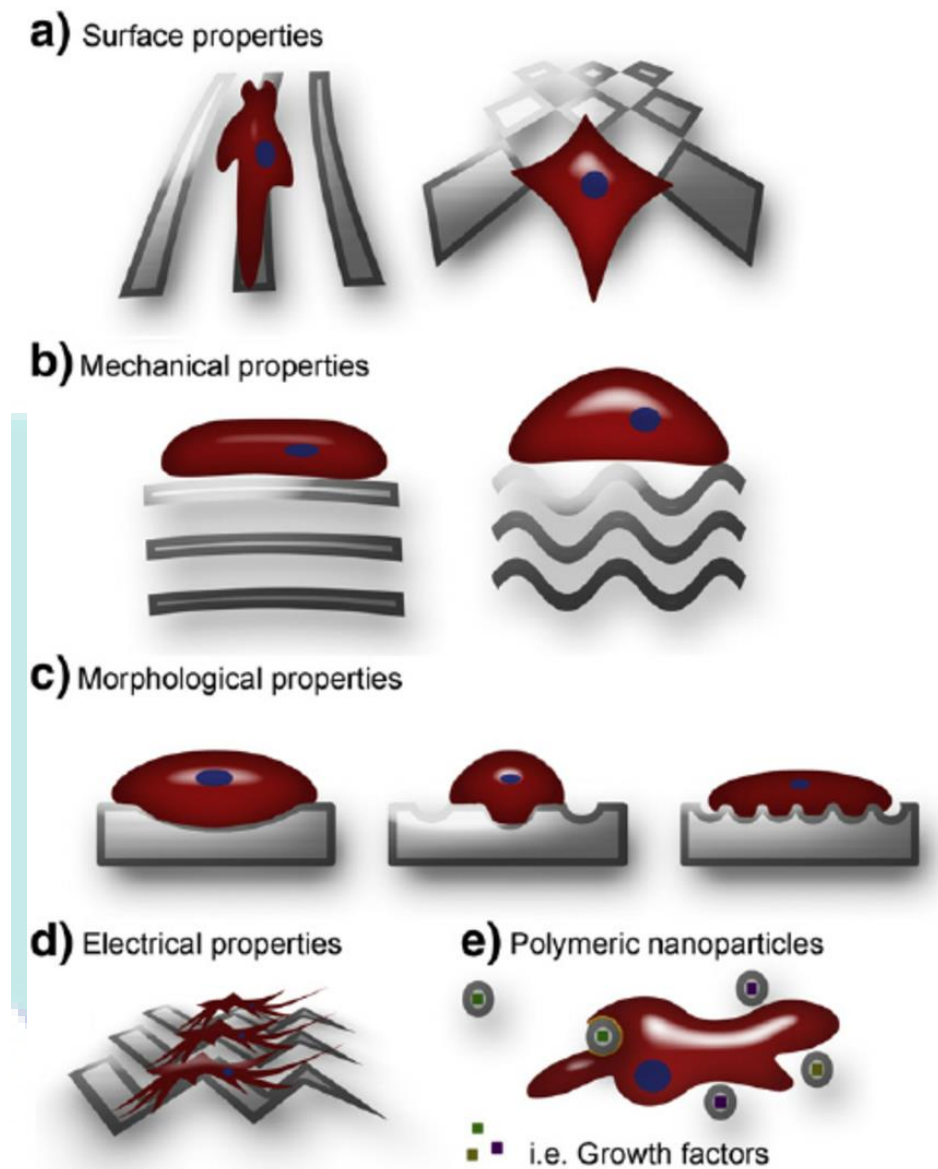
## 2.5 Biomimetic smart culture substrates and microenvironments

Biomimetics and microenvironments are becoming famous these days. Below shown Figure 2.14, Figure 2.15, Figure 2.16 and Figure 2.17 summarizes the factors and properties involved in cell culture substrates.



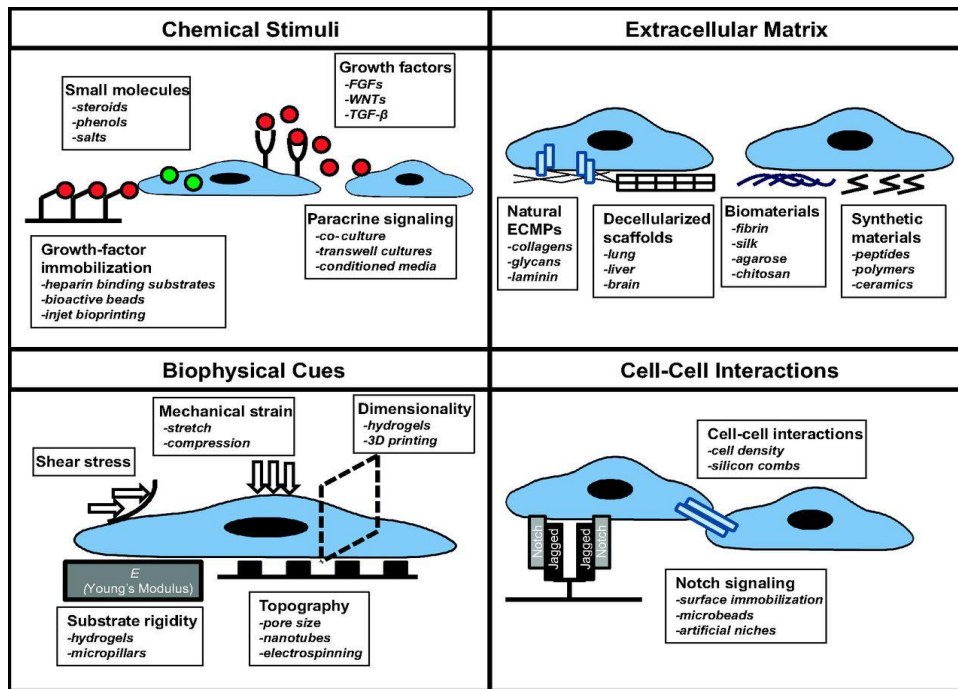
**Figure 2.14** Factors involved in cell culture substrates

Image source: Ross et al., (2012). Image showing some of the key factors which play major roles in cell culture substrates.



**Figure 2.15 Cell culture scaffold properties**

Image source: Martino et al., (2012). Image shows various properties of cell culture scaffold, which plays significant role in biomaterial research field. a) Surface properties. The surface topography could drive cell adhesion, proliferation, migration and differentiation. b) Mechanical properties. Cells respond to the mechanical properties of the substrate on which they are growing, thus changing their fate. c) Morphological properties. Scaffold morphologies for cell biomaterial interaction may vary in terms of interconnectivity, pore-size and shape. d) Electrical properties. Electrical properties of the substrates are important issues in biomaterial-cell interaction. e) Polymeric nanoparticles.



**Figure 2.16 Approaches in cell microenvironment**

Image source: Brafman, (2013)

Image showing engineering approaches used to study the cell microenvironment. Engineers are applying several novel approaches to dissect each of these components and understand how each regulates the cell behavior.

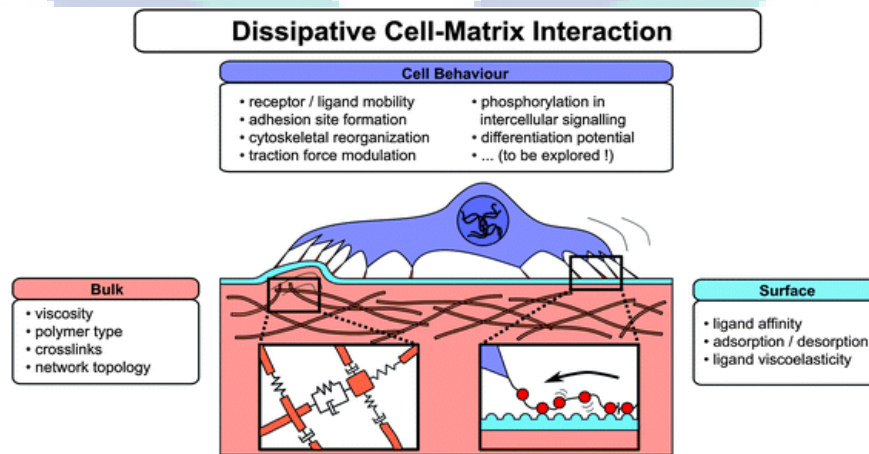
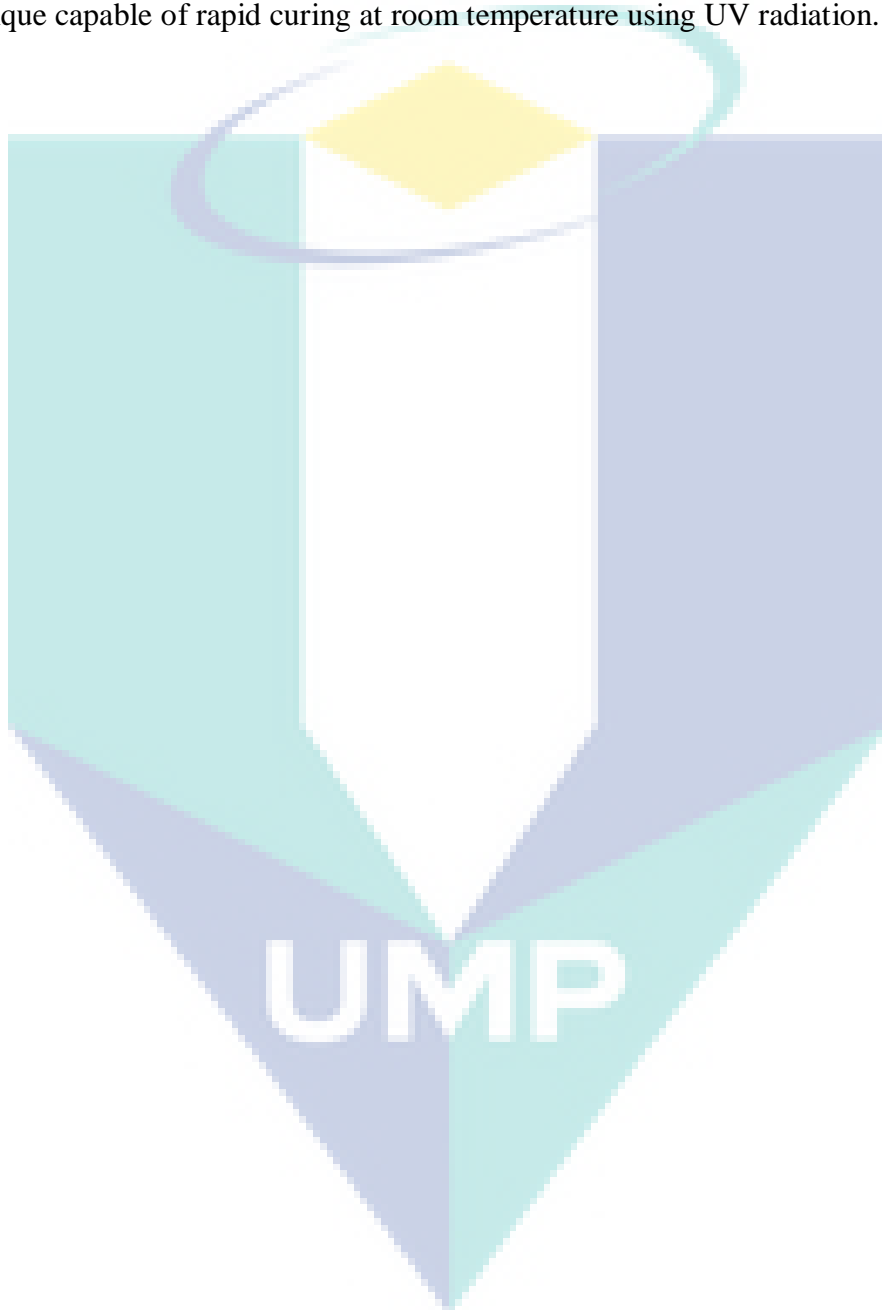


**Figure 2.17 Matrix-cell interactants**

Image source: Müller et al., (2013). Image showing the overview of material parameters that allow the incorporation of dissipative contributions in matrix–cell interactions leading to a distinct cell reaction.

## 2.6 Chapter summary

From the literature study, it can be concluded that the investigation of nanoparticle based composite cell imprint replica fabrication process was not reported. Herein the author introduced a novel superconductive carbon photo polymer composite and process technique capable of rapid curing at room temperature using UV radiation.



## CHAPTER 3

### PASSIVE HYDRODYNAMIC MICROFLUIDIC BIOCHIP PLATFORM FOR SINGLE CELL ANALYSIS

#### 3.1 Overview

Recently researches are focused to and being carried out in the development of new passive microfluidics and biochips for single cell analysis. Current direction is to analyze and focus on each specific single cell for better understanding of its insights.

#### 3.2 Microfluidic biochip platforms for single cell trapping

In order to create an imprint replica of single cells for single cell morphology analysis, researchers have incorporated a combined method of the imprint replica with microfluidic biochip platform (Nock et al., 2011, Alkaisi et al., 2007). Single cell investigation acts as the fuel to drive research in many spheres such as pharmaceutical, biology, health-care, etc. (El-Ali et al., 2006, Dittrich et al., 2006). The problems associated with conventional techniques such as cell sampling from a cultured population are multifold. The intricacies of these methods are the time involved to perform the analysis, the accuracy of the results and the homogeneity of the samples selected are some of the challenging that needs to be addressed. Certain solutions to bypass the above mentioned problems themselves are complicated or are associated with a subset of difficulties. For example, calculating mean responses from a population could lead to an erroneous result, but analyzing a single cell could yield far better results. Previous studies related to cell are conducted using large populations of cells and these measurements reflect only the average values of the cell response. This approach can be a source of misinterpretation as it ignores the statistical nature of many cellular events (Johann, 2006). Therefore, to overcome these drawbacks researchers are currently moving towards single cell analysis (SCA) method for analyzing the cells individually. This would lead



to a more accurate representation of cell-to-cell variations instead of the conventional method where the average is masked by bulk measurements. Ascendancy of using SCA is due to the fact that it will reduce biological noise from the target cell population, as each and every cell has different protein level and gene expressions (Fan et al., 2010). Moreover, each cell exhibits different cell cycle stages and therefore the cell metabolism may respond to slight variations towards external chemical, physical, or mechanical environments (Dittrich and Jakubowski, 2014). In addition to that SCA facilitates rare cells or events, scarce, precious sample and single-cell precision in populations. Single cells have been studied since the invention of the microscope. However, in recent years, due to the development of sophisticated fabrication technologies, increase of the sensitivity of many analytical instruments in the cell and fluid handling are attributed to the microfluidics technology has pushed the field of SCA to an advanced level. Figure 3.1 shows the trends and statistics on SCA. Applications involved in the SCA are shown in Figure 3.2.

### Publications on Single Cell Analysis

■ SCA (1980-2004) ■ SCA (2005-2016)

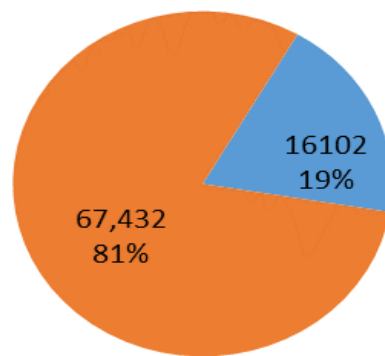


**Figure 3.1 Publications trend on single cell analysis**

A literature search was performed using Web of Science (provided by Thomson Reuters) to determine the number of publications on single cell analysis. Topic search was carried out for the term “single cell analysis\*”. To see the trends, search was made during two sets of time span (1984-2004) and (2005-2016). Statistics show that the number of publications was increased to several folds when compared to previous decades.

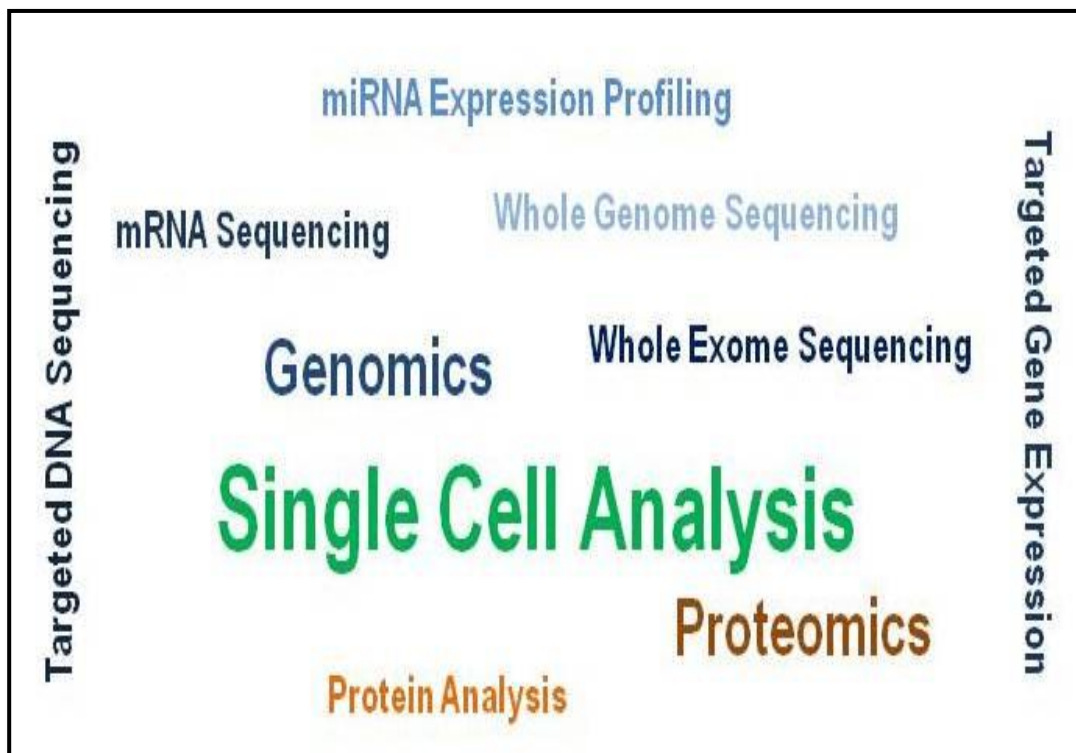


**Figure 3.2 Applications of SCA**

Word crowd shows some of the most common applications of single cell analysis. Some of the current key players in the market, for SCA are 10X Genomics (US), Accelerate Diagnostics, Inc. (US), Advanced Cell Diagnostics, Inc. (US), Affymetrix Inc (US), Agilent Technologies Inc. (US), Amphasys AG (Switzerland), Angle Plc (UK), Beckman Coulter, Inc. (US), Becton, Dickinson and Company (US), Bio-Rad Laboratories, Inc. (US), Clontech Laboratories, Inc. (US), Celsee Diagnostics (US), Enumeral (US), Epic Sciences (US), Fluidigm (US), Illumina, Inc. (US), Kellbenx Inc. (US), Merck KGaA (Germany), NanoString technologies (US), Qiagen NV (Netherlands), Sigma Aldrich (US), Thermo Fisher Scientific Inc. (US), Wafergen Bio-Systems Inc. (US), Yikon Genomics (China) and Zephyrus Biosciences Inc. (US).

To carry out single cell investigations, first single cells are required to be trapped and isolated. Some conventional methods such as usage of microscopes and patch-clamp have disadvantages like inability for single cell assays and high skill level requirement.

Even if the shortcomings are overcome the throughput of these methods are low. Microfluidics has come out as a powerful tool to study the complexities of cells (Whitesides, 2006). The micro level dimensions of flow channels used in biochips are the size of cells (Whitesides, 2006). It caters to every need of research and delivers accurate results. Apart from the quality of results, reduction in time, savings in space, reagents and small sample volumes involved (order of micro litres) are some of the remarkable discoveries made using microfluidics (Fan et al., 2010).

### **3.2.1 Techniques**

Several approaches were applied in microfluidics facilitating single cell trapping which can be broadly classified into contact based approach and contact less approach. Different cell trapping methods are hydrodynamic trapping, dielectrophoresis trapping, chemical trapping, gel trapping, magnetic trapping, acoustic trapping and laser trapping. Each method has its own merits and demerits. Figure 3.3 shows the diverse approaches involved in single cell trapping techniques and Table 3.1 (Lo and Yao, 2015) enlists each methods pros and cons. Mostly the process requires auxiliary equipment/facilities like a pump or a pressure-controlling system for fluid introduction and guidance, and some need specialized electronic or optical equipment which are not generally in a common medical or biological laboratory and induce extra obstacles for operation. The auxiliary parts occupy much space and thereby greatly lower the area density of single-cell arrays. Design structures of many microfluidic chips are complicated due to the need for multiple layers, channels, and valves, which are difficult to be fabricated and/or manipulated (Ferlay et al., 2015, Fujita et al., 2015, Eyer et al., 2012). Thus the practical applications in clinics or general biological laboratories are limited due to these drawbacks. (Nilsson et al., 2009) Increasing demand for trapping based on the design itself, involving unsophisticated basic laboratory instruments for single cell measurements led to the evolution of hydrodynamic trapping technique. This way, cells which may be affected due to the presence of an external field/ force are preserved in an unaffected form. Apart from the simplicity of the process, the natural state of the separated particles can be useful in many researches.

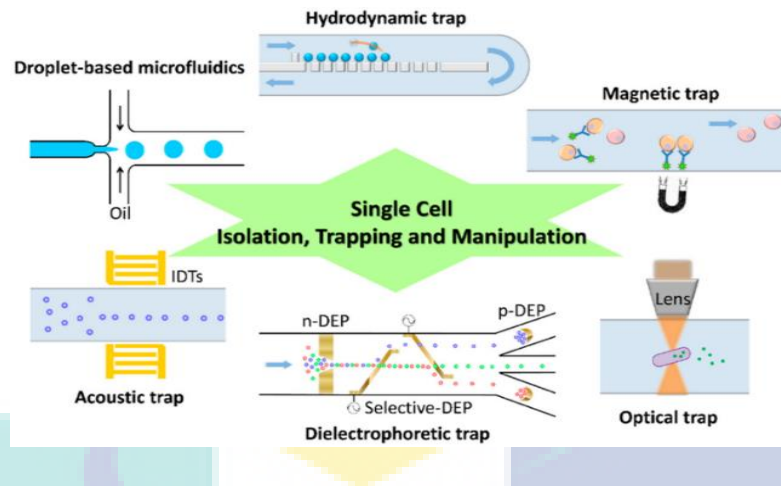


**Figure 3.3 Diverse approaches for single cell trapping**

Image source: Lo and Yao, (2015)

**Table 3.1 Comparison of various microfluidic techniques for single-cell trapping**

Source: Lo and Yao, (2015)

Approaches	Main Applications	Major Advantage	Major Disadvantage
Droplet-based microfluidics	<ul style="list-style-type: none"> <li>• Single cell isolation</li> <li>• Cell culture in droplet</li> </ul>	High throughput screening for specific single-cells	Challenge to encapsulate single-cells in each droplet
Hydrodynamic trap	<ul style="list-style-type: none"> <li>• Single cell isolation</li> <li>• Cell culture on chip</li> </ul>	Multifunction in one device	Complicated fabricating process
Magnetic trap	<ul style="list-style-type: none"> <li>• Specific cell trapping</li> </ul>	Efficient trapping of labeled cells	Requires antibodies or primers for magnetic label
Acoustic trap	<ul style="list-style-type: none"> <li>• Cell manipulation</li> </ul>	Good for cell positioning	May have negative effect to cells
Dielectrophoretic trap	<ul style="list-style-type: none"> <li>• Cell manipulation</li> <li>• Cell selection</li> </ul>	Easily select target cells via alternating frequency of AC	Heat problem during long-term manipulation
Optical trap	<ul style="list-style-type: none"> <li>• Cell manipulation</li> <li>• Cell mechanics</li> </ul>	Applicable in many fields of study	Requires expensive optical system

### 3.2.2 Hydrodynamic trapping

Hydrodynamic trapping is a method which utilizes mechanical barriers or obstructions to separate the target particle from the main flow. Once separated, the target particles are retained in hydrodynamic trapping sites where it could be of for various investigations. Typical particle screening structures include walls or pores. Arrays consisting of the pattern of trapping site could be made to capture single cells. The advances in research technologies during the past decade resulted in the development of various microfluidics systems for single cell trapping and its applications.

Changqing Yi et al. published a short review on the applications of microfluidic devices for cell-based assays over the years (2002–2005) (Carpenter et al., 2006). Kim et al., (Kim et al., 2008) has published a review with a focus on the microfluidic systems that are combined with physical micro/nanostructures or a topographically patterned substrate for cell research. Nilsson et al., presented a review article which focuses on the different technical approaches for trapping of particles and cells in a microfluidic system (Nilsson et al., 2009). Bhagat et al., has reviewed microfluidics-based cell separation techniques (Bhagat et al., 2010). Burger et al., has summarized the significant progress centrifugal microfluidic platforms for cell removal, filtering, lysis, separation, sorting, encapsulation, trapping, assaying sensing, cytometry and detection (Burger and Ducreé, 2012). In 2013, Karimi et al., presented an overview of the cell/particle sorting techniques using hydrodynamic effects in microchannels (Karimi et al., 2013). Barbaros et al., reviewed some of the manipulation techniques for bio-particles with a comparative study and recent applications (Cetin et al., 2014). Alireza Valizadeh et al., published a review of different approaches in single cell manipulation methods using fluidic systems (Valizadeh and Khosroushahi, 2015). Past decade's developments and updates on microfluidic systems for single cell analysis with an exclusive focus on hydrodynamics based approach are presented below.

In 2005, optimization of cell trapping in micro well for fibroblasts (as a model of adherent cell) and rat basophilic leukemia cells (as a model of non-adherent cell) was demonstrated. The results were able to derive a relation between well depth, well diameter and settle time. Figure 3.4 shows the results for cell trapping correlation with micro well diameter. For high SCC% required settle time was quite high. (Rettig and Folch, 2005).

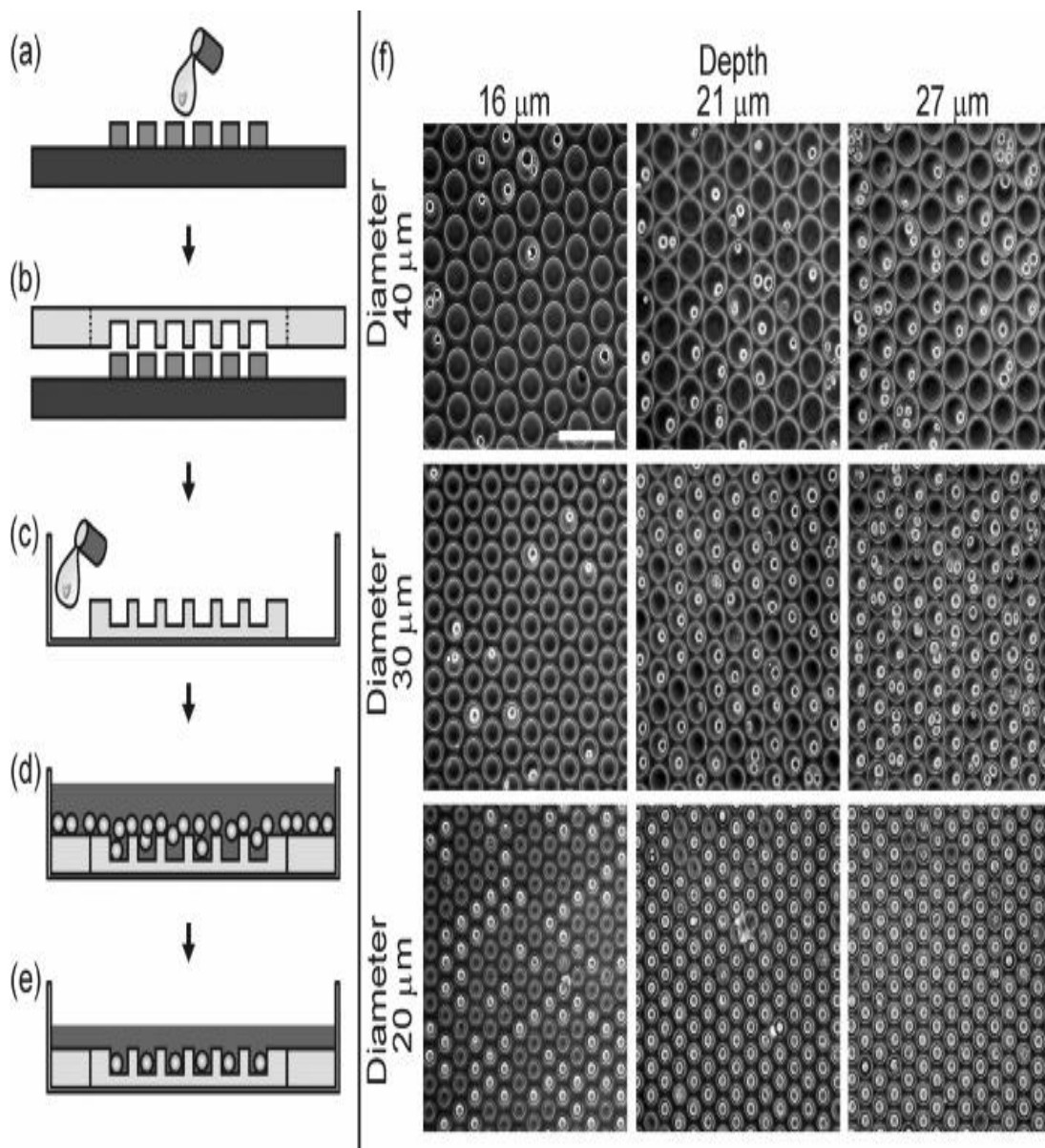


**Figure 3.4 Cell trapping correlation with micro well diameter**

Image source: Rettig and Folch, (2005). Image showing (a-e) Schematics of the fabrication and seeding procedure; (f) all the combinations of three different diameters and three different depths (Note the increase in the total number of trapped single cells as micro well gets deeper (left to right) and narrower (top to bottom)), Scale bar: 100 μm.

In 2006, an outstanding report was made where U-shaped microstructures were utilized to trap single cells. These facilitate the lateral trapping of cells. Figure 3.5 shows the cell trapping arrays and designs involved (Di Carlo et al., 2006).

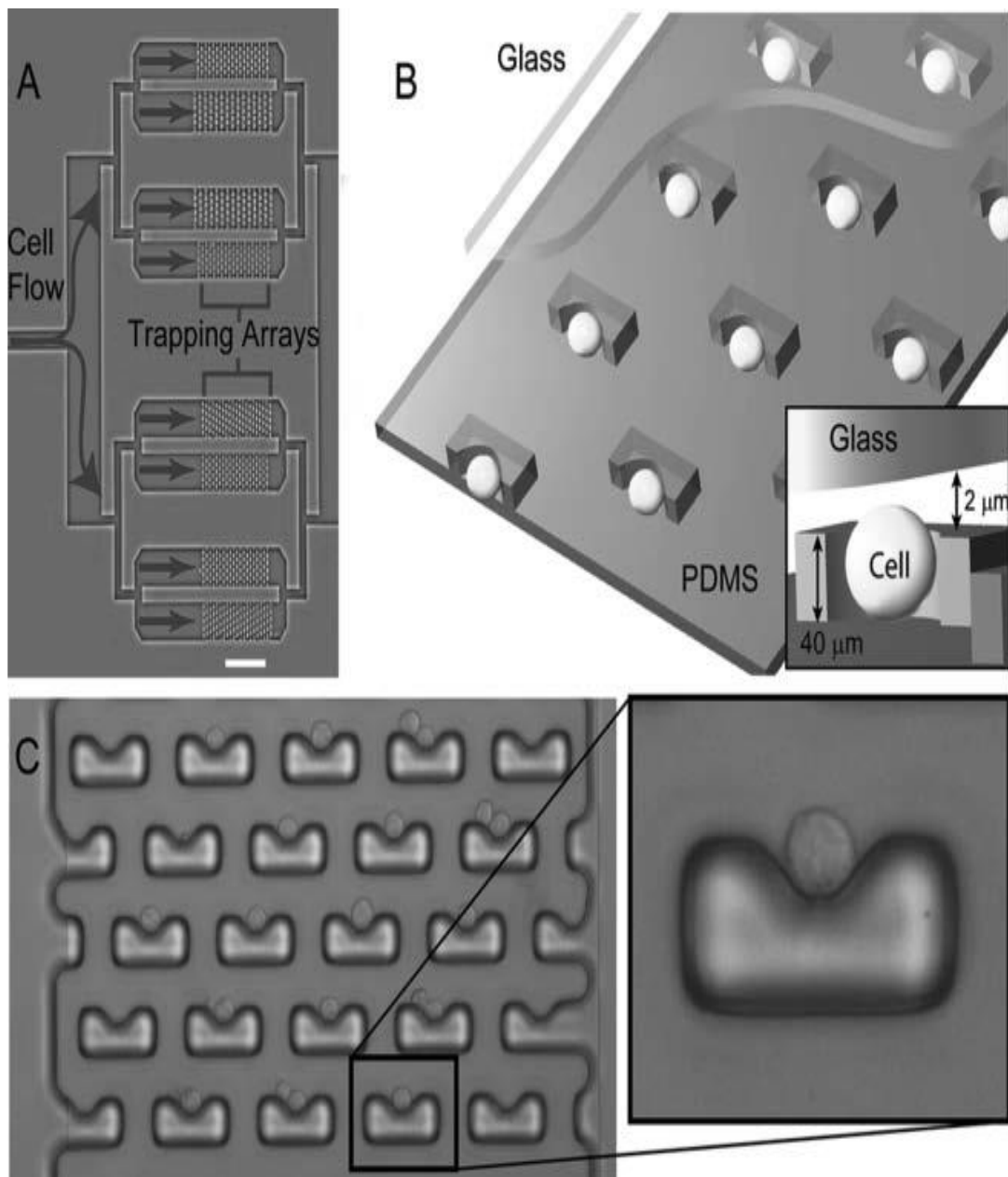
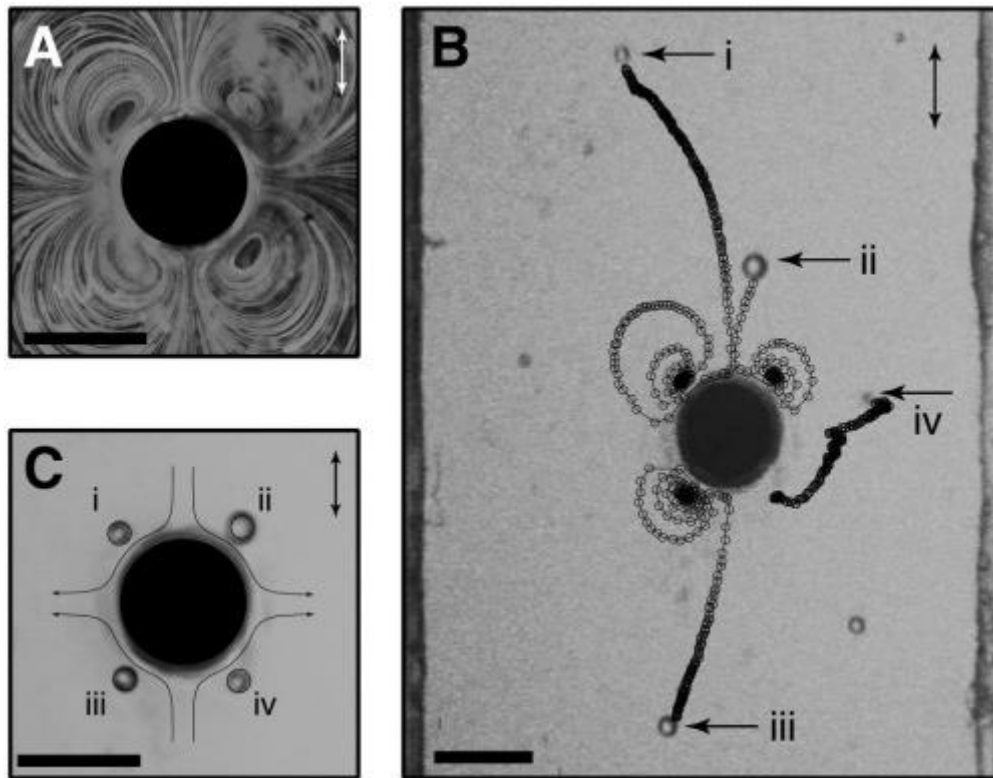


**Figure 3.5 Cell trapping in array of traps**

Image source: Di Carlo et al., (2006). (A) A photograph of the cell trapping device with arrays of traps, scale bar: 500 μm; (B) A diagram of the device and the mechanism of trapping presented, (C) A high resolution bright field micrograph of the trapping array with trapped cells shown.

Hydrodynamic based tweezers for non-contact trapping of single cells using steady streaming micro eddies was demonstrated in 2006. Figure 3.6 shows the non-contact trapping of cells. It involves the steady streaming eddies created from audible

frequency oscillations in the trapping process. Precise trapping of single cells were uncertain (Lutz et al., 2006).



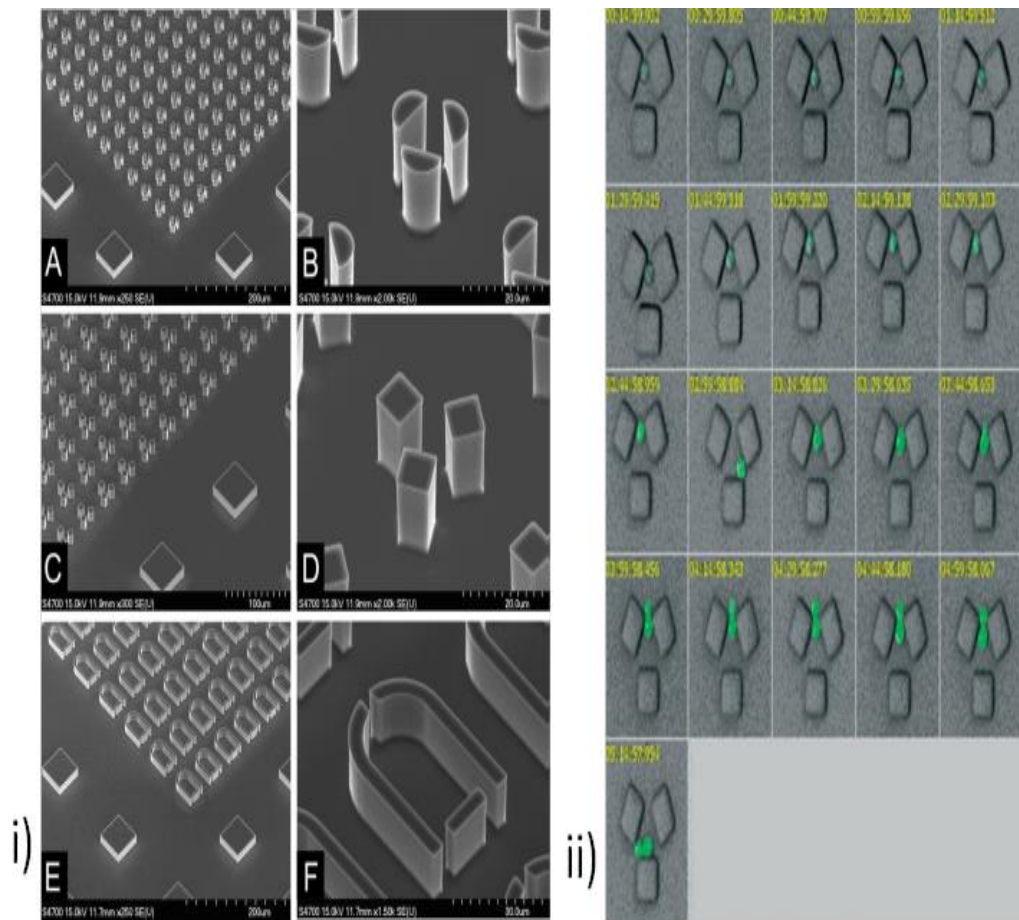
**Figure 3.6 Non-contact trapping of cells using steady streaming micro eddies**

Image source: Lutz et al., (2006). Steady streaming eddies created by audible frequency oscillations collect objects from a channel and trap them at specific locations in three dimensions, (A) Time-exposed image of flow tracer particles showing the formation of four symmetric steady streaming eddies adjacent to the cylinder, (B) Capture trajectories of four polystyrene microspheres. The initial location of each sphere were shown by arrows and number labels, and circles represent their positions at 100 ms intervals, (C) Time-exposed image showing the final trapping location of the four spheres from part B, (Double headed arrows indicate oscillation direction) (Scale bars, 250  $\mu\text{m}$ ).

Microfluidics device that can be used to study the single cell gene expression analysis in *Saccharomyces cerevisiae* was reported by Ryley and Smith (Ryley and Pereira-Smith, 2006). "Jail Bars" were used to confine mother cell into the patterns, which facilitates the escaping of daughter cell to be trapped into another "Jail Bars". Figure 3.7 shows the trap designs. Three different jail bar patterns were reported. This system



requires a timing circuit for the media flow to be periodically reversed, as an aid to dislodge the daughter cells (Ryley and Pereira-Smith, 2006).



**Figure 3.7 Array of jail designs for cell trapping**

Image source: Ryley and Pereira-Smith, (2006). Image shows i) Electron micrograph of silicon master for PDMS devices showing various jail designs; ii) Image series from HSP104-GFP heat shock time course (frames were taken 15 min apart).

In 2009, an array of lateral mechanical traps was demonstrated for single cell tumour apoptosis analysis. Over 85% of the hydro-dynamically trapped cells retained their positions during the course of the short-term experiments. Figure 3.8 shows the cell trap array. Trapping efficiency was between 10–20%. System involves a negative pressure driven flow which is controlled by syringe pump (Wlodkowic et al., 2009).

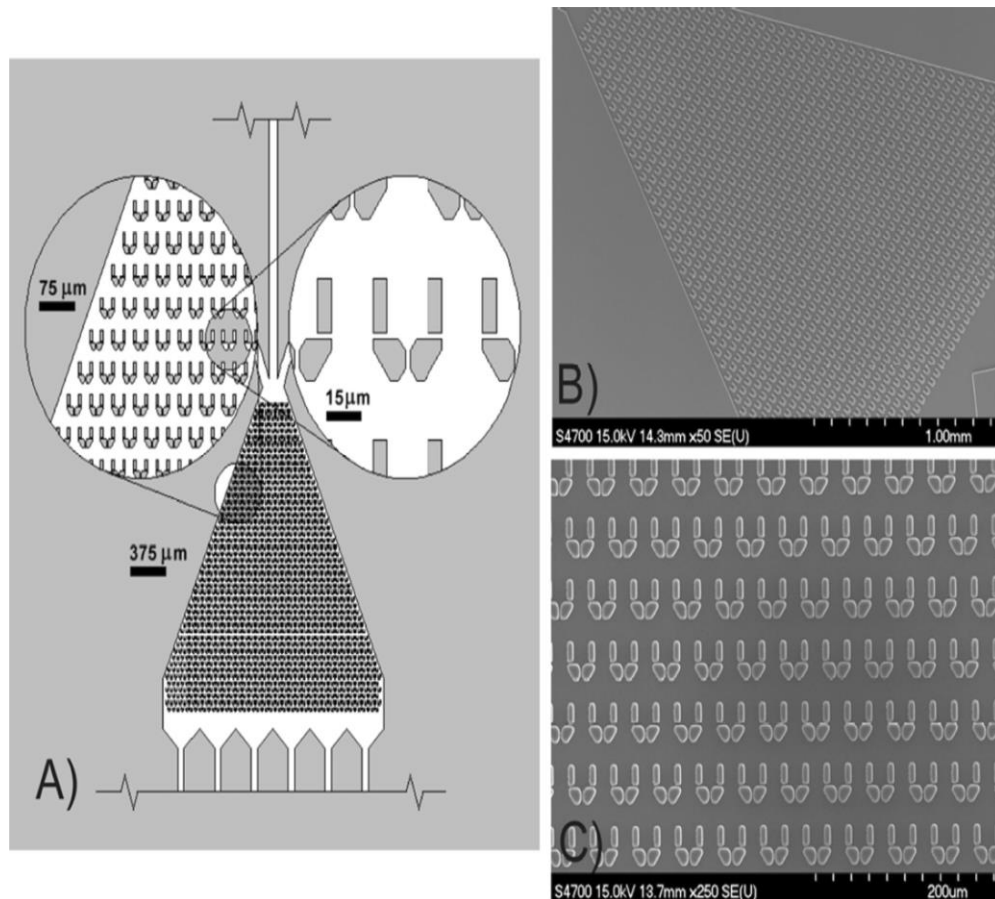


**Figure 3.8 Microfluidic cell array**

Image source: Wlodkowic et al., (2009). Image shows microfluidic live-cell array (A) Chip layout showing a triangular micro culture chamber, containing cell trapping array, (B–C) SEM images of the array of PDMS cell.

In 2010, an automated particle trap based on a stagnation point flow generated in a microfluidic device was reported. The hydrodynamic trap enables confinement and manipulation of single particles in low viscosity (1–10cP) aqueous solution. The trapped micro scale and nano scale particles were of the range (100 nm – 15 μm). Since hydrodynamic traps were created by a planar extensional flow field at the junction of two perpendicular microchannels, damages may be caused to cells (Tanyeri et al., 2010). A novel immuno-bio-sensing device for direct and rapid assessment of the antibody production of each of thousands of living cells being captured in a single slide was published. Each cell was trapped near a designated surface plasmon-resonant nano hole array immuno-biosensor to detect the binding of the cell secreted antibodies to an immobilized target antigen. Arrays of single-cell traps were consisting of concave

hydrodynamic structures and inset micro wells. Functionality of micro well traps were verified by testing, with 5-20 cells/well trapped following a 10 min settling time. Untrapped cells beyond the micro wells are removed via peristaltic pumping, with the minimal trade-off of trapped cell displacement. This system also involves multiple cell trapping. Figure 3.9 shows the hydrodynamic trap (Romanuik et al., 2010).

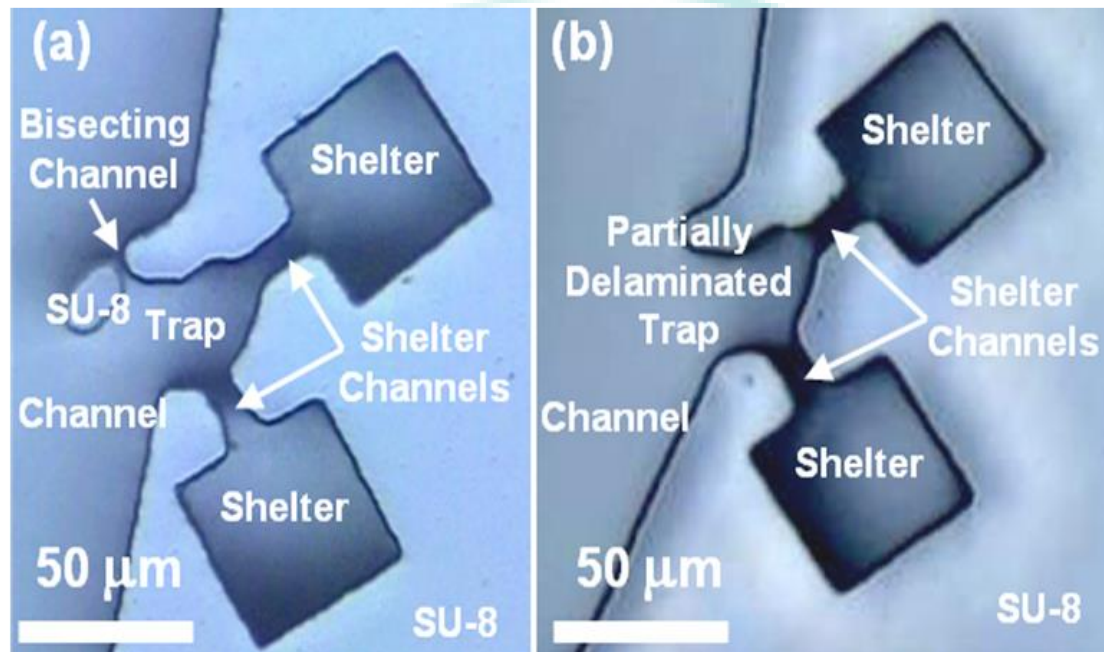


**Figure 3.9 Hydrodynamic cell traps**

Image source: Romanuik et al., 2010). Image showing (a) Hydrodynamic cell traps and nano hole array shelters inset into a SU-8 based spiral, (b) Partial cell trap delamination, due to poor SU-8 adhesion.

Single cell trapping and DNA damage analysis using micro well arrays were developed and reported. This method suits for high throughput DNA damage measurements providing information on multiple lesions and pathways. This method utilizes single cells captured by gravity into a micro well array with DNA damage revealed morphologically by gel electrophoresis. This platform enables high throughput assessment of multiple DNA repair pathways and sub pathways in parallel (Wood et al., 2010). Triangular micro well array capable of cell trapping was reported for short term study and this process involves recirculation system (Park et al., 2010). A microfluidic based single cell trapping for long-term on-chip culture was published. The investigated

biochip facilitates lateral trapping and trapping results are showed in Figure 3.10 (Kobel et al., 2010).

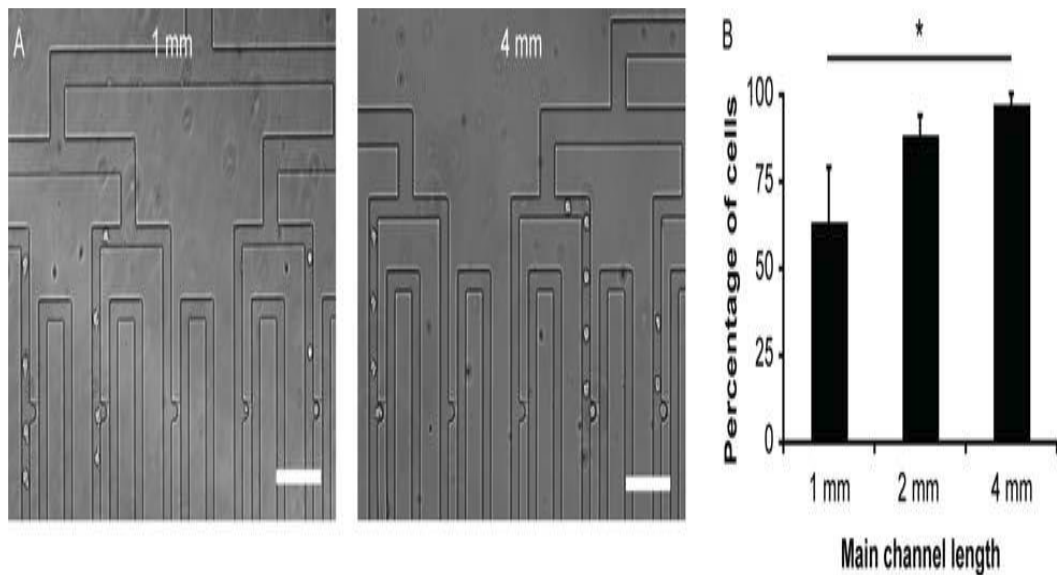


**Figure 3.10 Cell trapping correlation with channel length**

Image source: Kobel et al., (2010). Image showing (A) Overlay of a series of images (taken at a 100 ms interval) of a 1 mm and a 4 mm trap design showing cells missing the trap (1 mm design) and being trapped (4 mm design) (Scale bars are 100  $\mu$ m), (B) Trapping yield for single traps with 1 mm, 2 mm and 4 mm long main channels demonstrating that the trapping efficiency increases proportionally with main channel length.

In 2011, a microfluidic device for high density hydrodynamic cell trapping, growth and super-resolution imaging was reported. The fluidic design helps to trap the cells in a high-density array of wells and holds them very still throughout the life cycle, using hydrodynamic forces. The devices were compatible with the necessary criteria for Fluorescent Photo-Activation Localisation Microscopy (FPALM) imaging of *Schizosaccharomyces pombe*. A high trapping efficiency was observed in the first few rows, as once these sites were filled further cells tended to settle into pre-occupied sites. When too many cells were injected, crowding led to a pile-up and blocking of the main channel (Bell et al., 2011). Single particles were trapped in a stagnation point flow at the junction of two intersecting microchannels. The hydrodynamic trap was based on active flow control at a fluid stagnation point using an integrated on-chip valve in a monolithic

PDMS-based microfluidic device. Characterization of device design parameters, enabling precise control of stagnation point position for efficient trap performance was reported. Figure 3.11 shows hydrodynamic trap using stagnation point. Contactless trapping is possible using this method. The stagnation point position was actively controlled along the outflow direction via an integrated, on-chip valve by adjusting the relative flow rates in the two outlet channels. Involves linear feedback controller for particle trapping (Tanyeri et al., 2011).

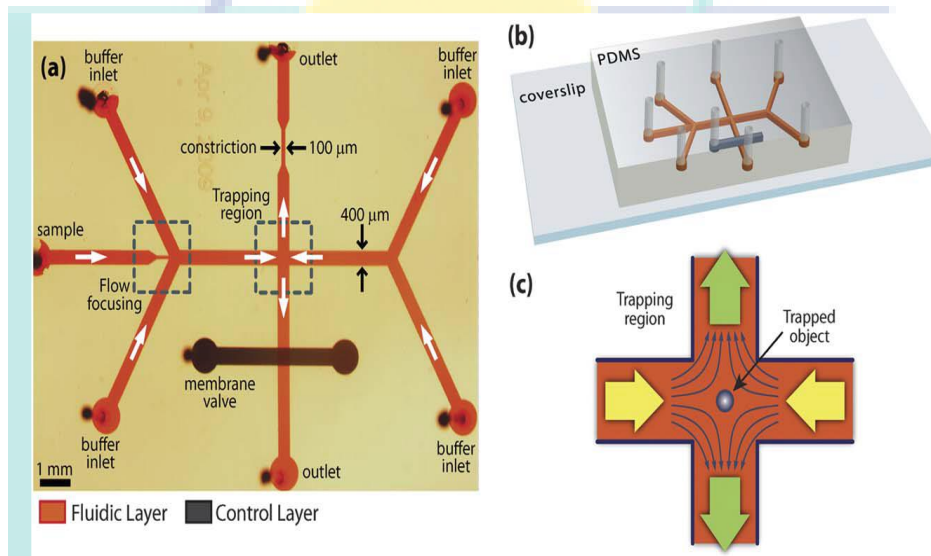


**Figure 3.11 Hydrodynamic trap using stagnation point**

Image source: Tanyeri et al., (2011). Image showing (a) Optical micrograph of a microfluidic trapping device, (b) 3-D illustration of the microfluidic trapping device, (c) Schematic of the trapping region of two opposing laminar streams meet at the intersection of two perpendicular microchannels, thereby creating a well-defined flow field containing a stagnation point where an object will be trapped.

Microfluidic system consisting of the successive single-cell handlings of single-cell isolation from a large number of cells in cell suspension, labelling each isolated single cell and the lysate extraction from each labelled single cells were reported. Microfluidic system was composed of main channels, cell-trapping pockets, drain channels, and single-cell content collection channels which were fabricated by polydimethylsiloxane. Demonstrated high-throughput and high-volume single cell isolation with 512 pocket type device. Figure 3.12 shows cell capture using pockets. Stained cell contents were extracted beside the cell membrane by cell lysis with a surfactant injected into the main

channel. The cell contents extracted from each captured cell were individually collected into each collection channel for analysis. This method can facilitate single cell analyte based applications (Arakawa et al., 2011).

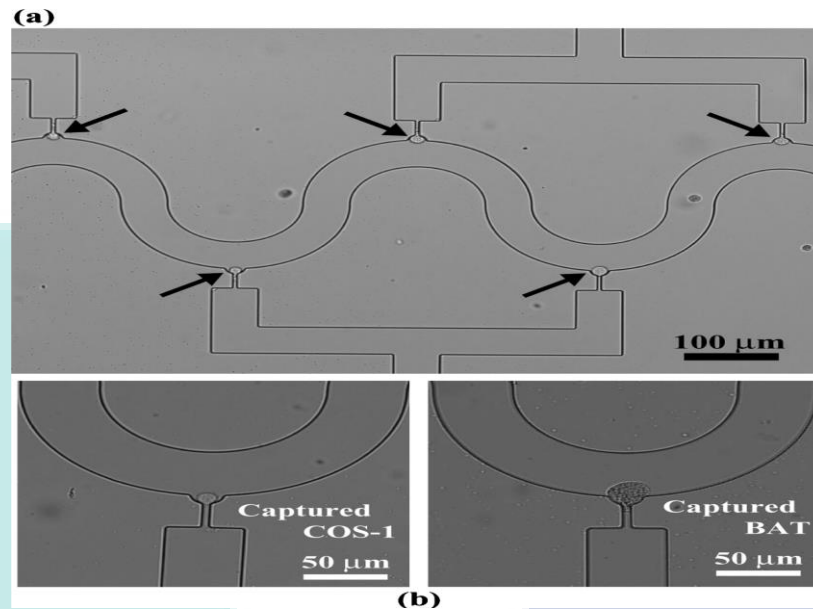


**Figure 3.12 Cell capture using pockets**

Image source: Arakawa et al., (2011). Image showing (a) cells captured in the trapping pockets, (b) Magnification of captured cells and intrusion in to drain channel.

A new method combining a simple micro well-based cell docking process inside a patterned microfluidic channel, with programmable time-course live-cell imaging and software-aided fluorescent image processing was demonstrated. Budding yeast, *Saccharomyces cerevisiae* (*S. cerevisiae*), cells were individually captured in micro wells by multiple sweeping processes. The authors reported that the micro wells of 8 mm diameter and 8 mm depth were suitable for an optimal docking efficiency (>90%) without notable flooding issues. For quantitative SCA, time-course fluorescent images of the cells stimulated by mating pheromone were captured using computerized fluorescence microscope. Figure 3.13 shows cell trapping in different micro well size. This method requires the optimization of cell-containing solution plug actively migrating back and forth several times by a finger-pressure induced receding meniscus for efficient docking process. As the meniscus recedes over the micro wells, the yeast cells were spontaneously captured into the micro wells by lateral capillary force at the single-cell level. By repeating these sweeping processes, the cell docking was completed (Jeon et al., 2011).

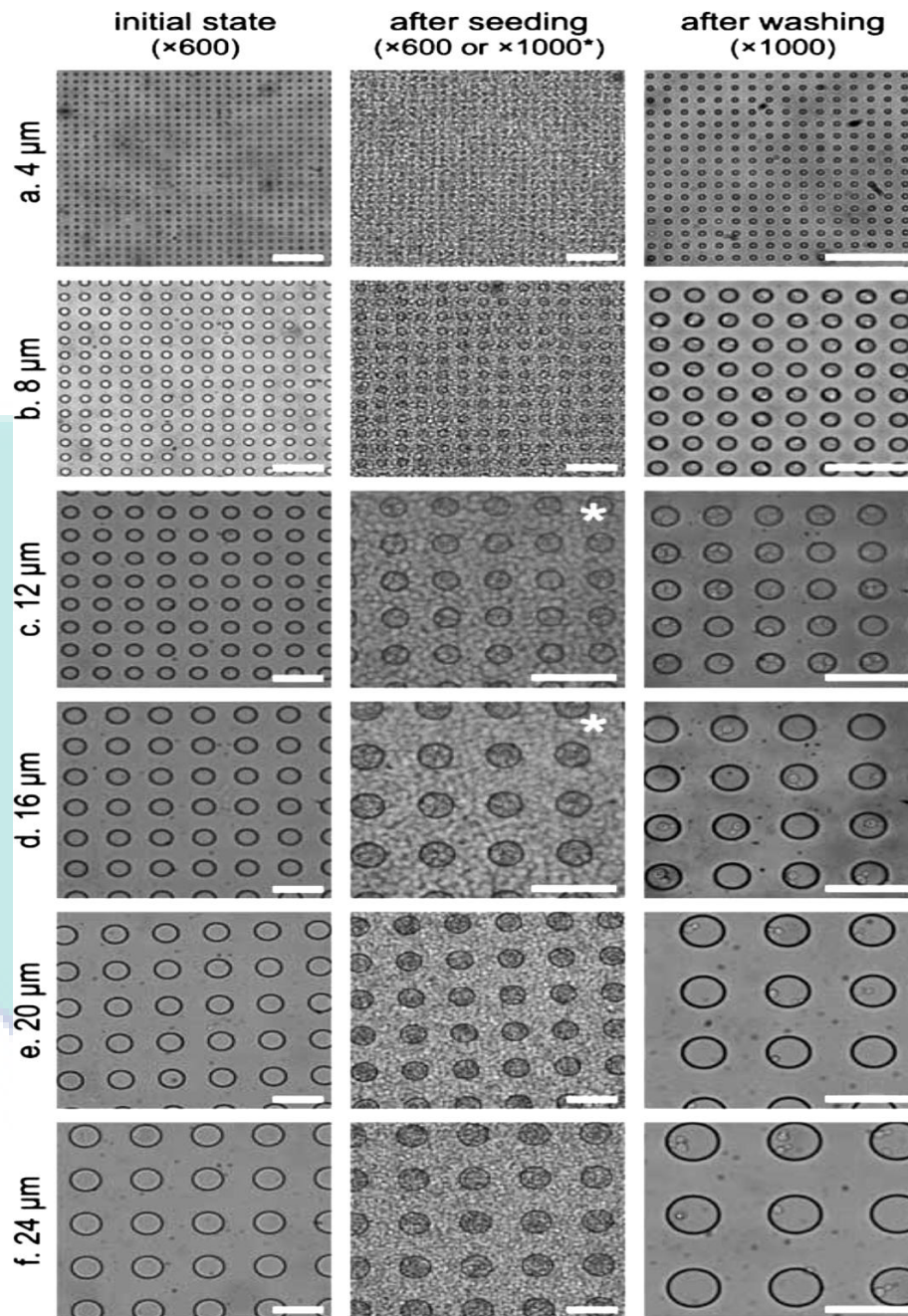
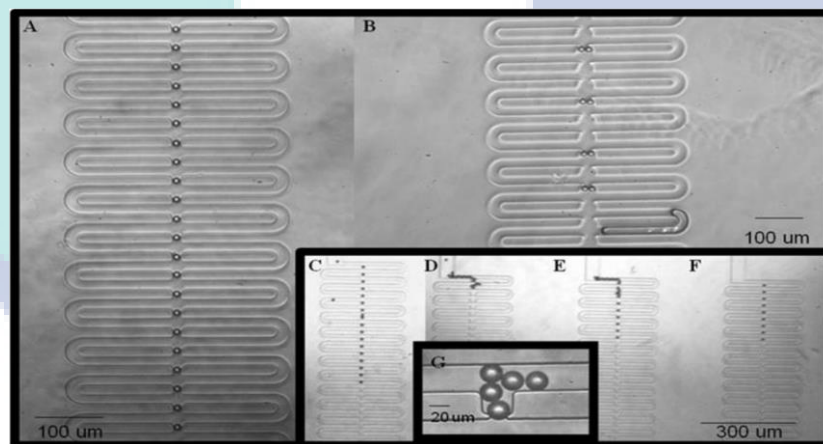


**Figure 3.13 Cell trapping correlation with different micro well diameter**

Image source: Jeon et al., (2011). Image shows bright field images of various micro wells at initial state, after cell seeding, and after washing step, respectively: (a) 4, (b) 8, (c) 12, (d) 16, (e) 20, and (f) 24 mm (Scale bar: 40 mm).

In 2012, detailed numerical and experimental investigation into the optimisation of hydrodynamic micro-trapping arrays for high-throughput capture of single polystyrene micro particles and three different types of live cells at trapping times of 30 min or less were reported. Figure 3.14 show trapping of micro particle in traps. Based on

investigation with four different geometries concluded that, i) The calculated device dimensions permitted partitioned flow between the main channel and the trap channel, and further, preferential flow through the trap channel in the absence of any obstruction; (ii) Different trap shapes, all having the same dimensional parameters in terms of depth, trapping channel lengths and widths, main channel lengths and widths, produce contrasting streamline plots and that the interaction of the fluid with the different geometries can produce areas of stagnated flow or distorted field lines; (iii) Once trapped, any motion of the trapped particle or cell or a shift in its configuration within the trap can result in significant increases in pressures on the cell surface and variations in the shear stress distribution across the cell's surface. Also reported that a reduction of the average carrier fluid velocity by 50% resulted in an increase from 80% to 92% occupancy of single algae cells in traps. Reported article also act as a guideline for microfluidic design considerations for better results (Lawrenz et al., 2012).



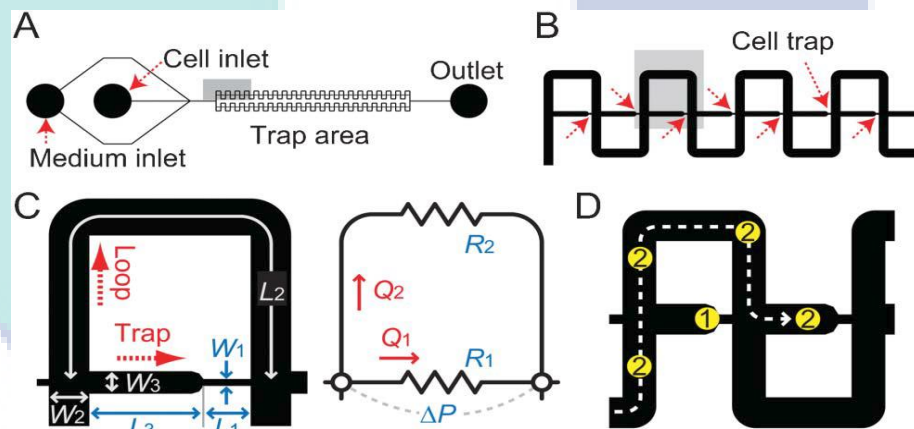
**Figure 3.14** Single micro particle trapping using different trap designs

Image source: Lawrenz et al., (2012). Single micro particle capture in devices: (A) triangular arrays, (B) elliptical arrays, (C) triangular arrays, (D) elliptical arrays, (E) conical arrays, (F) square arrays, and (G) particle aggregation at square traps.

In 2012 (Kim et al., 2012), introduced a method for trapping and releasing micro beads, using dual-function elastomeric valves. The fluid flow was controlled to ensure that beads flowing in a main stream enter into a branch channel. Trapping and releasing of single beads was successfully performed under an optimized pressure and flow rate ratio. This technique utilized elastomeric valve as a dual-function removable trap instead of a fixed trap and a separate component for releasing trapped particles. The process



requires controlling of elastomeric valves driven by pneumatic pressure and a fluid flow action (Kim et al., 2012a). Kumano et al., (Kumano et al., 2012) demonstrated the real-time observation of cell division and phagocytic digestion. The conditions that enable effective and long-term trapping of a prominent model ciliate (*Tetrahymena thermophile*) within a hydrodynamic microfluidic device were discussed in much detail. This method demands continuous pulling of a syringe containing cells at a slow rate to prevent cells from entering the channel by swimming. Conflict requirements between cell retention and trapping efficiency were discussed. Author also discussed that width and length of trap need to be optimized according to the applications. Figure 3.15 shows trapping in microchannels (Kumano et al., 2012). Cells were trapped on a stretchable micro well array for SCA. System involves an optimized stretching using plastic tube for this process (Subashini et al., 2012).



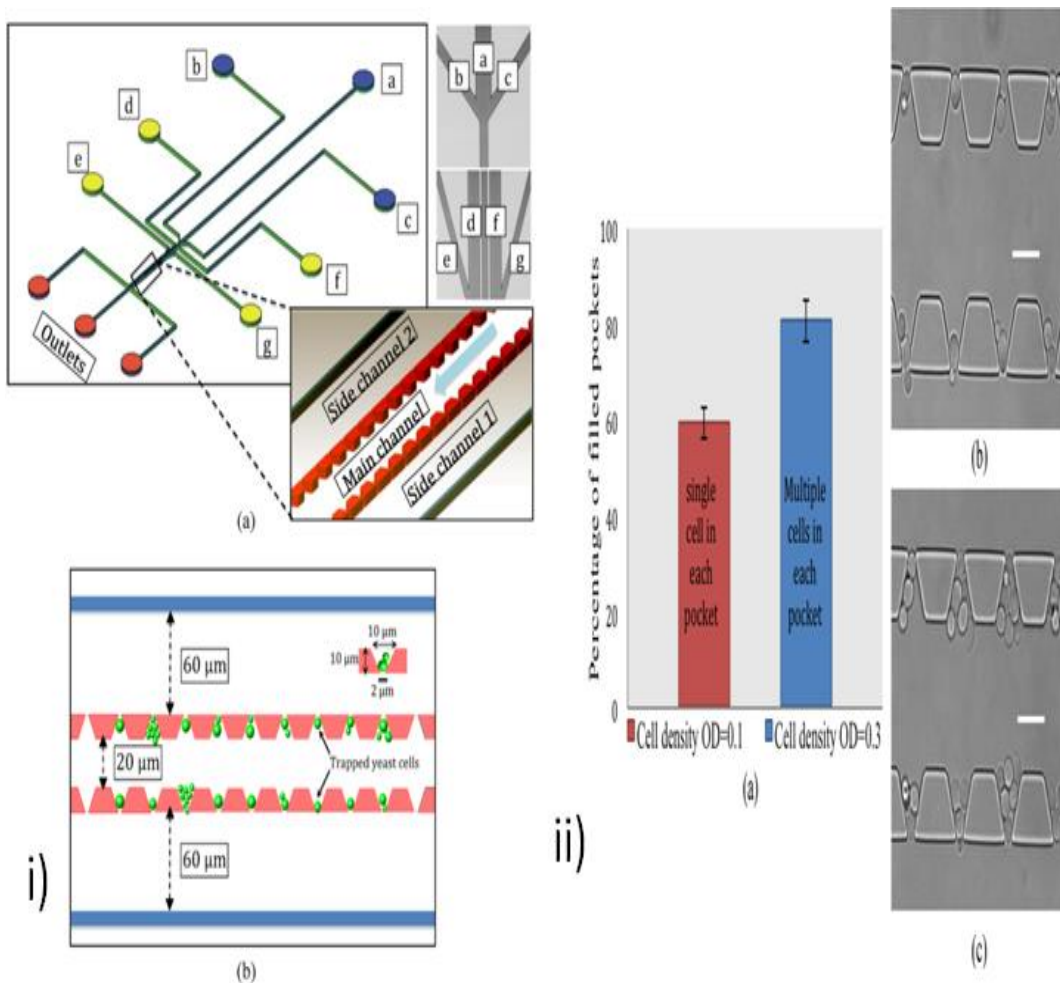
**Figure 3.15 Trapping using microchannel**

Image source: Kumano et al., (2012). Schematic illustration of the micro channel design for trapping (A) The whole structure of the micro channel, (B) A close-up of the trap area, marked as the gray area in A, (C) A close-up of one trapping unit (left), marked as the gray area in B, and the corresponding resistance circuit diagram (right), (D) A conceptual scheme of cell trapping).

In 2013, deterministic high-density single-cell trap array were developed. In this article lateral trapping of cells were involved (Chung et al., 2013). Microfluidic cell trapping device to measure single cell exocytosis was reported. Quantal exocytosis measurement was achieved by targeting single or small clumps of chromaffin cells on top of the  $10 \times 10 \mu\text{m}$  indium tin oxide microelectrodes arrays with the developed micro

device. About 72 % of the trapping sites were occupied by cells with the hydrodynamic trapping method and the recorded amperometric signals are comparable to the results with traditional carbon fibre microelectrodes. Precise amperometric measurements require electrode surface areas small enough to minimize non-faradic information such as electrical noise and capacitive currents, because larger electrodes cannot ensure all the quantal release events be detected due to the high background noise, although, electrodes need to remain large enough for allowing a quantitative collection of released molecules from releasing point distributed on the surface of a single cell or from a collection of cells depending on the scope of the measurements. Compromise between these conflicting requirements was provided by using indium tin oxide planar microelectrodes with sizes of 10  $\mu\text{m}$  by 10  $\mu\text{m}$  and the amperometric detection system involves the fabrication of microelectrodes (Gao et al., 2013).

Investigations on hydrodynamic trapping of microspheres in a microfluidic particle-trap array device by finite element simulations were reported. The investigations were based on the fluid velocity field, pressure field, and force and stress on the microsphere in the device. They explored the trap array's geometric parameters and critical fluid velocity, which affected the microsphere's hydrodynamic trapping. The simulated hydrodynamics in the microfluidic channel impacting the moving microsphere agree well with the experimental observation. The author concluded that the FEM simulations provide a powerful explorative tool in designing and implementing microfluidic devices. Lateral cell trapping were examined and reported. This article provides a design guidelines for further improvements (Xu et al., 2013). Hydrodynamic cell trapping for high throughput single-cell applications were developed. Reported technique facilitates lateral trapping in to V-shaped pockets. Figure 3.16 shows cell trapping in "V" shaped pockets. (i and ii) (Banaeiyan et al., 2013). 2-D micromanipulation of single particles using fluid flow was published. Sample trajectory of a single particle (2.2  $\mu\text{m}$  diameter fluorescent polystyrene bead) was manipulated in two dimensions using the trap. A predetermined trajectory was programmed to spell the letter "C" and "I". Figure 3.17 shows single particle trajectory manipulation (Tanyeri and Schroeder, 2013).



**Figure 3.16 Cell trapping using V shaped pockets**

Image source: Banaeiyan et al., (2013). Image shows i) (a) Overview of the microfluidic device with inlets and outlets. Inlets “a”, “b” and “c” were connected to the main channel and used to inject the cells and stress substances into the device. Inlets “d” and “f” were used as the side inlets for hydrodynamic cell loading and reagent injection into the side channels. Inlets “e” and “g” were sheath flow inlets, (b) Device dimensions engineered for experiments with yeast cells; ii) (a) Trapping efficiency based on cell density, (b) at lower cell density, single cells occupy 60% of the traps, and (c) in higher cell concentration, multiple cells are trapped in 80% of the pockets (Scale bar: 10 μm).

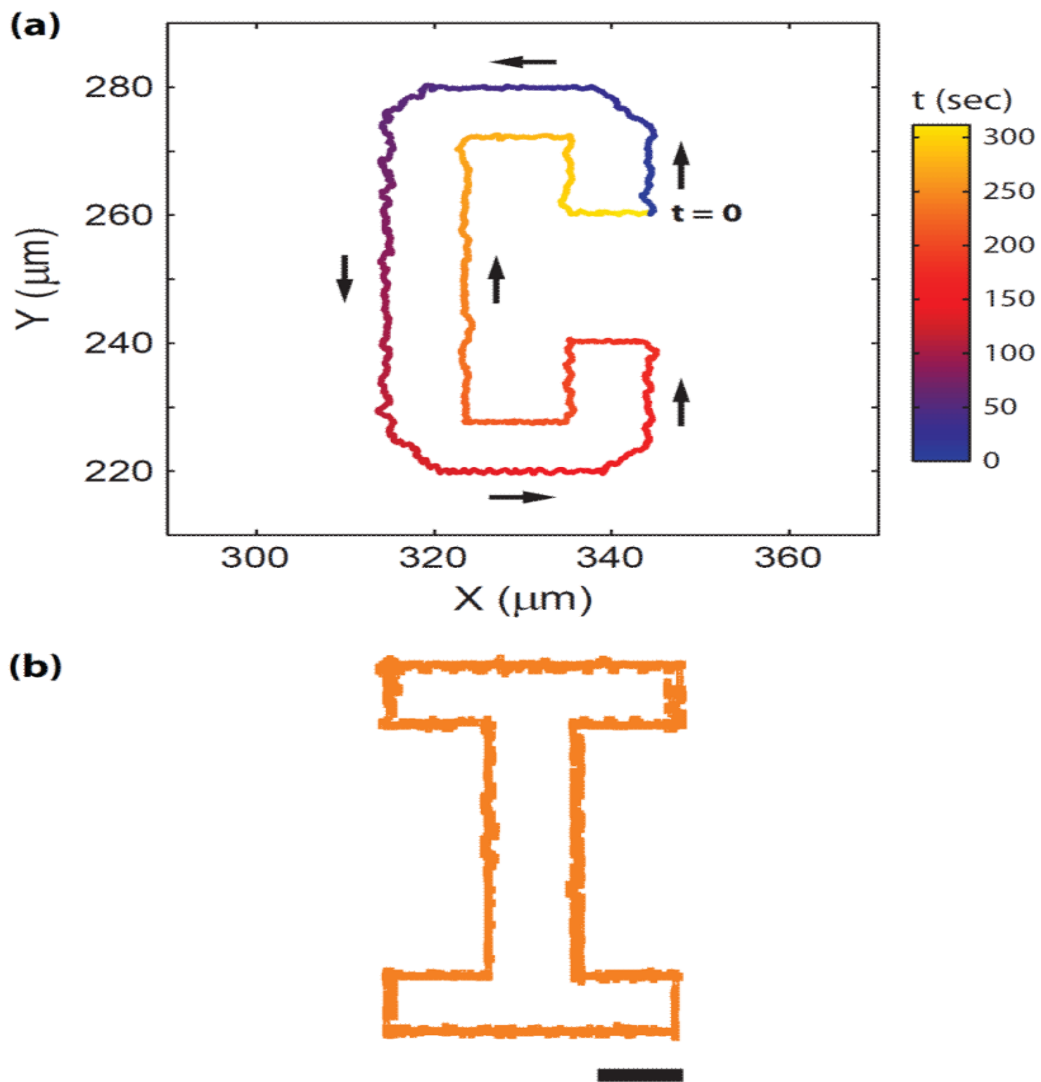


**Figure 3.17 Single particle trajectory manipulation**

Image source: Tanyeri and Schroeder, (2013). Image showing (a) Sample trajectory of a single particle manipulated in two dimensions using the trap, (b) Sample trajectory of an individual particle tracing the letter “I” using the flow-based trapping and manipulation method (Scale bar: 10  $\mu\text{m}$ ).

Xu et al., reported a microfluidic microsphere-trap array device on a single platform. Different types of targets were captured on the surfaces of microspheres of different sizes. By optimizing the geometric parameters of the traps, the trap arrays in the device can immobilize microspheres of different sizes at different regions with microfluidic hydrodynamic trapping. The targets are thus detected according to the microspheres’ positions (position-encoding). Figure 3.18 shows particle trapped in array

of traps. Preliminary microsphere trapping experiments was performed on a fabricated device using microspheres of one size. Device's single cell capture (SCC) efficiency was around 99% and this process facilitates lateral trapping. Process was validated with the microspheres (Xu et al., 2013).

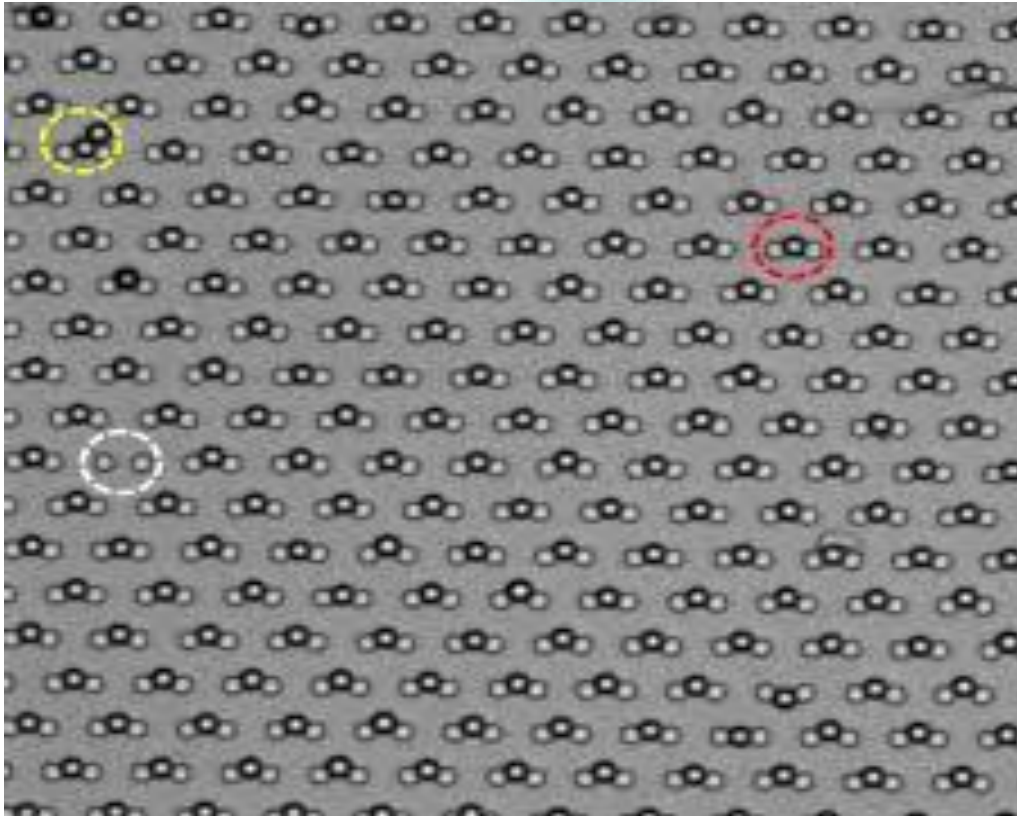


**Figure 3.18 Spheres being trapped in the array of traps**

Image source: Xu et al., (2013). Image showing trapped spheres, single (red dashed circle), multiple (yellow dashed circle), and empty (blue dashed circle).

In 2014, Kim et al., reported a hydrodynamic fluid flow through the sieve-like microfluidic channel sequentially fills the trap positions with particles of the trap size, and particles smaller than the trap size pass through the sieve and are trapped by smaller traps downstream. Results showed that more than 85% of the polystyrene microspheres (of sizes 15  $\mu\text{m}$ , 6  $\mu\text{m}$  and 4  $\mu\text{m}$ ) were sorted in the correct segment of the device that targets their respective sizes. Trapping efficiency of the device was manipulated by controlling the channel dimensions of the device. Size sorting was achieved through the gaps in the trap positions. To enable both trapping and sorting to work at the same time, side channels were added to isolate and decouple fluid flow between each stage in the

device. Capture efficiency was high, although the SCC efficiency was minimal and suitable for size-based sorting. Kim et al., commented that single trap occupancy can be accomplished in future works by tapering the channel height to match with the zone's target trapping size (Kim et al., 2014).

Microfluidic device was designed and developed specifically for the reversible immobilisation of *Schizosaccharomyces pombe* cells to facilitate live cell super-resolution microscopy. Photo-Activation Localisation Microscopy (PALM) was used to create detailed super-resolution images. Technique was suitable for SCA when high-throughput was not much of consideration and this process facilitates lateral trapping. This process used flow system to control the fluid flow. Figure 3.19 (i) shows the cell being trapped (Bell et al., 2014). In this work, a method for facile hydrodynamic trapping and anchoring of bacterial cells using nano wire array with fishnet-like structure in microfluidic channel was published. Vertically well-aligned ZnO nano wires were directly synthesized onto the side walls of micro slit structures by hydrothermal method to form mesh-like cage structures, which were effective in trapping and anchoring of *Escherichia coli* cells as model bacteria. Two anchoring modes; impaling and wedging were reported. This is suitable for multiple trapping of cells with certain damages to the cells. This process requires complex fabrication steps and demands ZnO vertical nano wire synthesis on walls. In this method, multiple cells were captured and impaling anchors caused irreversible damages to cells (Kwon et al., 2014).

Lab-on-a-chip device with a knot shaped microfluidic network was presented enabling trapping of single pollen grains at the entrances of a series of microchannels (Ghanbari et al., 2014). The set-up serves to create identical growth conditions for serially arranged tip growing plant cells such as pollen tubes. Microchannels were to harbour the individual pollen tubes. Experimental results showed that the pollen tubes can be trapped and start to grow inside the microfluidic chip 30 min after the injection of pollen suspension. The application was regarding single pollen grain trapping (Ghanbari et al., 2014). An article was published to address the compromise between cellular loading efficiencies and trapped cell densities. The cell trapping efficiency of a microfluidic device with two parallel micro channels interconnected with cellular trapping sites were reported. The author mentioned that by using fine tuning parameters, more than 95% of trapping sites were taken by individual cells. The article reported the optimized  $Q_{trap}/Q_{mc}$  ( $Q_{trap}$ : the flow at trap path and  $Q_{mc}$ : the flow at main channel path) value

for high efficiency trapping of SCC. The design patterns or parts used in the experiments were much similar to previously reported articles (Deng et al., 2014).

Khalili et al., reported the optimisation of Qtrap/Qms for efficient trapping. Appropriate Qtrap/Qmc ratio to perform cell trapping using the hydrodynamic resistance concept was the ratio value above 1 (Khalili et al., 2014). A special article by Benavente et al., demonstrating single-cell trapping and selective treatment via co-flow within a microfluidic platform involving grooves was reported. Lateral trapping were possible and involves optimizing of the co-flows (Benavente-Babace et al., 2014).

In 2015, a microfluidic chip with hydrodynamic traps for isolating single cells was proposed (Kukhtevich et al., 2015). 2D motion analysis of particles in COMSOL was used to determine the shape and size of hydrodynamic traps. Experimental conformance of the MFC's ability with semicircular traps was presented. A single trap could arrest multiple cells if the diameter of the cells were very small or if a cell was fractured and thus segregating individual cells were not always possible (Kukhtevich et al., 2015). A microfluidic device enabling high-efficiency single cell trapping was proposed based on least flow resistance path. T and inverse T junction structures formed the hydrodynamic trapping sites with a view to optimize the existing channel shape and size. Experimental results showed a 100% conformance to cell trapping and 90% single cell trapping. It was rare, yet possible for the biggest cells to clog the main channel and nullify the performance. Cell density plays an important role and higher density could lead to a faster trapping, but should be regulated carefully to make sure that cluster of cells does not fall into the same trap site. Figure 3.19 (ii) shows the micro array for cell trapping (Jin et al., 2015).

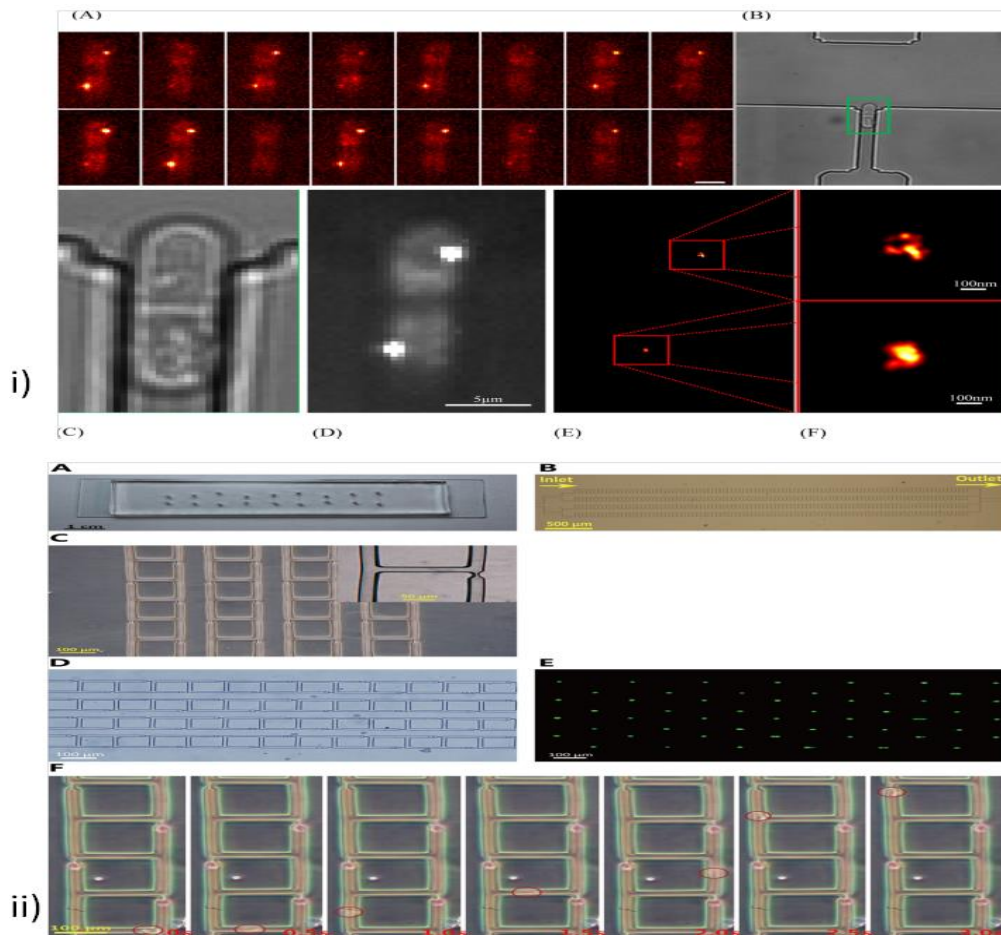


**Figure 3.19 Microfluidic device showing cells being trapped**

Image adapted from source i) Bell et al., (2014) and ii) Jin et al., (2015). Image shows i) (A) Time montage of raw single image frames for a trapped *S. pombe* cell, (B) A cell was immobilized and imaged with transmitted white light, (C) A zoomed image where septum clearly visible, and the cell nearing fission, (D) Epifluorescence image of the same cell showing the fluorophores clustered around the two separate centromeres, (E) Corresponding PALM image of the fluorophore positions, (F) Increased resolution image of the fluorophore centres showing the level of detail achieved; ii) (a) A picture of the micro-fabricated PDMS micro-device, (b) Microscopic picture of the single cell trapping array, (c) Zoom-in view of the microarray, (d) Bright-field microscopic image of cells trapped in the constrictions, (e) Fluorescent microscopy image of the same cells shown in (d), (f) Time elapsed view of trapping of a single cell.

A microfluidic digital single-cell assay for the evaluation of anticancer drugs was proposed (Jin et al., 2015). A microfluidic hydrodynamic trapping chip was made for digital single-cell assays with the ability to monitor the dynamics of cell over a period.



90% single cell trapping efficiency was reported after numerically and experimentally determining the right bypass structure. Inhomogeneity of the cell volumes had caused reduction in efficiency of capturing single cells (Jin et al., 2015). Centrifugation-assisted single-cell trapping in a truncated cone-shaped micro well array chip for the real-time observation of cellular apoptosis was demonstrated. In this approach, the trapping process required centrifugation. The process involved centrifugation with varying parameters like size of the micro well, centrifugation rate, cell concentration, centrifugation duration, and centrifugation cycles. Since these parameters vary for different cells and analysis, all these parameters needed to be optimized according to each analysis. Figure 3.20 (i) shows the truncated cone shaped micro well array (Huang et al., 2015).

Guan et al., reported the characterizing of the performance for the hydrodynamic trap using a control-based approach. The performance of a hydrodynamic system actuated by varying combinations of proportion-integral-derivative controllers were investigated by implementing three types of controllers, P, PI & PD. Proportional and derivative controllers produced enhanced trap stability, quantified by the tightness of confinement or the amount of cell oscillation around the set point. Due to the nature of the process, integral control could not be proved to improve the trap stability. By adding integral controller used to monitor the effect of integral gain  $K_i$ , no visible improvements were seen in tightening the confinement. By adding a PD controller it was observed that with high values of  $K_d$  fluctuations in the flow field, particle position jump were increased (Guan et al., 2015).

Design and verification of a bi-layered microfluidic platform to capture single cells, culture and followed by clonal proliferation were intended by the authors (Chen et al., 2015). By using U-shaped hydrodynamic trapping sites and letting microfluidic to flow into the downstream wall of each micro-well, single cells were trapped and expanded over a period of time. For microspheres in the range of 20-25  $\mu\text{m}$  when the  $Re$  was increased from 1.4 to 2.8, the single cell trapping efficiency dropped, but microspheres with 15  $\mu\text{m}$  size experience increased trapping for the same  $Re$  range. Also, when the microsphere diameter was very small compared to the well size, multiple cells were collected in a single well. It was recorded that the first generation cell division time was longer. For cells used in the study a delay of around 39 hours was reported before cell divisions were initiated. Cell doubling time of cells used in the study was reported to

be more than the time taken by culturing populations. Figure 3.20 (ii) shows the serpentine channel with micro well array (Chen et al., 2015).

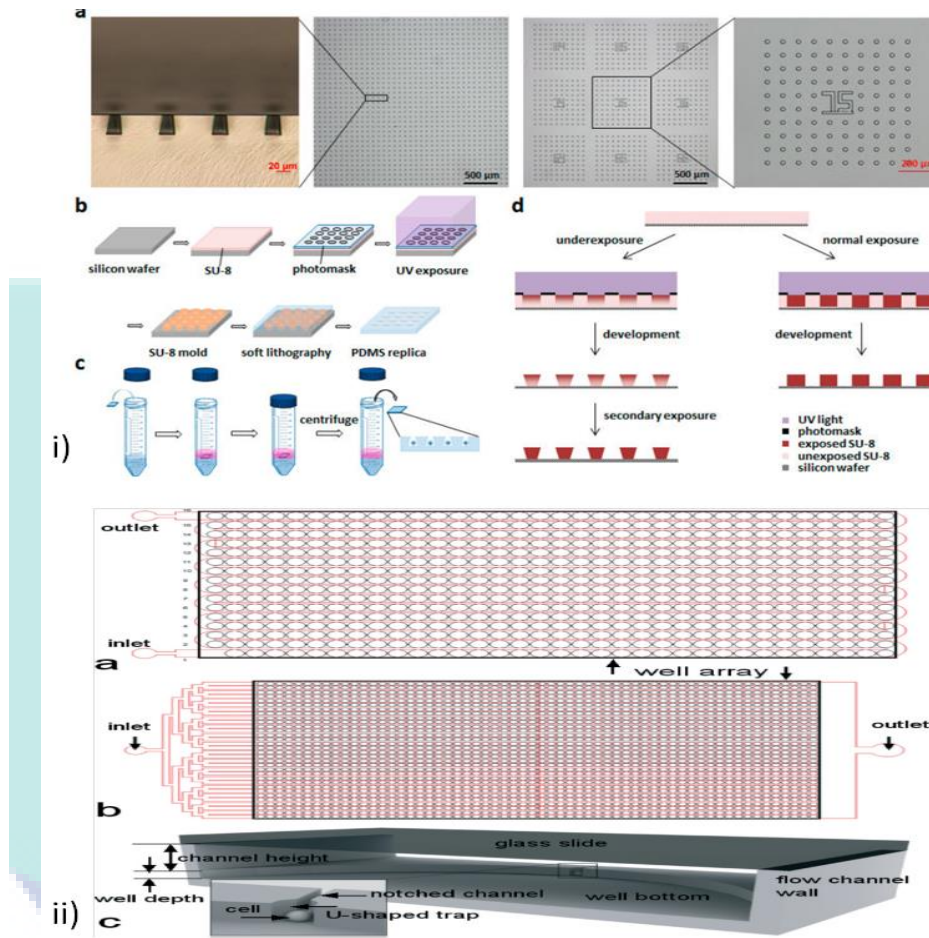


**Figure 3.20 Microfluidics with TCMA and different fluid channels**

Image from source i) Huang et al., (2015) and ii) Chen et al., (2015). Image showing i) (a) Cross-sectional view of micro wells and a representative number-coded block on an addressable truncated cone-shaped microcell array (TCMA) chip (from left to right), (b) Procedures for the preparation of a PDMS chip with a truncated cone-shaped micro well array, (c) Steps for centrifugation-assisted single-cell trapping, (d) Schematic illustration of the principles for the fabrication of inverse truncated cone-shaped micro posts (left) and normal columnar micro posts (right); ii) (a) Design with a serpentine channel on top of wells, (b) Design with a tree-pattern flow channel, (c) Cross section of one well for both design.

Article by Guan et al., (Guan et al., 2015) described an analytical design guideline for deterministic single cell hydrodynamic trapping by optimizing streamline

distributions that fell under laminar flow with cell dimension as the key factor. By carefully considering the target particle size, increased trapping efficiency could be achieved as compared to optimizing flow rates alone. Factors like cell density, cell size distribution, quantity of trap sites, and velocity of flow may have an impact on the efficiency of trapping. For example, high cell density could lead to choking of channel, non-uniform cell size could lead to loss of smaller cells if the traps were not designed to trap them. Lower cell trapping sites may lead to overflow. If the flow regime was not laminar or if flow pressure was too high, the cells could pinch through traps by deforming. Figure 3.21 shows cell being trapped in fluidic trap (Guan et al., 2015). The authors intended to develop a finite element simulation model (ABAQUS) of single-cell trapping system that could trap any type of cells or particles based on the hydrodynamic trapping in the main channel. Optimization of design was carried out by trapping out yeast cell model. The effect of the hole position (trapping site), parameters involved in trapping (back pressure etc.) and size were investigated. Cells with dimensions smaller than that of the trapping site could collect multiple cells in a single site. Trapping greatly depended on the geometric parameters of the channel (Khalili and Ahmad, 2015).

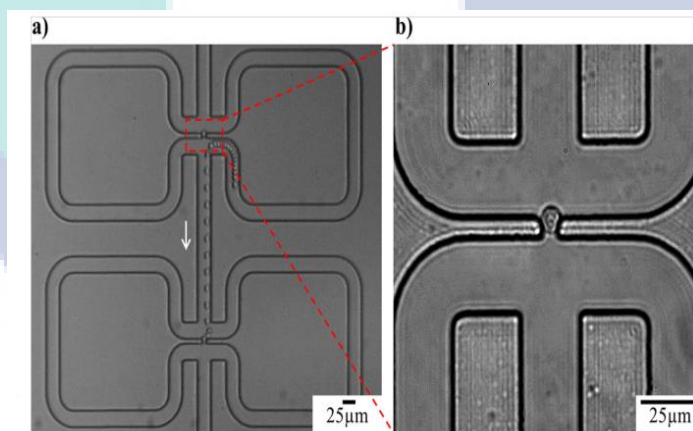


**Figure 3.21 Cell being trapped in a fluidic trap**

Image source: Guan et al., (2015). Image showing (a) Superimposed time-lapse image of white blood cell trapping and (b) close-up of captured white blood cell, white arrow indicates the direction of flow.

### **3.3 Critical Review**

Microfluidic devices are creating new breakthroughs in the field of SCA. These devices are helping pharmaceutical industry, medical diagnosis, healthcare, life science

research and many other different spheres in advancing to newer frontiers. In coming years, this research will extend to cater its service in all aspects of single cell dynamics. The industry trend and interest in this field have grown multifold in recent years and is expected to proliferate further. Even though hydrodynamic microfluidic systems have many advantages in single cell studies, several demerits such as time consumption for optimizing fluidic device, fabrication reliability, and user interface need to be addressed to advance the application of the systems further. Moreover, the integration of the hydrodynamic microfluidic platform to omics technology and its standard characterization needs to be addressed for SCA with a special focus. Literatures are critically summarized in this section, based on the earlier presented literatures and Table 3.2 summarizes the single cell vertical trapping systems. Each method was critically summarized highlighting their upside and downside.

The future devices will focus on overcoming some of the drawbacks of the current microfluidic systems for single cell analysis, along with its adoption towards new applications. Future systems can be further improved in many ways, as discussed below. Passive systems: microfluidic system with non-auxiliary devices will be of interest, thus leading to the reduction in cost and lab space. System complexity: complexity in fabrication methods or process will be of least interest and considered demerits. Less complex systems will be more preferred in the market. Handling: less expertise requirement for handling will be the need of the market. High throughput: systems with a high throughput of single cell analysis will be of interest. Cell trapping: high single cell trapping will be of interest with least or no cell cluster trapping. Trapping resolution: the focus will be on the improvement of the trapping resolution. Operation time: low operation time is very much essential. Reduction of running and settling time will be the crucial factors to focus. Compatibility: microfluidic systems that are compatible with the existent modalities will be advantageous. Evaporation: the evaporation of reagents during operation acts as a barrier for an efficient cell separation and manipulation.

With these focus areas, effective strategies need to be developed by utilizing the full potential of microfluidics to address the issues. These directions facilitate further exploration of growing demand for SCA.

**Table 3.2 Critical summary of contact-based hydrodynamic vertical trapping**

Cell used	Inlet cell density	Well / trap area dimensions	Flow rate	Auxiliaries involved	Time taken	Applications	General practical implications / downside	Reference
NIH3T3 fibroblasts or rat basophilic leukemia (RBL-1) cells	2500-6200 cells/mm <sup>2</sup>	For fibroblasts (Microwells of $D = 25 \mu\text{m}$ , $H = 27\text{-}\mu\text{m}$ ), for RBL-1 cells (Microwells of $D = 20 \mu\text{m}$ , $H = 21\text{-}\mu\text{m}$ )	-	-	5-40 min	Single cell assay	Microwell size needs to be optimized for each specific cell	(Rettig and Folch, 2005)
Human PC3 prostate cancer cells	$1.5 \times 10^6$ cells/mL	Triangular microwells (side length of $50 \mu\text{m}$ with depth of $20 \mu\text{m}$ )	0.05 - 0.15 mL/h	Used a syringe pump	20 min	Short term, single cell analysis	Requires fluid pumping system, for providing varying flow	(Park et al., 2010)

Polystyrene microspheres and 17/9 mouse B cell hybridoma cells	In the order of $10^5/\text{mL}$	Microwells (30-200 $\mu\text{m}$ diameters, 60-80 $\mu\text{m}$ depths)	In the order of tens of $\mu\text{L}/\text{min}$	Used a peristaltic pumping	10 min	Immunobiosensing applications	Involves peristaltic pumping system. Suitable for multiple cell trapping applications	(Romanuik et al., 2010)
TK6 human lymphoblasts; Human B-lymphocyte lines GM15268, GM15242, and GM15224 (Coriell Institute); and OVCAR-8 human ovarian cancer cells	$5 \times 10^4$ cells/mL	Microwells depth and width were varied from 20–50 $\mu\text{m}$	-	Agarose-PBS gel was applied to seal the cells within the microwell	15 min	Single cell DNA damage analysis applications	Complex process. Custom software were used for analysis	(Wood et al., 2010)



UMP

<i>S. cerevisiae</i> (SH129)	$5.0 \times 10^9$ cells/mL	Microwells - (4–24 $\mu\text{m}$ diameter and 8 $\mu\text{m}$ depth)	Direct Seeding	Manipulation of solution plug by applying hand pressure after closing one side of reservoir	5–10 min	Single cell imaging and quantification applications	cell	Flooding effect occurs at cases. Requires manual manipulation of solution plug.	(Park et al., 2011)
Ba/F3 cells	$1.25 \times 10^6$ cells/mL	Microwells diameter 12 $\mu\text{m}$ (stretched 20 $\mu\text{m}$ ), height of 15 $\mu\text{m}$	Direct seeding	Stretching and withdrawal were precisely controlled by a manual micromanipulator	5-10 min	Single cell analysis	cell	Involves precise stretching and withdrawal of PDMS microwell array for cell trapping. Different cell size requires different design optimization	(Wang et al., 2012)
HeLa cells	$2 \times 10^5$ cells/mL	Microwells with diameter sizes of 10–24 $\mu\text{m}$	-	Centrifugation assisted at rate of 1500 rpm (453g).	Few seconds	Drug screening, Cancer diagnosis		Requires centrifugation	(Huang et al., 2015)

Microspheres (25  $\mu\text{m}$ ), Human dermal fibroblasts (HDFs, CRL-2429) and K562 cells (human immortalised myelogenous leukaemia Line)

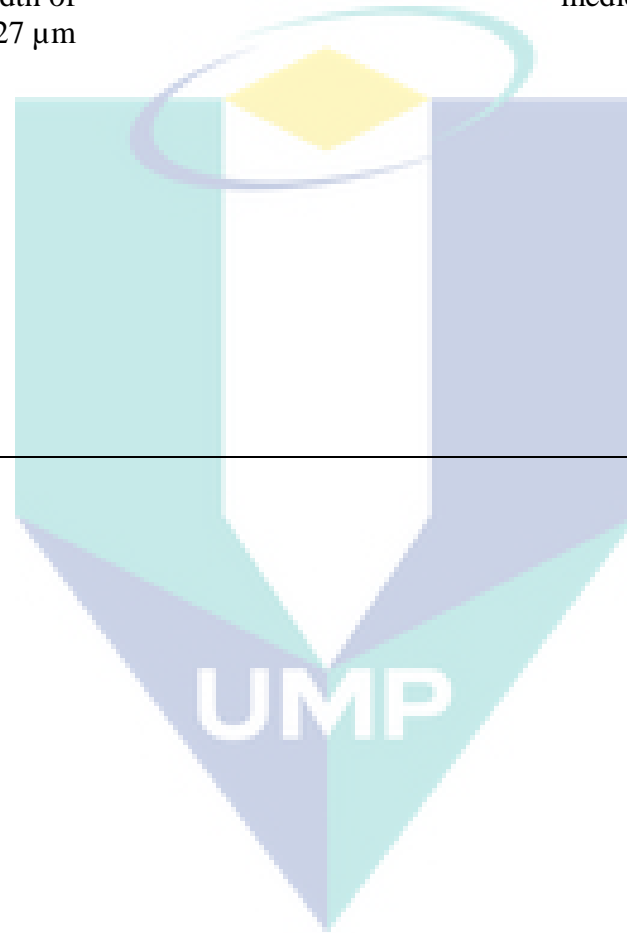
$5 \times 10^5$  cells/mL

Microwell diameter (0.5 – 1 mm), Trap width of 18 and 27  $\mu\text{m}$

10 min

Stem cell research, Regenerative medicine

(Chen et al., 2015)

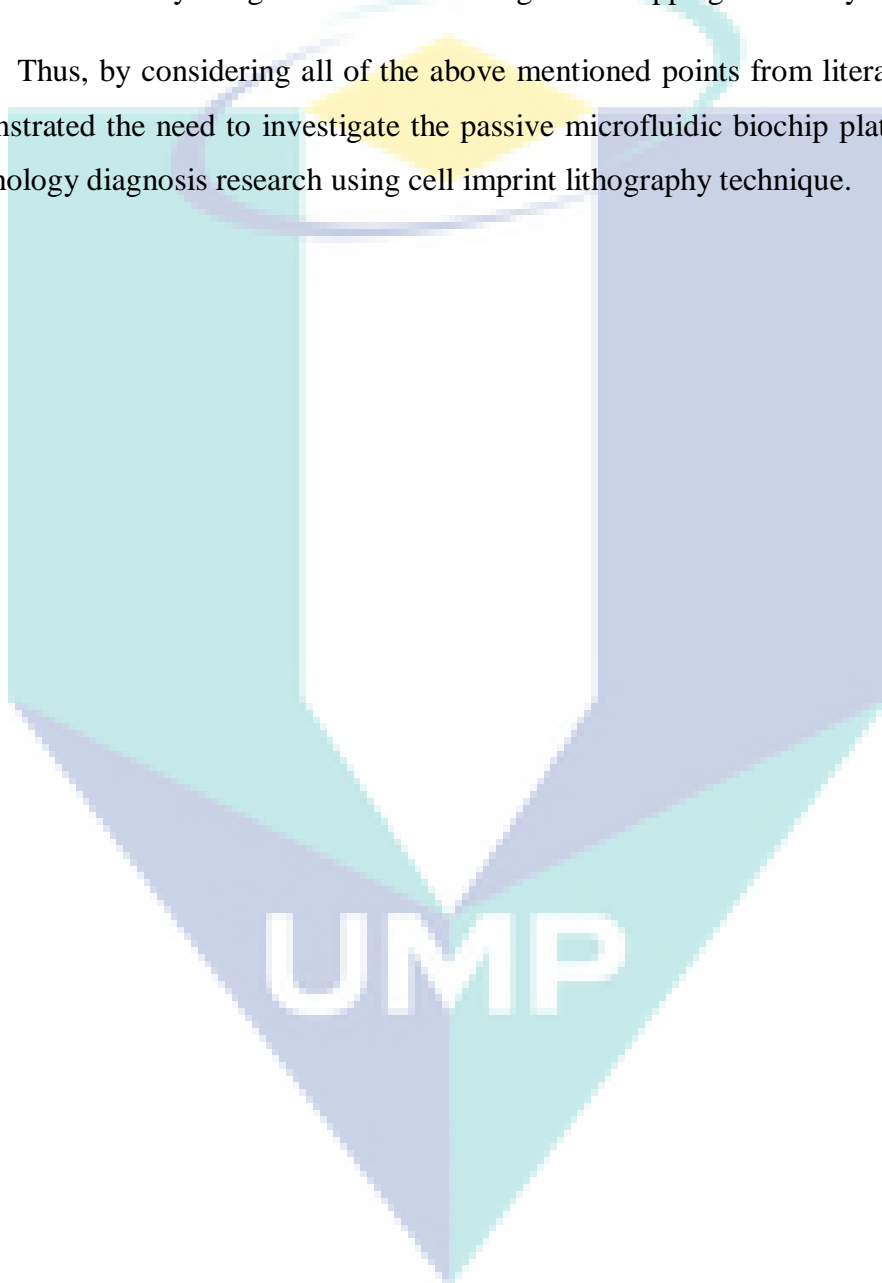




### 3.4 Chapter summary

To the best of the author's knowledge, none of the studies in the literature have investigated the relative efficiency of hydrodynamic-based fluid channel designs on SCC. The effort of this work has been taken to investigate the effects of fluid channel design and micro well array design orientation for single cell trapping efficiency.

Thus, by considering all of the above mentioned points from literature study, it demonstrated the need to investigate the passive microfluidic biochip platform for cell morphology diagnosis research using cell imprint lithography technique.



## CHAPTER 4

### CARBON NANO PARTICLE-POLYMER COMPOSITE CELL IMPRINT LITHOGRAPHY

#### 4.1 Organization of this chapter

This chapter describes in detail the methodologies. Methods involved in this research can be broadly divided into four sections,

- 1) Carbon-polymer cell imprint lithography
- 2) Microfluidic biochip platform
- 3) Cell morphology feature detection
- 4) *In-vitro* evaluation of the fabricated polymer composites

Figure 4.1 shows the overall flow chart of the research. The flow chart shows the directions of the research methods involved. In Figure 4.2, it illustrates the overall methodology used in this study. Following sections present cell imprint lithography polymer preparation and optimization study; cell imprint lithography with and without stimulation for diagnosis; cell imprint lithography for drug therapy applications for extracellular diagnosis; cell response study for polymer; polymer composites *in-vitro* evaluation for biomedical applications; biochip fabrication and operational optimization for achieving high single cell trapping; and detection of extracellular morphology features obtained from cell imprint lithography.

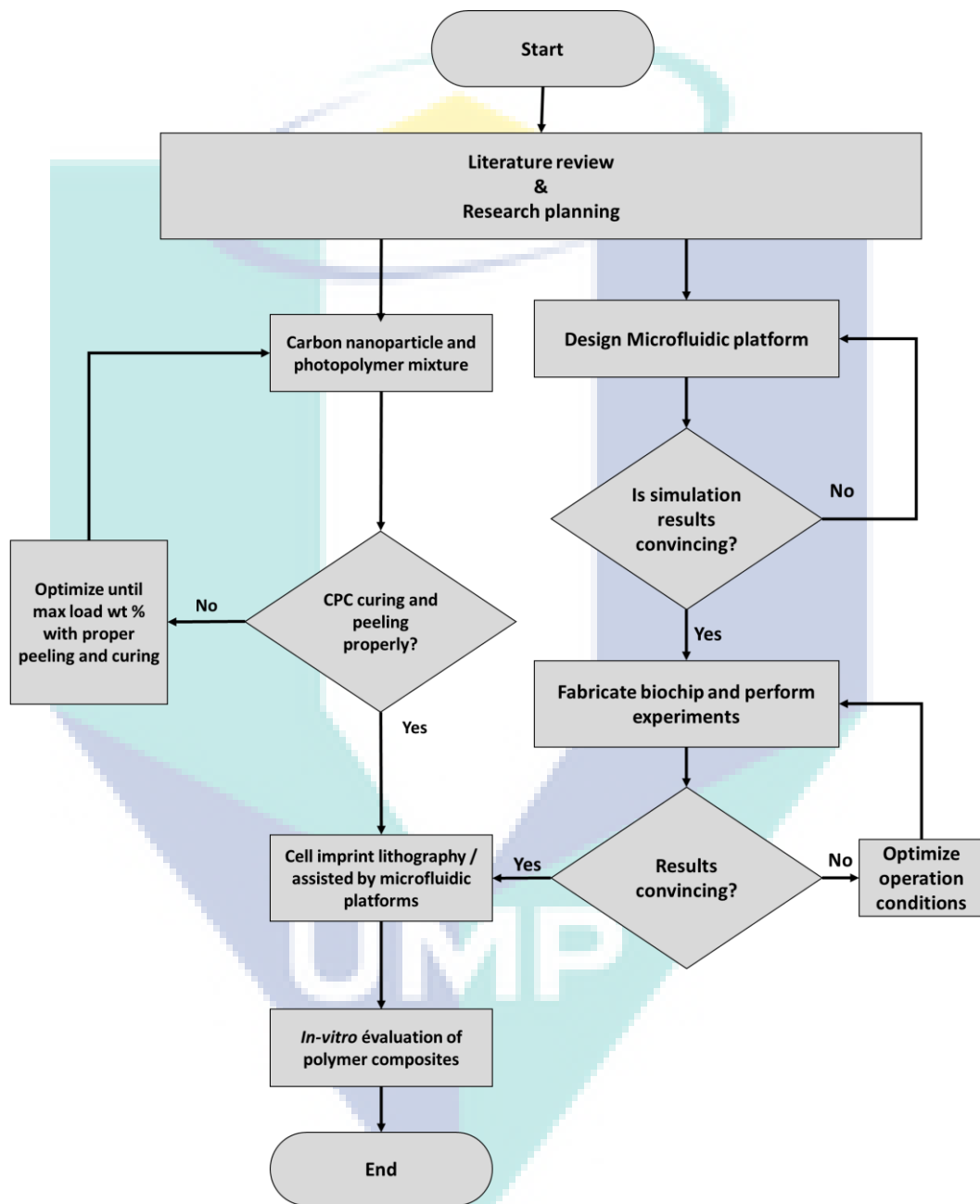


**Figure 4.1** Flow chart of research methodologies

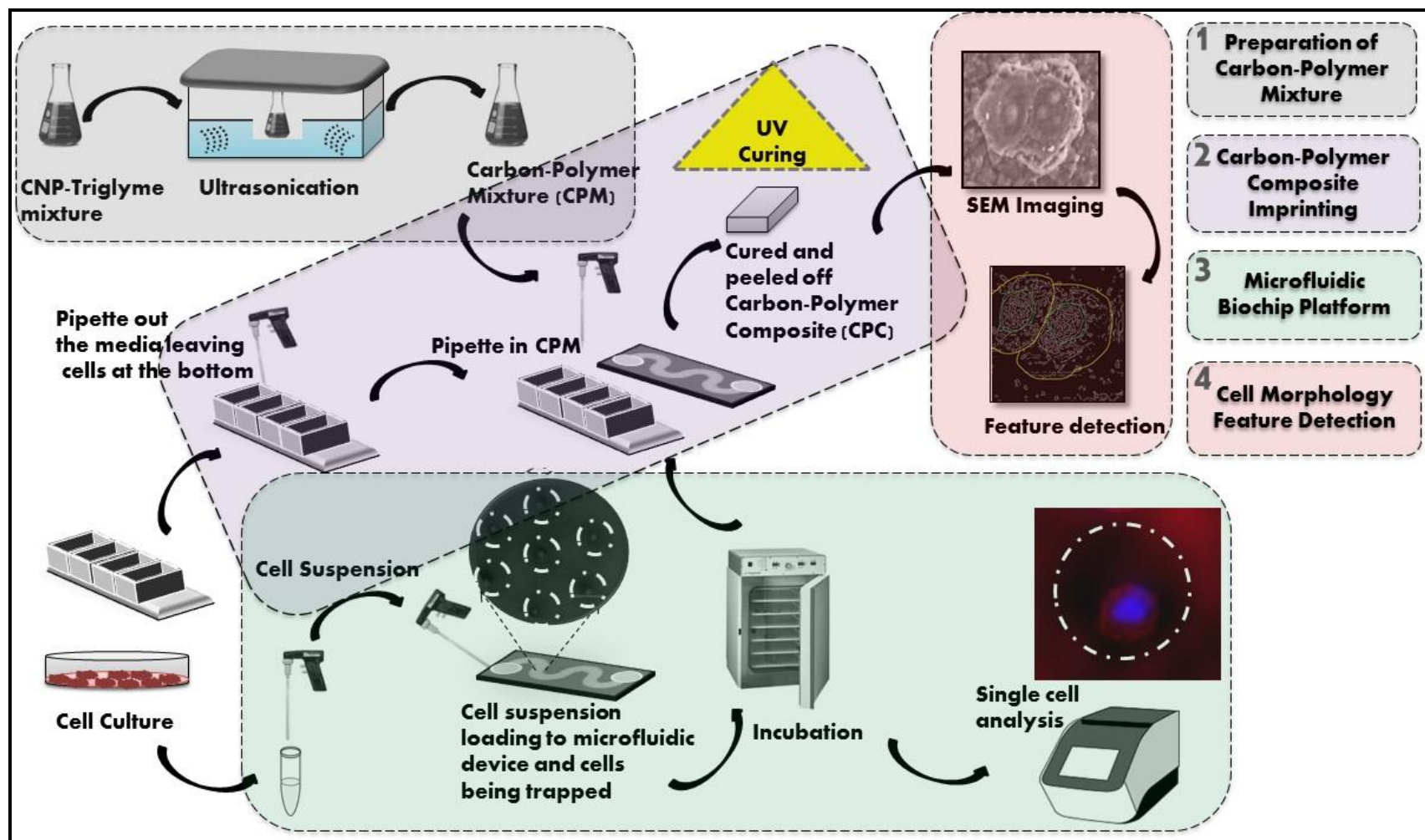


Figure 4.2 Graphical representation of overall methodology used in the study

## **4.2 Cell culture and maintenance**

Cells used in this study were human breast adenocarcinoma (MCF-7), human cervical cancer cells (HeLa), human lung carcinoma (A549), colorectal adenocarcinoma (HT-29), human gingival fibroblast (HGF-1), mouse fibroblast cells (3T3-L1) and mouse connective fibroblast cells (L929). All cells were from American Type Culture Collection, USA. A549, MCF-7, HGF-1, HT-29, HeLa and 3T3-L1 were cultured in DMEM medium (Gibco, USA). The L929 cells were maintained in MEM supplemented with 3% glutamine, 7.5% NaHCO<sub>3</sub> and 10% FBS and 1X Antibiotics. The cells were maintained at 37°C under humidified atmosphere, with 5% CO<sub>2</sub> and 95% air in the incubator (Mettler, Germany). All procedures involving the cells were conducted under biosafety cabinet (ESCO, Singapore) to maintain sterility and to avoid contamination. Complete cell culturing methods and protocols used are described detail in the Appendix A.

## **4.3 Carbon-polymer composite preparation and imprinting**

This section describes in detail the methods involved in carbon-polymer composite imprinting process.

### **4.3.1 Carbon nanoparticle characterization**

Carbon-nano-particle (CNP) (Ketjenblack EC-600JD - AkzoNobel) was characterized using SEM (Zeiss, EVO 50, Germany) and TEM (Zeiss, Libra 120, Germany), in order to see the carbon particle shape, size and surface morphology at different magnifications. The SEM samples were prepared by blowing CNP particles over the carbon tape stuck to the stub. The TEM samples were prepared by depositing two to three droplets of the nanoparticle suspension onto a grid, which was air dried prior to the TEM analysis.

The chosen super conductive CNP is a very pure carbon black extremely suitable for antistatic and electro conductive applications. Low loading is sufficient to achieve the significant conductivity increase, due to its unique morphology and the extremely high surface area of approximately 1400 m<sup>2</sup>/g (BET), thereby minimizing loss in mechanical and rheological properties. Because of these properties, many researchers have used and

reported CNP (Carbon Black) composites for many applications (Kozłowski and Kozłowska, 1996, Holade et al., 2014, Moss et al., 2011, Oki et al., 2013, Molaire, 2012).

### 4.3.2 Carbon-polymer mixture preparation and optimization:

Polymer preparation and optimization involved three stages, which are CNP-triglyme ultrasonication, carbon-polymer mixture (CPM) and UV photo polymerization. Figure 4.3 shows the process flow chart for the fabrication of carbon polymer composites for cell imprint lithography.

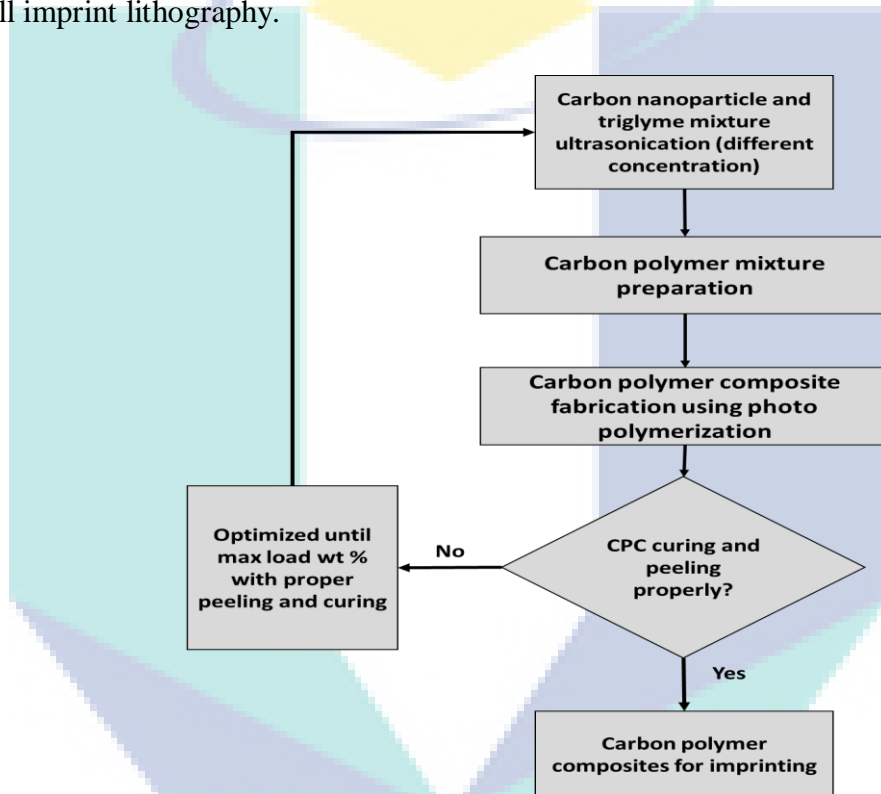


Figure 4.3 Flow chart for carbon photopolymer fabrication

#### 4.3.2.1 Carbon nanoparticle-triglyme ultrasonication

CNP-triglyme stock solutions with concentrations of 0 wt %, 0.14 wt%, 0.28 wt%, 0.42 wt%, 0.56 wt % and 0.70 wt % were prepared by ultrasonating CNP in triglyme (Sigma Aldrich). Ultrasonication was performed at room temperature for 90 min. While performing ultrasonication, the glassware containing CNP-triglyme mixture was covered with aluminium foil to protect it from light.

#### **4.3.2.2 Carbon-polymer mixture**

CPM is prepared using the mixture of CNP-triglyme, ethylene glycol dimethacrylate, methacrylic acid (Sigma Aldrich) and IRGA cure 2022 (CIBA Specialty Chemicals) with proportions of 71.1%, 25.2%, 2.5% and 1.2% respectively. This yielded CPM with final concentration of 0 wt%, 0.1 wt %, 0.2 wt%, 0.3 wt %, 0.4 wt% and 0.5 wt % through the respective CNP-triglyme stock solutions. CPM were vortexed for 5 min by covering the container with aluminium foil to protect them from light. CPM was prepared instantly.

#### **4.3.2.3 UV photo polymerization**

Prepared CPM was then applied over the glass slide (flat surface) and cured using UV source (100W, 250–450 nm) for 7 min. Cured polymer was peeled off from the glass slide and herein will be referred as non-carbon polymer composite (N-CPC), 1-CPC, 2-CPC, 3-CPC, 4-CPC and 5-CPC for 0 wt %, 0.1 wt %, 0.2 wt %, 0.3 wt %, 0.4 wt % and 0.5 wt % respectively. For optimization, CPM was applied over the plain glass slide and then cured. The obtained polymer will be termed in general as carbon polymer composite (CPC). Optimization was performed based on two factors, which are CNP wt % and CPM volume. Based on the optimization study, the 0.3 wt % CPM was able to rapidly cure and peeled off without any damages or distortions on the bottom surface. Thus, this composition was used for further studies.

#### **4.3.3 Photopolymer effect and cell cytoskeleton study**

In order to study the effect of the process to cells, two stages of experiment were performed, cell reaction to photopolymer and bioimprinting process effect.

##### **4.3.3.1 Polymer-cell response**

The effects of the polymer to cell morphology were studied using 3T3-L1 and A549 cells. The fibroblast cell line was chosen as it met the requirements of international standards (ISO 10993-5) (Wallin and Arscott, 1998). To investigate the effect on cancer cells, A549 lung cancer cell line was considered. The 3T3-L1 fibroblast and A549 lung cancer cells were seeded on a glass slide in a petri dish. After 24 hours, the glass slides were washed with phosphate buffer solution (PBS) (Sigma-aldrich) thrice, then cells were exposed to polymer mixture for 5 min. Polymer mixture exposure to cells were carried

out in dark environment. Exposing time was chosen to be 5 min because during the bioimprinting process the CPM would polymerized in less than 5 min. Thus, any change in morphology within this time frame was crucial. Consequently the cells were washed with PBS thrice and media (Sigma-aldrich) twice. Cells were observed and captured in inverted microscope (EVOS). The exposed glass slides were incubated and after 24 hours of incubation, the cells were washed with PBS and observed under an inverted microscope (EVOS).

#### **4.3.3.2 Bioimprinting effect to cells**

To study the effect of bioimprinting process to cell morphology, 3T3-L1 fibroblast and A549 lung cancer cells were seeded in 4 well glass slides (Nunc™ Lab-Tek™ II Chamber Slide™, ThermoFischer Scientific). After 24 hours of incubation, the cells were washed with PBS and bioimprint processes were performed as mentioned earlier. After the curing and peeling processes, the glass slides were subsequently washed with PBS thrice and with media twice, then observed under inverted microscope.

#### **4.3.4 Carbon polymer composite (CPC) electrical resistance measurement**

In order to investigate the changes in electrical properties of CPC due to doping of CNP, a simple electrical resistance measurement was performed. Samples were prepared with a CPM volume of 300  $\mu$ l and cured blocks were sliced at the uneven surface to make it as a rectangular cuboid block. Electrical resistance was measured by placing electrodes at the two side surfaces which was separated by the long edges of the rectangular cuboid block ( $2.7 \times 1.0 \times 0.3$  cm). Electrical resistance was measured using a multi-meter in resistance mode. Schematics of measurement is shown in Figure 4.4.



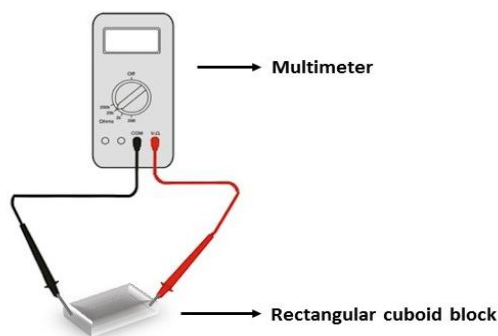


**Figure 4.4 Schematic illustration of resistivity measurement setup**

This diagram describes the CPC resistivity measurement setup using multi-meter

#### 4.4 Passive hydrodynamic microfluidic biochip platform

In order to capture and imprint the single cell, microfluidic biochip platform was employed. Three designs namely straight channel, branched channel and serpent shaped channel were considered. The effects of fluid channel design and microwell array design orientation for single cell trapping efficiency were investigated. Demonstrated a micro fluid dynamics based biochips, capable of vertical cell trapping with high SCC for short term study.

##### 4.4.1 Biochip design

Biochip designs with the straight channel, branched channel and serpent fluid channel were designed, fabricated and investigated. Biochip consists of a fluid channel of width 2 mm with a hexagonal microwell array of diameter around 35  $\mu\text{m}$  and depth of 30  $\mu\text{m}$ . Straight channel design consists of ~3500 microwells, branched channel design consists of ~5000 microwells and serpent shaped design consists of ~1100 microwells. The cell suspension was pipetted out into the inlet well which flows through the channel and to be collected at the outlet well. During the process, the cell gets captured in the hexagonal array of the microwell. The microfluidic platform was tilted to an angle of around 10-15° during the operation to assist the flow. This angle range was chosen so that the flow was moderate for cell trapping, and if the angle was too high or too low, the cell trapping would not be efficient. Figure 4.5 (a) shows the biochip illustration.

#### 4.4.2 Biochip design simulation analysis

Comsol Multiphysics 4.3 was used for simulation, with no-slip boundary conditions, and the simulation was done by specifying the cell (particle tracing) properties like mass and size. Particles of mass ( $2e-12$ kg) and particle diameter ( $10e-6$ m) were considered in this simulation study. Fluid properties were also mentioned. Fluids were modeled with the density value of  $999.97$  kg/m<sup>3</sup> and dynamic viscosity value of  $1.0016$  m.Pa.s at  $293.15$  K. Inflow velocity of the fluid ( $0.1$  mm/s) was mentioned and corresponding boundary conditions were specified in the software. Drag force was also considered in the simulation. Boundary conditions specified were shown below in Table 4.1.

**Table 4.1** Boundary conditions of modelling

<b>Initial Values</b>	<b>Microchannel Inlet</b>	<b>Microchannel Wall</b>	<b>Microchannel Outlet</b>
$U_x = 0$ m/s $U_y = 0$ m/s $P = 0$ Pa	A constant velocity, $U_o = 0.0001$ m/s	The flow is assumed as no slip, $U_{wall} = 0$ m/s.	Static pressure, $0$ Pa, is imposed at channel outlet. $P_o = 0$ Pa

#### 4.4.3 Biochip fabrication

Biochips were fabricated using emulsion mask grayscale photolithography process (Lee and Mohamed, 2016). The biochip patterns were designed using CorelDraw X7. Due to the 5:1 shrinking rate of the mask fabrication equipment, the designed pattern was drawn 5 times larger than the original dimension. The percentage of grayscale concentrations were used to control the height of developed photoresist obtained after the UV exposure process. The designed grayscale mask was printed on a transparent polyethylene terephthalate (PET) film by using image setter technique. The printed transparent film was also known as master mask film. Then, a Simple Mask Fabrication Machine MM605 (Nanometric Technology Inc.) was used to project the image from the printed master mask film in a 5:1 reduction scale onto a High Precision Photo Plate (Konica Minolta, Inc.), also known as emulsion mask. The emulsion mask was coated with a light-sensitive silver halide. The entire mask exposure process was carried out in a dark room condition due to the high light sensitivity of emulsion mask. Prior to the emulsion mask exposure process, the silver halide coated surface was placed facing

towards the light source with the exposure time adjusted to 8 seconds. After the exposure process, the exposed emulsion mask was immersed into an emulsion mask developer at room temperature for 2 min. The emulsion mask developer was a mixture of 1 part of high-resolution plate developer (CDH-100) from Konica Minolta Opto, Inc. and 4 parts of distilled water. The immersed emulsion mask was stirred continuously to ensure uniform development process. During the development process, the previously exposed silver halide had formed a high optical density metallic silver that could be functioned as an excellent optical filter on the emulsion mask. Dark-field emulsion mask was created during the development process.

The substrate used was (3x1)-inch size microscopic glass slides (DURAN Group). Glass substrate was selected due to its transparent property in order to create 3D relief surface structure by using the back UV exposure method. The glass slides were first cleaned to remove surface contaminants by using an ultrasonic bath (GT sonic VGT-1613QTD) with acetone for 5 min, followed by an ultrasonic bath with methanol and isopropyl alcohol (IPA) each for 5 min before being rinsed with distilled water. Immediately after the surface cleaning process, 2 ml of SU-8 2010 photoresist (MicroChem) was dispensed and spread over the entire surface of the (3x1)-inch glass substrate to produce a 700  $\mu\text{m}$  thick SU-8 film. During this process, the coated SU-8 film was self-planarized. The resultants were a flat and uniform layer due to the surface tension and high mobility. The SU-8 coated glass substrate was soft baked at the temperature of 95 °C for 10 hours using a conventional oven. It was important to make sure that all the SU-8 coated samples were placed flat in the conventional oven as the gravity force may affect the flow of photoresist. The photoresist coated glass substrates were then exposed using one side mask aligner LA4100\_R1 (Sanei Electric Inc.) with back exposure method. The power density of the i-line (365 nm) mercury lamp was set to 180 W and the SU-8 coated glass substrates were exposed for 30 seconds. Post exposure bake was performed right after the UV exposure process. The exposed samples were first baked at a temperature of 65 °C for 2 min on a hot plate. Then the temperature of hotplate was gradually ramped up to 95 °C for 10 min. After 10 min of baking, the hot plate was switched off while the samples were still left on top. The samples were allowed to cool down slowly to a room temperature. This slow cooling process reduced stress built up in the cross-linked SU-8 and further avoiding cracking and deformation of patterns during the development process. The developing process was carried out by

immersing the exposed samples into SU-8 developer solution (MicroChem). An ultrasonic cleaner was used to enhance the development process. With the help of ultrasonic cleaning, the development process took only 2 min to completely dissolve all unexposed SU-8 photoresist from the glass substrate. After the first development, the developed samples were rinsed by using another batch of clean SU-8 developer solution, then followed by the IPA and distilled water. Finally, the developed samples were blown dry by using a stream of nitrogen gas. Fabricated biochips were shown in Figure 4.5 (b-d).

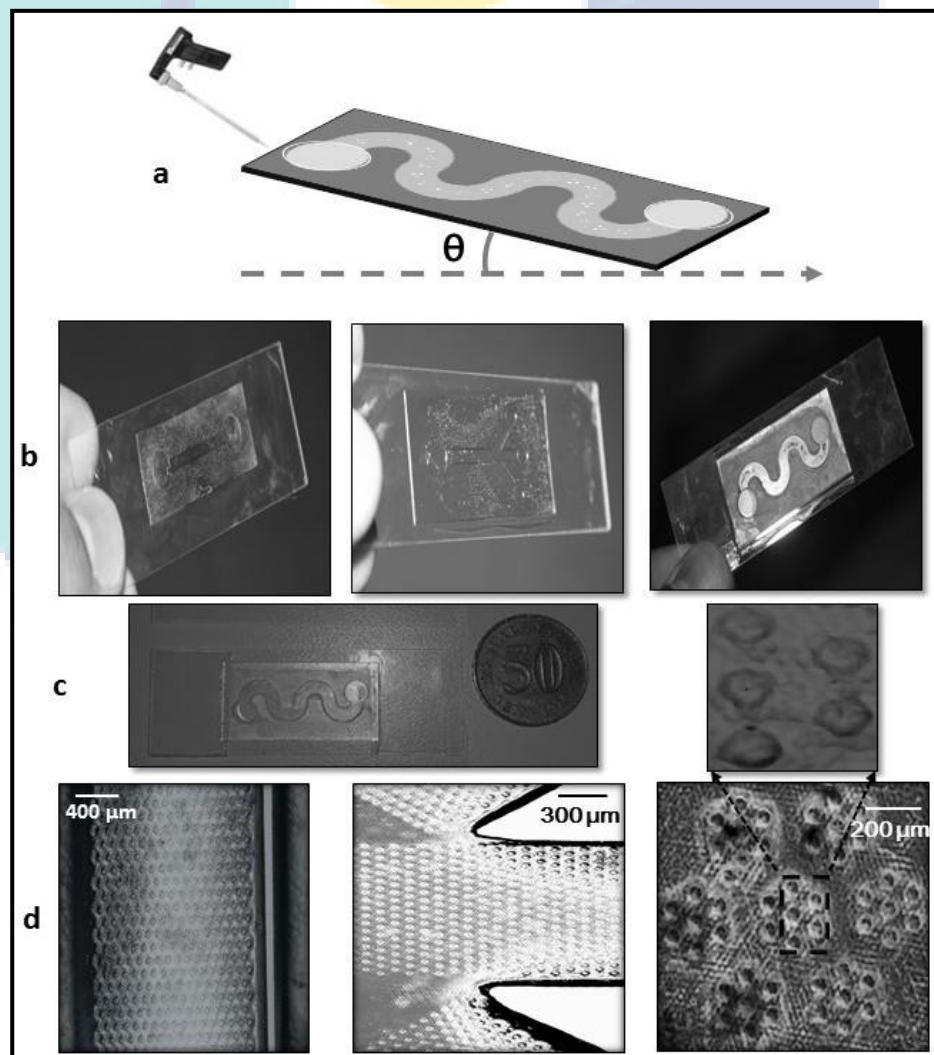


**Figure 4.5 Fabricated biochip and its operation**

Images showing (a) Illustration of biochip operation, where  $\theta$  corresponds to the tilt angle; (b) Fabricated biochips; (c) Biochip scale with a Malaysian 50 sen coin used as a reference and (d) Microwell array on fabricated biochip, images taken from InfiniteFocus measurement system (ALICONA).

#### **4.4.4 Microfluidic biochip for single cell trapping and cell viability test**

Prior to operation, the biochip was covered with a coverslip and sealed. Biochips were sterilized with 70% ethanol and UV for a few min before using. Once cells (A549) grown attained 80% confluency, they were trypsinized and centrifuged (Eppendorf 5810, USA) at 700 rpm for 5 min. Cells pallet was resuspended in complete growth media. 100  $\mu$ l cell suspension with a density of  $3.5 \times 10^4$  -  $7.5 \times 10^4$  cells/ml were mixed with Trypan Blue (Sigma-Aldrich, USA) and were pipetted down into the biochip, which was tilted at an angle of around 10-15° (achieved by placing biochip edge with inlet, on the side wall of the petri dish size brand) to enhance the fluid flow in the channel. Pipetting was done gently and slowly. After the fluid was drained out from the outlet and the channels were filled with fluid, the biochip was gently placed into a petri dish and incubated. During the transfer to the petri dish, caution was taken not to shake the biochip, as it may result in moving the cell out of the microwell before attachment. A hexagonal array of microwell was observed under a microscope (Leica DM 2000 LED) for its trapping and viability. Overall techniques were kept simple and not much complex process handling was done on the cells.

#### **4.4.5 Single cell fluorescent measurements**

In order to confirm the cell morphology and attachment of cells in biochip, fluorescent signals from single cells were captured. After loading cells, the biochip was incubated at temperature of 37° C under humidified atmosphere, with 5% CO<sub>2</sub> and 95% air for 3 hours for cells attachment. Once attached, the biochip was washed with PBS to fully remove remaining media. Cells were fixed with 4% paraformaldehyde (Sigma, USA) for 30 min and subsequently washed with PBS. For 5 seconds, cells were permeabilized using 0.1% Triton-X (Sigma, USA) prior to wash. Fixed A549 cells were dyed with DAPI (Sigma, USA) and Rhodamine Phalloidin (Molecular Probe, USA) for 10 min, washed subsequently and mounted with glycerol (Sigma, USA) for fluorescence imaging. Fluorescent images were taken by using a microscope (Nikon Eclipse TE 2000-S Tokyo, Japan).

#### **4.5 Fabrication of cell imprinted carbon polymer composite (CI-CPC)**

In this section described in detail the process involved in the fabrication of imprinted CPC.

#### 4.5.1 Fabrication of plain carbon polymer composite CPC

Plain CPC was prepared as described in section 4.3.2. This experiment was conducted to test the capability of the CPC to peel off without any deformations at the bottom surface.

#### 4.5.2 Fabrication of cell imprinted carbon polymer composite (CI-CPC)

Monolayer cell culture was preferred and once the cells cultured in 4 well glass slide (Nunc™ Lab-Tek™ II Chamber Slide™, ThermoFischer Scientific) attained a confluent state, media were pipetted out. By placing absorbent paper at all the four corners of each well, it was made sure that no solution was left at the glass slide. Then the glass slides were air dried for 5 min. Prepared CPM were pipetted over the cells in the glass slides. Based on the optimization, 250  $\mu$ l of CPM with concentration of (0.3 wt %) was applied and cured using UV light (100 W, 250–450 nm) for 7 min. Cured polymer was peeled off from the glass slide and washed in DI water to remove any debris or cell particles attached. The obtained polymer herein will be referred as cell imprint-carbon polymer composite (CI-CPC). The imprinting process is shown in Figure 4.6.

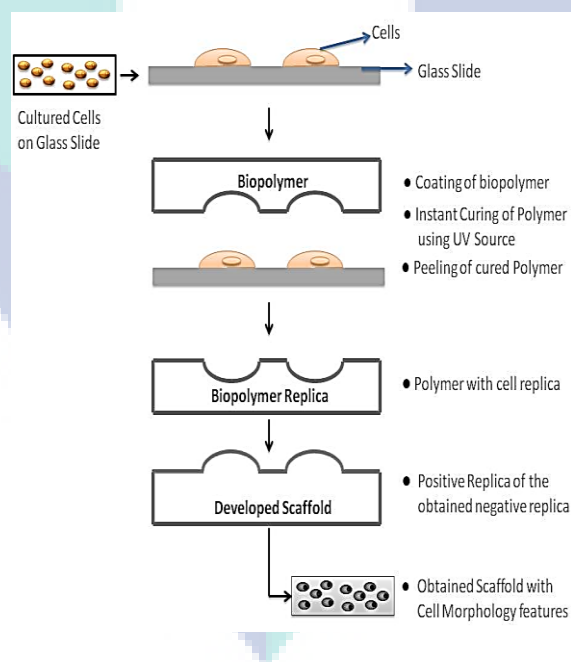


**Figure 4.6 Imprinting process**

This diagram describes the sequential step by step process involved in fabrication of cell imprinted carbon composite.

To facilitate the single cell imprinting capability, developed microfluidic biochip platforms were used. After 24 hours of incubation (time sufficient for cells (A549) to attach and spread) of cells trapped in biochip, bioimprinting process was performed. This process enabled the capture of single cells imprints.

#### **4.5.3 Scanning electron microscope imaging**

The fabricated polymer samples were imaged under SEM (Zeiss EVO 50, Germany). In order to image in SEM, the samples were stuck to stub using double sided carbon tape. Prior to imaging samples were stored in desiccator.

#### **4.6 Cell imprinted carbon polymer composites (CI-CPC) for cell diagnosis**

In order to evaluate the imprinting capabilities of the CPC for cell morphology based diagnosis, experiments were conducted on two types of cells, namely A549 and MCF-7.

##### **4.6.1 Bezoar extract preparation**

In preparing bezoar (BZ) extract stock solution, 100.0 mg of BZ powder were mix with 50.0 ml of hot distilled water and placed on hot plate stirrer (Lab Tech Daihan Labtech Co. Ltd, Japan) at speed of 1000 rpm, 60°C for 24 hours, until the solution colour changed from transparent into dusky grey solution. Then, the BZ extract solution was kept at room temperature for another 3 days before filtered with 0.22 µm syringe filter (Millipore, USA) to get a sterile stock solution which was kept in 4°C for storage. Working solution of BZ extracts was prepared fresh by diluting the stock solution with CGM prior being used.

##### **4.6.2 Vincristine sulphate solution preparation**

Vincristine sulphate (VC) powder (Sigma-Aldrich, USA) was dissolved in ultra-pure water to yield 50 mg/ml clear and colourless solution of stock solution. Working solution of VC was prepared fresh by diluting the stock solution with CGM prior use.

##### **4.6.3 Experiments on A549**

Two sets of experiments were performed on A549, one with the VC and another with BZ. For A549 VC experiment, A549 cells were seeded with  $1.0 \times 10^3$  cells/ml of

cell density in four well chamber slides for 24 hours of incubation. After 24 hours of seeding, cells were observed for their confluency, attachment to flask and morphology. Media was discarded with pipette pump (Eppendorf, Germany), and cells were washed with PBS twice, then 1 ml fresh CGM with 10 ng/ml of VC was added prior incubation at 37 °C, 5% CO<sub>2</sub>. Once reached the incubation period of 24 hours, media was discarded from the well and washed with PBS 3 times gently. Then CPC imprinting was performed as mentioned in previous section to obtain CI-CPC replica which was imaged under SEM.

For A549 BZ experiment, A549 cells were seeded with  $1.0 \times 10^3$  cells/ml of cell density in four well chamber slides for 24 hours of incubation. After 24 hours of seeding, cells were observed for their confluency, attachment to flask and morphology. Media was discarded with pipette pump, and cells were washed with PBS twice, and then 1 ml of fresh CGM with 20.0 µg/ml of BZ extract was added prior incubation at 37 °C, 5% CO<sub>2</sub>. Once reached the incubation period of 72 hours, media was discarded from the well and washed with PBS 3 times gently. Then CPC imprinting was performed to obtain CI-CPC replica which was imaged under SEM.

#### **4.6.4 Experiments on MCF-7**

For MCF-7 BZ experiment, MCF-7 cells were seeded with  $1.0 \times 10^3$  cells/ml of cell density in four well chamber slides for 24 hours of incubation. After 24 hours of seeding, cells were observed for their confluency, attachment to flask and morphology. Media was discarded, cells were washed with PBS twice, and then 1 ml of fresh CGM with 20.0 µg/ml of BZ extract was added prior incubation at 37 °C, 5% CO<sub>2</sub>. Once reached the incubation period of 72 hours, media was discarded from the well and washed with PBS 3 times gently. Then CPC imprinting was performed to obtain CI-CPC replica which was imaged under SEM.

#### **4.6.5 Comparative interpretation on various imaging modalities**

After cells were exposed to treatments, three set of observations were made using three different imaging modalities known as optical observation, fluorescent imaging observation and SEM replica observation. For optical microscope observation, after treatment, the cells were observed under optical microscope. For fluorescent imaging observation, after treatment, the cells were fixed and fluorescent stained as explained in section 3.3. For SEM CI-CPC observation, after cell treatment CPC imprinting was performed to obtain CI-CPC replica which was imaged under SEM. These experiments



were performed to compare the information extraction through three modalities and to correlate the data for further investigations.

#### 4.7 Cell morphology feature detection

The cell-imprint replica images were further processed for feature detection. Image processing algorithm were used with series operations like region of interest selection, RGB to colour plane extraction, edge detection and feature detection, which is shown in Figure 4.7. This diagram depicts the series of step by step process involved in the image processing. Region of interest was used to specify the interested regions of the image. It was then followed by colour plane extraction and in this process green plane was used as it contained the needed information. Canny edge detection algorithm was used as it is one of the methods that provide good and reliable detection. It becomes one of the most popular algorithms for edge detection.(Chou et al., 2002) The program was designed in National Instruments LabVIEW Vision 2014, which can autonomously detect the features.

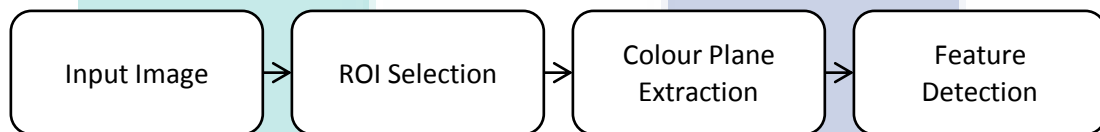


**Figure 4.7 Series of image processing steps for feature detection**

A region of interest (ROI) is a selected subspace of the input sample image. In the wide variety of applications the ROI selection plays a vital role such that, in medical imaging the boundaries of the tissues and the tumour regions was segmented. Different dimensions of the data sets can be viewed, for example the 2D dataset provides the boundaries of the image, and 3D dataset provides the contours outlining the object. The edges can be extracted by means of several algorithms in the image processing. The algorithms may differ for both colour images and the gray scale images. In general, for the colour images the geometrical clustering was used to extract the region of interest and for the greyscale images, canny operator is the best technique for the extraction of edges. The feature extraction from the raw image can be done by the colour plane extraction. This can be done in two ways. One method converts the colour image to the greyscale image and by using bit plane technique, the different intensities of the input image can

be extracted. The other method considers the original colour image and by using different colour models, the features were extracted. The number of planes may vary depend upon the input and the application. The hierarchical models are used to extract the colour planes in the previous works. Incorporating the images with the models and the gathered data provides the plane extraction. In general the algorithms such as probabilistic models, Expectation maximization can be used to extract the features.

To examine an image, the feature detection algorithm was adopted. The geometrical features, textural features were considered in the feature detection. Some of the features were edges, corners, ridges. The edges were the features which can describe the structural properties. The local two dimensional structures were described by the corners. A ridge descriptor computed from a grey-level image could be seen as a generalization of a medial axis and a ridge can be thought of as a one-dimensional curve that represented an axis of symmetry, and in addition has an attribute of local ridge width associated with each ridge point. Blobs provided a complementary description of image structures in terms of regions. The primary purpose of the edge detection was the reduction of dataset in the input image and also the structural properties of the image could be extracted. The edges characterized the boundaries of the image, as well as the structural property or the boundaries as the important tool for the diagnosis of such problems. Many algorithms such as sobel, prewitt, Robert algorithms are used for the edge detection but this operator is the prominent operator for the edge detection and known as optimal edge detector (Shrivakshan and Chandrasekar, 2012, Canny, 1983). This algorithm consisted of the basic steps such as smoothing the image in order to remove the noise, finding the gradients to highlight the regions with higher order derivatives, and the pixels with minimum value was suppressed by non-maximum suppression, double thresholding and the remaining pixels was tracked by the edge tracking.

Gaussian filter equation kernel of size  $(2k+1) \times (2k+1)$  is given by:

$$H_{ij} = \frac{1}{2\pi\sigma^2} \exp\left(-\frac{(i-k-1)^2 + (j-k-1)^2}{2\sigma^2}\right) \quad (4.1)$$

The edge detection operator (Roberts, Prewitt, Sobel) returns a value for the first derivative in the horizontal direction ( $G_x$ ) and the vertical direction ( $G_y$ ), which can be used to determine the edge gradient and direction.

$$G = \sqrt{(G_x^2 + G_y^2)} \quad (4.2)$$

$$\theta = \text{atan2}(G_y, G_x) \quad (4.3)$$

where  $G$  can be computed using the hypot function and  $\text{atan2}$  is the arctangent function with two arguments.

#### **4.8 In-vitro study of polymer composites for biomedical applications**

*In-vitro* methods for assessing cytotoxicity and cytocompatibility have become popular due to its fast, reasonable result and low cost. Polymer was evaluated for cytotoxicity and cytocompatibility by various methods as described below. Cytotoxicity is the quality of being toxic to cells. Measurement of cytotoxicity assays was performed to determine toxicity nature of the compounds. Assessing cell membrane integrity is one of the most common ways to measure cell viability and cytotoxic effects. Compounds that have cytotoxic effects often compromise cell membrane integrity (Riss and Moravec, 2004).

##### **4.8.1 Sample preparation**

Polymer composites after peeling out from glass slide were processed for cytotoxicity analysis. Since the samples were acidic in nature, they were neutralized by washing with 0.1N NaOH followed by thorough rinsing with PBS. Then samples were sterilized by 70% ethanol and washed thrice with culture medium prior to test.

##### **4.8.2 Cytotoxicity studies**

Cytotoxicity of polymer was analyzed by direct contact and tested on extract assays.

#### **4.8.2.1 Direct contact**

L929 cells were harvested using trypsin–EDTA solution and seeded in 24 well plate at a cell density of 30,000 cells/well and maintained till confluent. 4 mm piece of polymer was placed carefully over the subconfluent monolayer of cells and incubated for 24 hours. After 24 hours, cytotoxicity was evaluated as per ISO 10993-5 standard and graded under inverted phase contrast microscope. In order to visualize viable cells the monolayer was stained with neutral red solution (0.5% in physiological saline) for 15 min.

#### **4.8.2.2 Test on extract**

Polymer was extracted using culture media at 37°C for 24 hours at an extraction ratio of 3 cm<sup>2</sup>/ml. Extraction at different concentration were placed on subconfluent monolayer of cells seeded in 96 well plate. 100% extracts were diluted with culture medium to get 50% and 25% concentrations. Diluted phenol and high density polyethylene (HDPE) were considered as positive and negative control respectively. Different dilutions of test sample extracts, positive control and 100% extracts of negative control in triplicate were placed on subconfluent monolayer of L-929 cells. After incubation of cells with extracts of test sample and controls at 37 ± 1°C for 24 to 96 hours, cell cultures were examined microscopically for cellular response and graded as per ISO10993-5 standard under inverted phase contrast microscope. MTT assay was also done after cytotoxicity evaluation of test sample. Culture medium was removed and 50 µl (1 mg/ml in medium without supplements) was added and incubated for 2 hours. After 2 hours formazan crystals were solubilised using 100 µl of isopropanol and activity was read at 570 nm using spectrophotometer (Biotek, USA)

#### **4.8.3 Cytocompatibility studies**

Cytocompatibility studies were evaluated using MTT assay, live dead analysis, and actin-phalloidin staining.

##### **4.8.3.1 Cell adhesion**

L929 cells were sub cultured and seeded at a density of 1x 10<sup>4</sup>/cm<sup>2</sup> on top of the materials and incubated for 48 hours. The test materials after 48 hours of cell adhesion were analyzed for live –dead staining. Percentage metabolic activity was quantified by

MTT assay and samples were fixed in 4% paraformaldehyde for actin phalloidin staining. Cells cultured in glass cover slip were considered as control.

#### **4.8.3.2 Live dead analysis**

Briefly the medium was removed from cell culture plates and cell monolayer was stained with fluorescein diacetate (FDA) from Sigma Aldrich (10 µg/ml) for 15 min and subsequently by propidium iodide (PI) from (High Media) for 1 min and examined under inverted fluorescence microscope immediately (exit/emis I3/N21 in Leica DMI 6000E).

#### **4.8.3.3 Cytoskeleton analysis**

Cell cytoskeleton was observed using actin-phalloidin staining, and cell monolayer after fixation was rinsed with PBS thrice and permeabilised cells using 0.1 % Triton X-100 (in PBS) (Sigma) for 1 min followed by washing with PBS thrice. Cells were then stained with 1 : 100 diluted rhodamine conjugated phalloidin (Invitrogen) staining for 15 min and nucleus was counter-stained with Hoechst 33428 (Sigma) for 1 min and visualized under inverted fluorescence microscope (exit/emis A/N21 in Leica DMI 6000E)

#### **4.8.3.4 Cell adhesion with MTT assay**

Samples after cell adhesion were rinsed thrice with medium and 400 µl of MTT solution (1 mg/ml MEM without serum) was added and incubated for 2 hours. After 2 hours the formazan crystals formed were solubilised by 800 µl of isopropanol and transferred to a 96 well plate, absorbance was read at 570 nm using UV/visible spectrophotometer (Biotek, US). The data were analyzed statistically. Cell activity was determined by the below mentioned formula.

$$\text{Cell activity (\%)} = \frac{OD \text{ test cells}}{OD \text{ control cells}} \times 100 \quad (4.4)$$

## CHAPTER 5

### RESULTS AND DISCUSSIONS

#### 5.1 Carbon-polymer composite imprinting

In this section, the characterization and process optimization results of CPC imprinting were provided.

##### 5.1.1 Carbon nanoparticle characterization

Prepared carbon nanoparticle were investigated by SEM and TEM at different magnifications to characterize the morphology of the CNP. Figure 5.1 presents the SEM micrographs of CNP. Figure 5.2 presents the TEM micrographs of CNP at various magnifications. Shape, size and surface morphology of CNP from observations revealed the grape-like agglomerates. Each particle with average diameter size range of between 25-35 nm. Results matches with the earlier characterization report made by (Marinho et al., 2012).

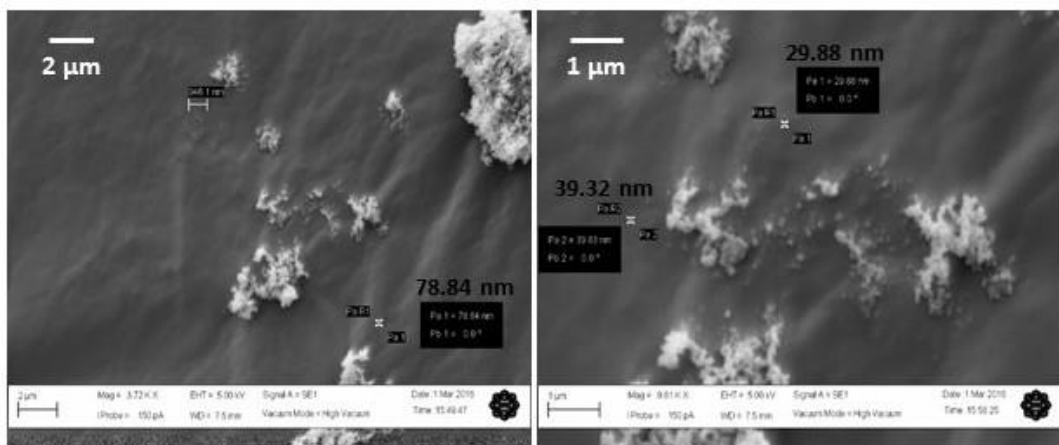


**Figure 5.1** CNP SEM characterization

Pictograph showing CNP under SEM.

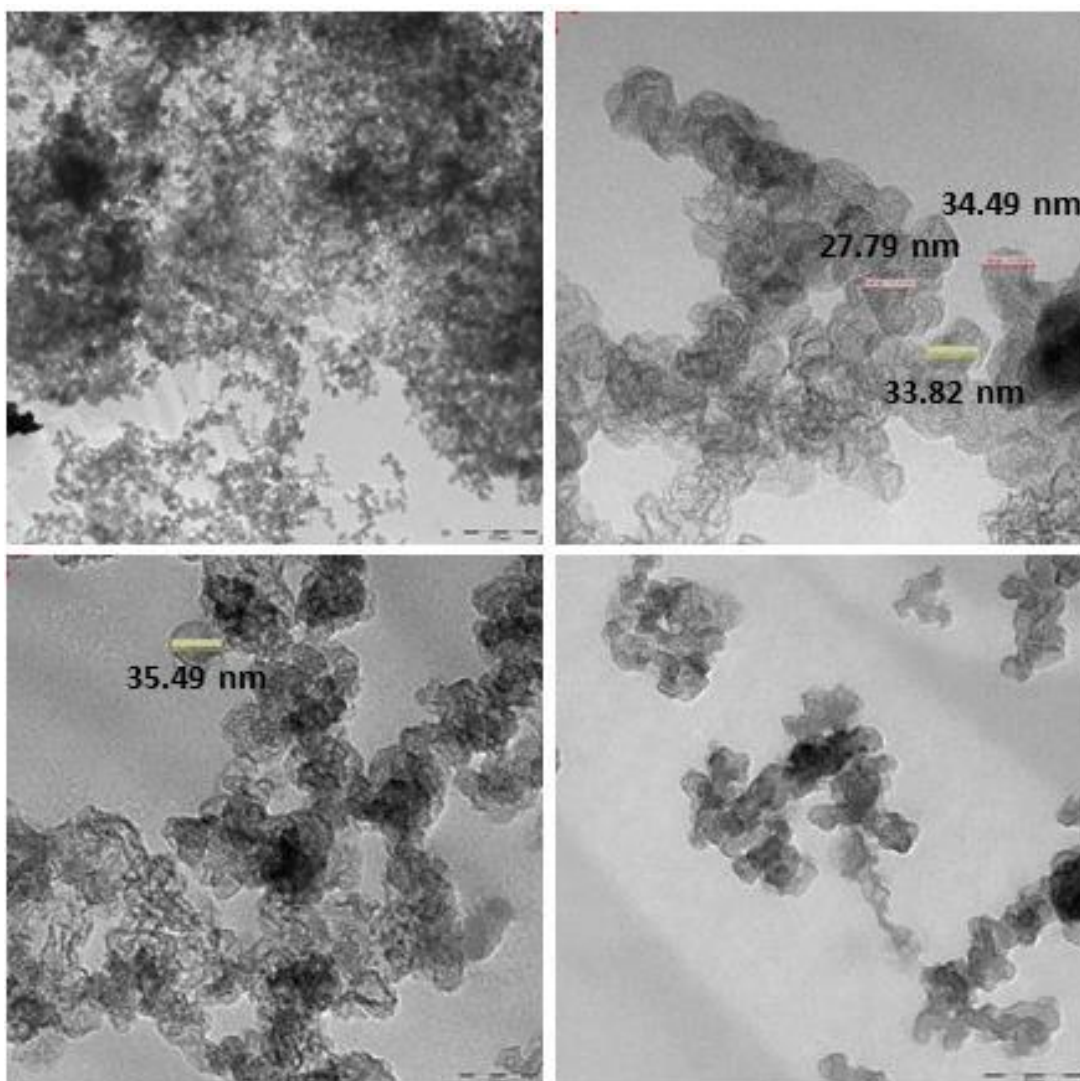


**Figure 5.2 CNP TEM Characterization**

Pictograph showing CNP at various magnifications under TEM.

### **5.1.2 Carbon-polymer mixture preparation and optimization**

From CNP characterization results, it is clear that the CNP were in agglomerates form. Agglomerates are held by weak Vander-walls force, which can be easily separated using ultrasonication. CNP was mixed initially with triglyme and ultrasonicated. Mixing of CNP directly with the polymer mixture composition was avoided, as the solutions may tend to react (during the ultrasonication and storage) and may produce different results. CPM was prepared instantly for efficient polymerization and repeatability. As the CNP loading wt % were increased gradually in CPM, at certain point the imprinting capability of the polymer was lost which will be termed as Imprinting Threshold (IL). Figure 5.3 shows the relation between filler wt % and imprinting capability.

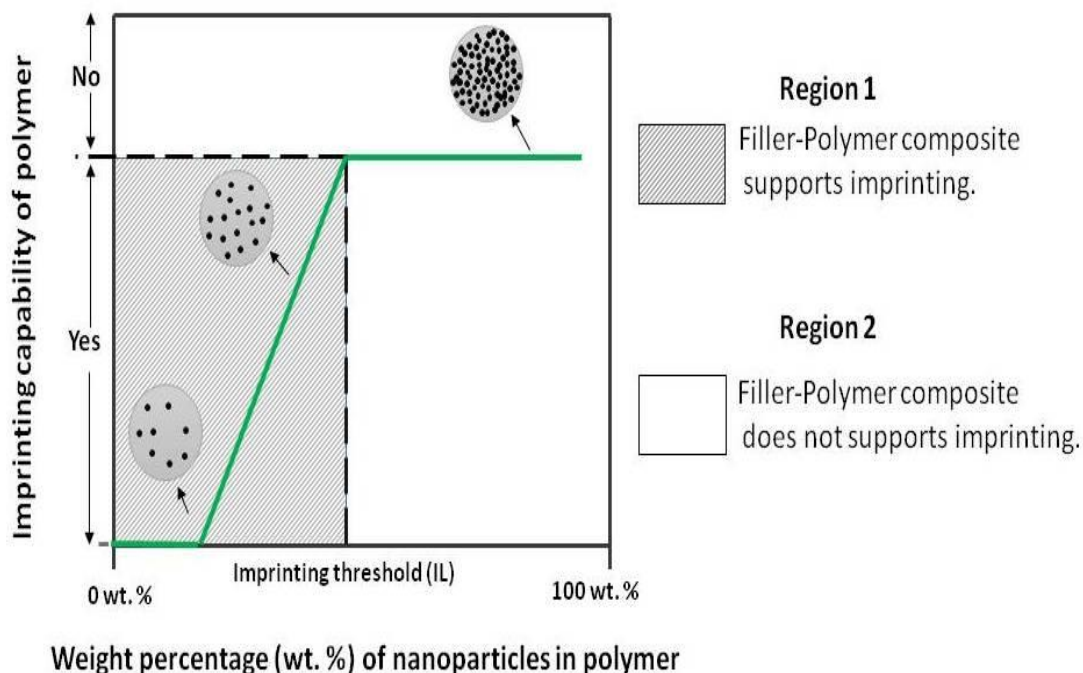


**Figure 5.3 Filler wt % vs imprinting capability of the polymer**

It was observed that beyond 0.3 wt % CNP in CPM, imprinting capability of the polymer was lost. This indicated that the IL of the CPM was 0.3 wt %. CPC's were observed to be more brittle as the CNP wt % increased. Optimization was performed by considering two factors which were CNP wt % and CPM volume. Based on the optimization study, among N-CPC, 1-CPC, 2-CPC, 3-CPC, 4-CPC and 5-CPC, 250  $\mu$ l of 3-CPC (concentration 5.06 mg/ml of CNP in polymer mixture) in each chamber of 4 chamber slide produced best results in terms of proper polymerization, rapid curing time and proper peeling off after curing for the minimal applied volume without any damage or distortions at the bottom surface. After the polymerization, a small temperature rise was observed which was felt by finger touch at bottom of the glass slide. This result indicates the reaction to be exothermal.

### 5.1.3 Photopolymer effect and cell cytoskeleton study

#### 5.1.3.1 Polymer-cell response

From the cell reaction to the photopolymer experiment, evidence reveal that there were no sign of abnormal morphological changes nor sign of cell death, thus indicating



that the cell morphology were preserved during the process. Figure 5.4 shows the images of the cell reaction to photopolymer.

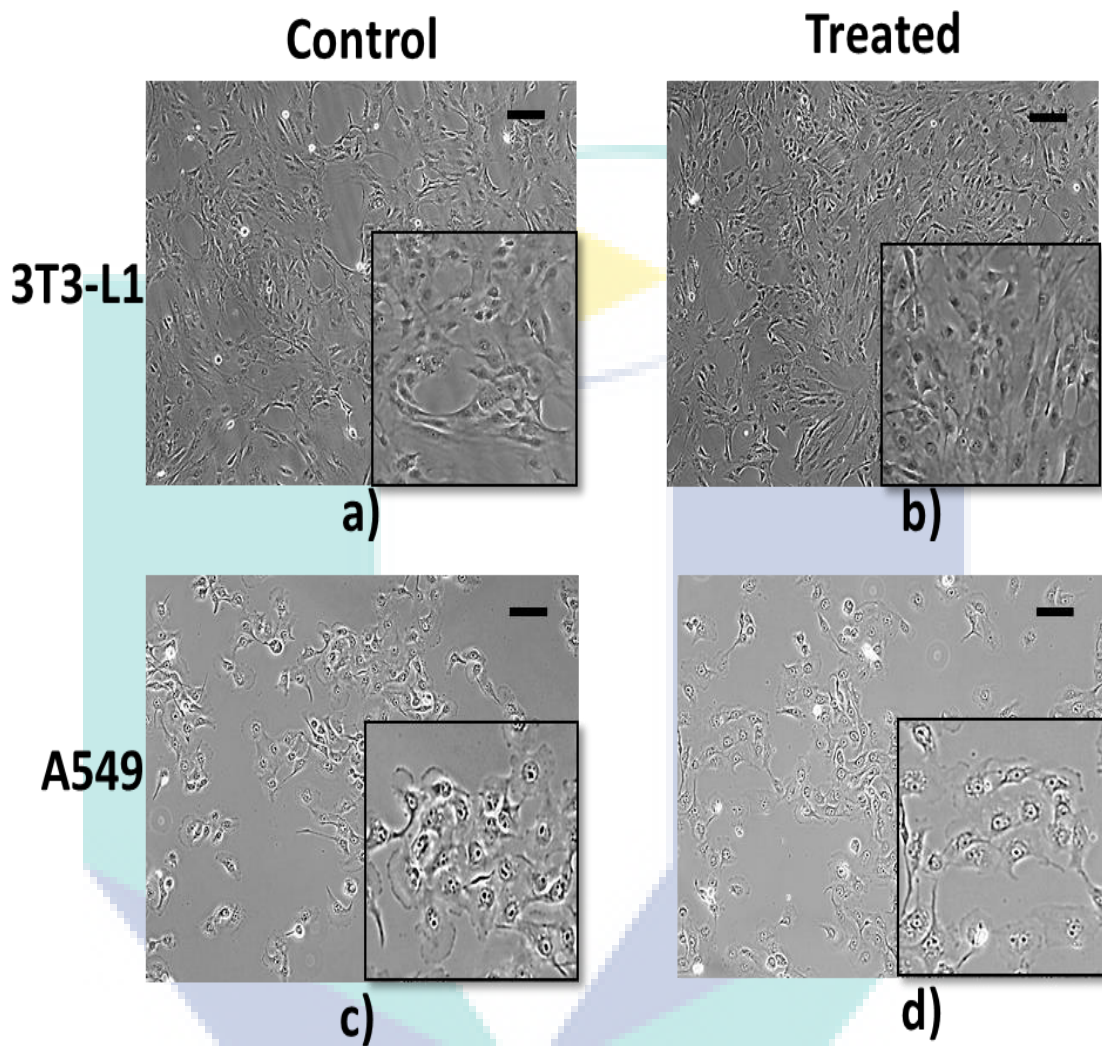


**Figure 5.4 Polymer-Cell response**

(a),(b) show the morphology of 3T3-L1 cells unexposed and exposed to polymer respectively; (c),(d) show the morphology of A549 cells unexposed and exposed to polymer respectively; it is evident that there was no significant change in morphology due to polymer. Scale bar is 50  $\mu\text{m}$ .

### 5.1.3.2 Bioimprinting effect to cells

Evaluation of cell morphology after the process of bioimprinting showed that the cell morphology was still preserved. Figure 5.5 shows the comparative images of the cell morphology after the bioimprinting process respectively. Figure 5.6 shows the effect of

imprinting on cell morphology under fluorescence microscopy. It can be seen that the extracellular morphology details of the cells were preserved.

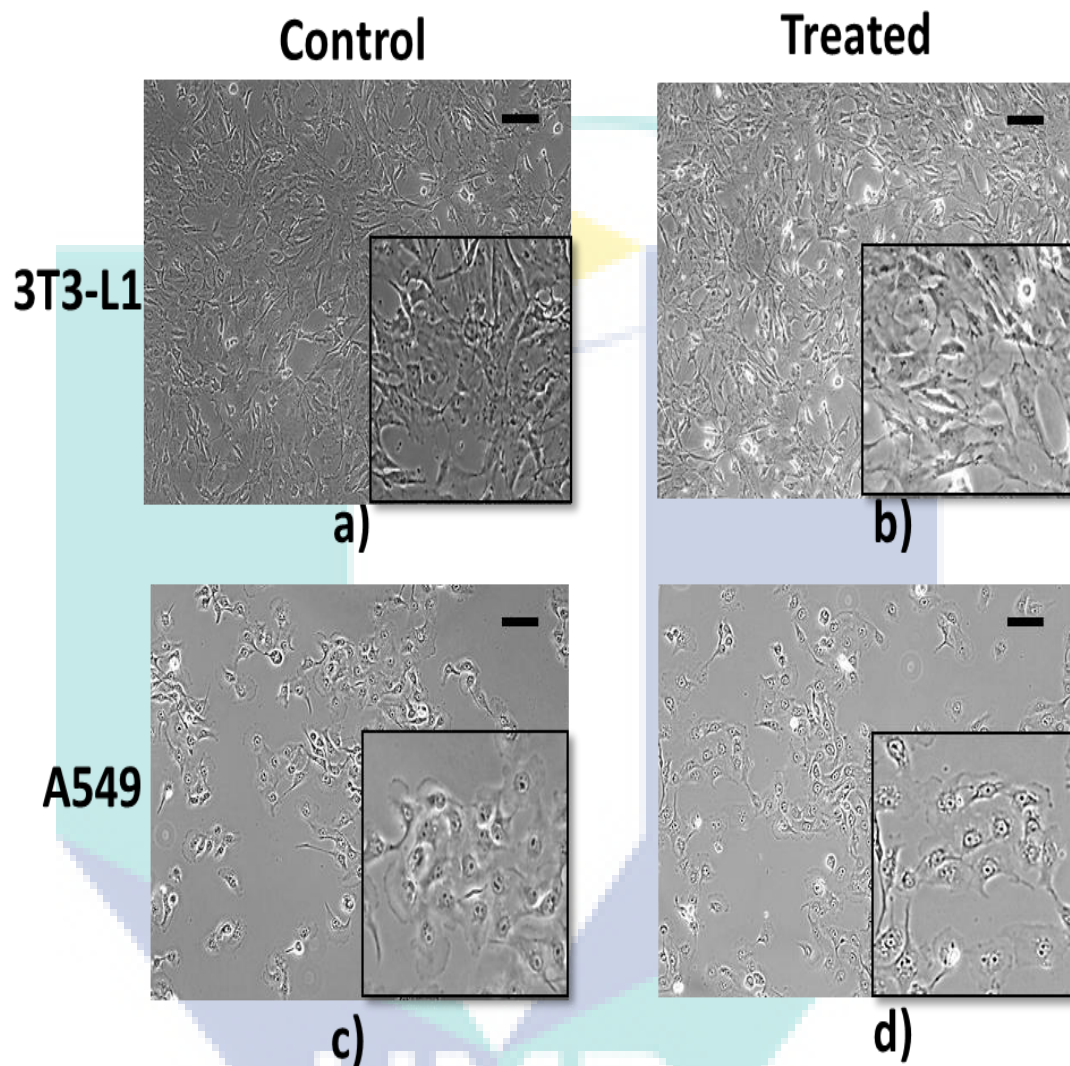


**Figure 5.5 Bioimprinting effect to cells**

(a),(b) show the morphology of 3T3-L1 cells control and after bioimprint process respectively; (c),(d) show the morphology of A549 cells control and after bioimprint process respectively. Evidences show that there is no change in morphology after the bioimprint process. Scale bar is 50  $\mu\text{m}$ .

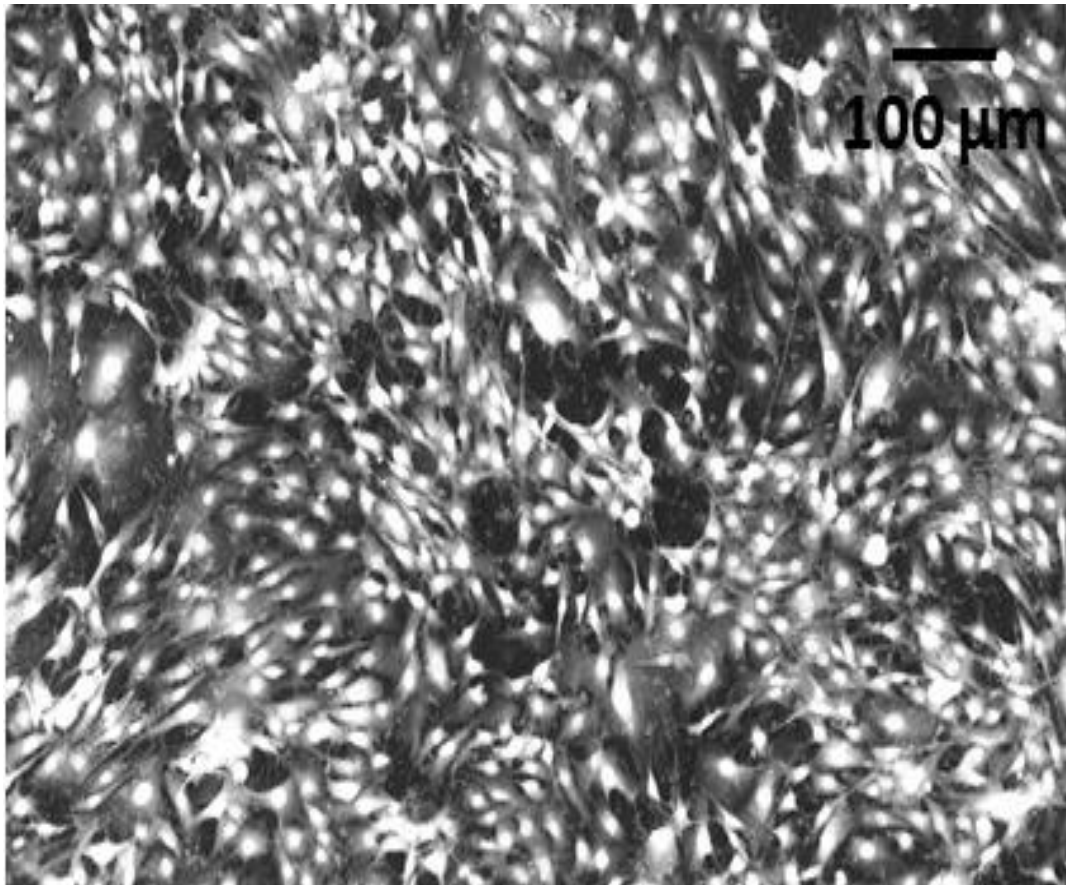


**Figure 5.6** Fluorescent imaging of bioimprinting effect to cells morphology

Fluorescent pictograph shows the cell morphology of 3T3-L1 cells at the bottom of the glass slide after peeling off from the composite when polymerized. This shows that the morphology were unaffected and preserved during the process.

#### **5.1.4 Carbon polymer composite (CPC) electrical resistivity measurement**

Due to doping of CNP, the electrical resistivity of the CPC was changed. Changes in electrical resistivity of the CPC were measured and presented. The resistivity of the polymer was decreased as the CNP wt % was increased. As shown earlier (literature review chapter) in Figure 2.8, it can be clearly seen that after the percolation threshold ( $p_c$ ), resistivity dropped drastically. Addition of CNP can be tailored based on the resistivity requirement of the polymer. Figure 5.7 shows the resistivity change for various load of CNP wt % of CPC. It can be seen that resistance were significantly reduced when compared to N-CPC.

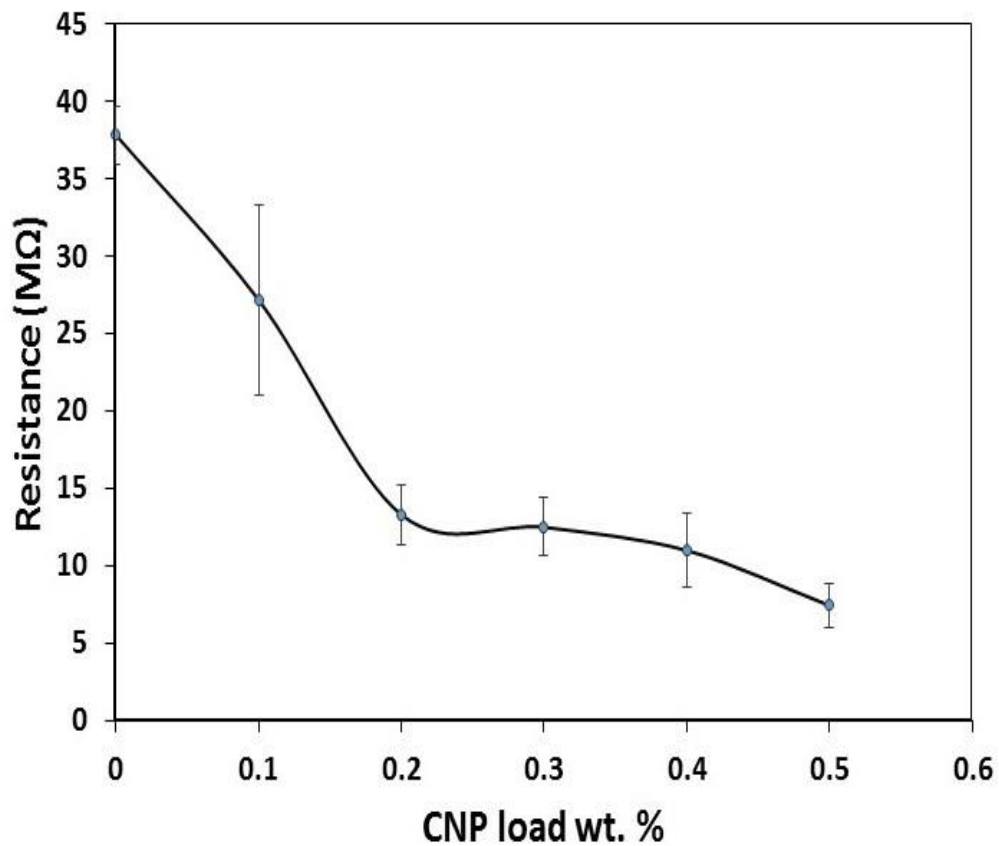


**Figure 5.7 CNP load wt. % vs resistance of CPC**

Figure shows CPC resistance for load CNP filler wt. %. Data represents means  $\pm$  SD of the triplicates.

## 5.2 Passive hydrodynamic microfluidic biochip platform

To facilitate single cell replica fabrication, microfluidic biochip platforms were designed and used. Results obtained for microfluidic biochip platform has been presented below.

### 5.2.1 Microfluidic design simulation study

Serpent channel has better dispersed velocity profile when compared to other two designs. Velocity was higher at the middle and slowed at the edges of the serpent channel. The dispersed velocity profiles provided varying probability for a single cell to be trapped while avoiding equal probability, thereby reducing multiple cell trapping. Figure 5.8 shows the simulation results of the biochip.

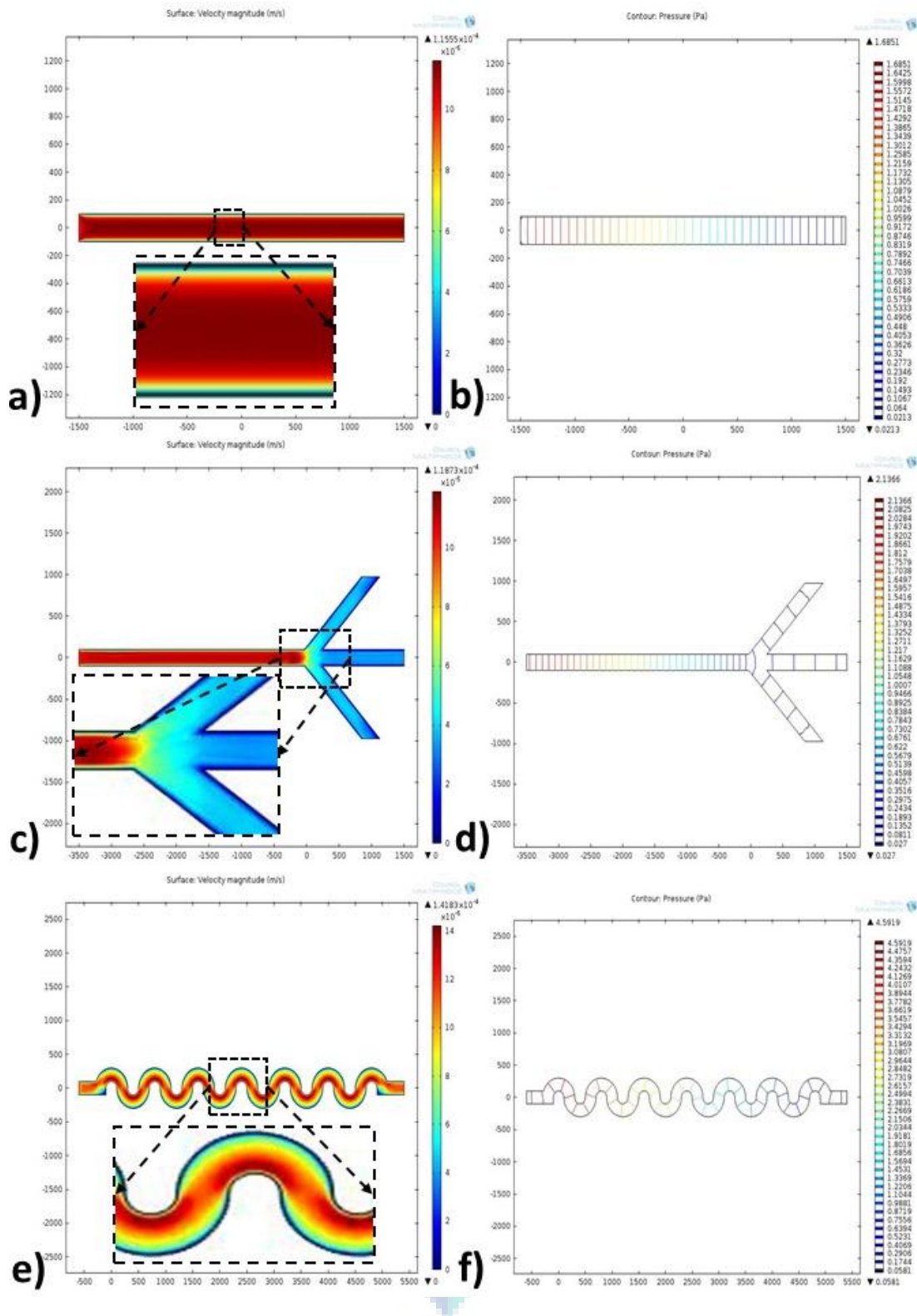


**Figure 5.8 Microfluidic design simulation study**

(a, c, e) Velocity profile in three fluid channels, insets show the close-up view and  
 (b, d, f) Contour plot of pressure in three fluid channels.

### 5.2.2 Microfluidic biochip for single cell trapping and design analysis

Observations from the three biochip designs revealed that the single cell trapping was more in serpent shaped biochip followed by branched channel design and straight channel design. In serpent design, SCC was higher and multiple cell capture (MCC) was less when compared to other two designs (shown in Figure 5.9 and Figure 5.10).

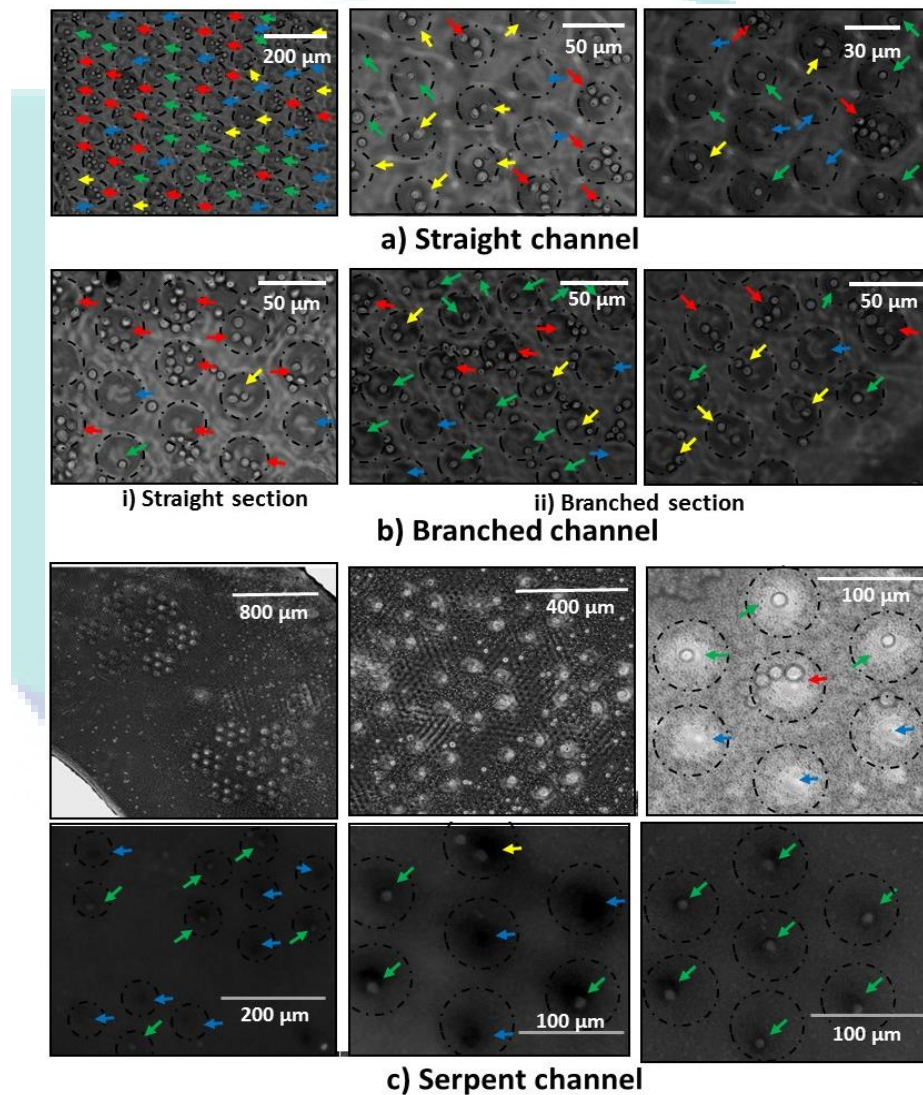


**Figure 5.9** Single cell trapping in three biochips

Trapped A549 cells in (a) straight channel design, (b-i) straight section in the branched channel design, (b-ii) side branched section in the branched channel design, and (c) serpent channel design. The blue arrow points to no capture, green arrow points to SCC, the yellow arrow points to dual cell capture and the red arrow points to three or more cell capture. Dotted black circles were just for clear; it did not resemble the exact scale with the biochip.

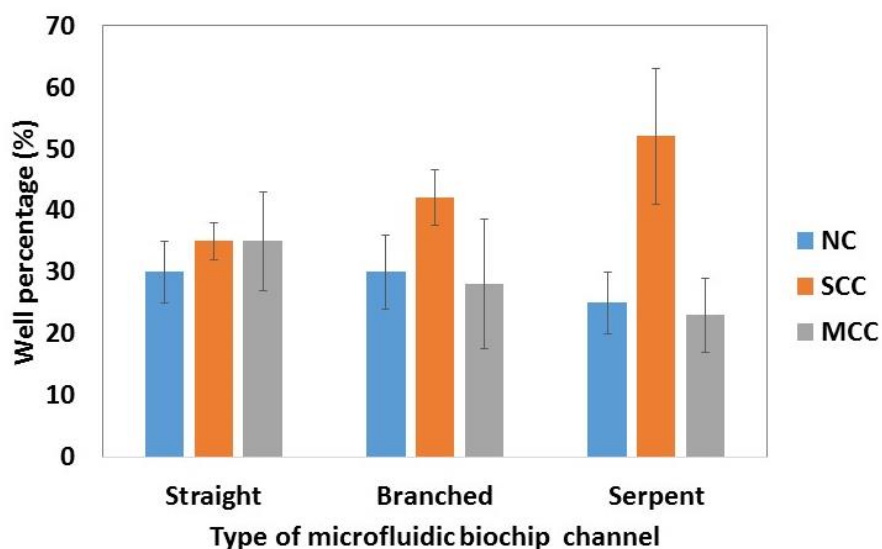


**Figure 5.10 Microfluidic biochip trapping capabilities**

Cell trapping capabilities of three channel designs with comparison of no capture (NC), SCC and MCC based on the study conducted. It can be seen that in serpent design NC and MCC were least, SCC was maximum with comparison to others. Error bars show the standard deviation.

### 5.2.3 Cell viability

It is evidenced by the results that viable A549 cells were trapped in microwells. The cells observed were shining as the cells did not take up trypan blue (shown in Figure 5.11 (a-c)). If cells were dead it will take-up the trypan blue. Almost no dead cells were observed.

### 5.2.4 Single cell fluorescent measurements

Single cell fluorescence signals were observed. Results revealed that the A549 cells were not damaged and had intact morphology. DAPI (blue) signal from the nucleus and Rhodamine Phalloidin (red) signal from filament actin, which holds the cytoskeleton of the cells were captured in the images. These results confirmed that the cells showed attachment at the bottom of the microwell as shown in Figure 5.11 (d and e)).

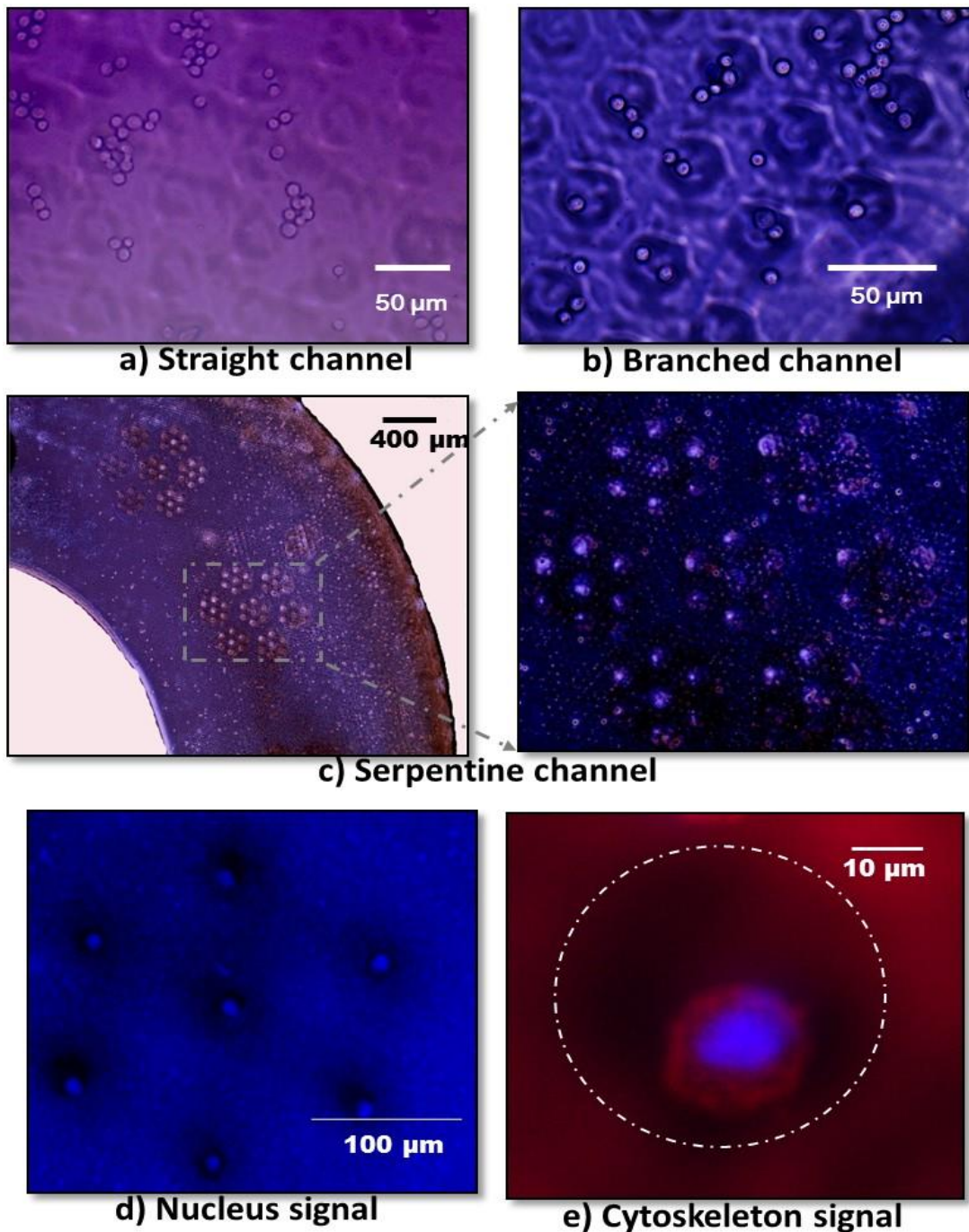


**Figure 5.11 Cell viability and cytoskeleton study**

(a-c) show cell viability test (cells did not take up the trypan blue) on straight channel, branched channel, and serpent channel respectively; (d) fluorescence signal from the nucleus (DAPI) of single cells being captured in serpent channel and (e) single cell cytoskeleton (fluorescence image) after 3 hours of incubation for serpent channel biochip, blue signal from nucleus (DAPI) and red from actin (Rhodamine Phalloidin).



Conventional approaches to cell trapping involved auxiliary systems supported microfluidic platforms which added to the complexity, lab space and cost. Mostly the developed approaches involve experienced handling and others involved application and exposure to electric fields and magnetic fields. The method which does not require experienced handling is in great demand. These biochips can be used in the environment where access to any external forces or electric source is absent. The system consisted of four parts: inlet reservoir where the cell suspension was introduced, main channel, microwells patterned on the bottom surface of the main channel, and the outlet reservoir. As the system was not supported by any auxiliaries, the platform was tilted to an angle of around 10-15° to assist the fluid flow. Furthermore, this biochip did not caused harm to the cells which were proven through the viability tests. Comparative summarizations of simulated and experimental results are shown in Table 5.1.

**Table 5.1 Comparative interpretation of simulation and experimental results**

<b>S.No.</b>	<b>Channel design</b>	<b>Simulation results</b>	<b>Experimental results</b>
1	Straight channel	No change in flow trajectories throughout the channel	No change in trapping efficiency throughout the channel
2	Branched channel	Change in flow trajectories at branched section curing	SCC was improved at branched section.
3	Serpentine channel	Varying trajectories throughout channel	SCC was improved significantly

From the results, it was revealed that the geometry of fluid channels affected the trapping rate and efficiency of SCC rate. There were more possibilities for trapping multiple cells in the straight and branched channel. This was because when cells traveled over any regions of the straight or branched channel they travel nearly the same distance, speed, and trajectory profile to the well, providing high chances of multiple cells being trapped anywhere in the channels. In the branched channel after the branch section, cell trapping was found to be better. This is due to the varying trajectory profile at the branched section of branched channel.

On the contrary, the serpent channel with hexagonal microwell array provided efficient single cell trapping possibilities. This was due to varying trajectories of the flow in the channel. This enabled the cells to travel in the varying trajectory path with less clumpy, thereby providing high SCC with least MCC. Achieving high SCC with no or minimal MCC would be great if that demand could be achieved without involving specialized and no auxiliary equipment would definitely add to the upside. Single cell fluorescent images revealed that the cell morphology was intact, which would be suitable for short-term investigation of a single cell.

Thus, these observations acted as design guidelines for the hydrodynamic-based passive biochips to achieve higher SCC. Factors that most likely to affect the cell occupancy were listed, (1) shape of the channel, (2) size, positioning, and orientation of microwells, (3) size of the cells, (4) the cell concentration, (5) biochip tilt angle, (6) pipetting out rate and pipette angle. These factors must be considered when designing hydrodynamic-based microfluidic biochip for high SCC.

Apart from using this microfluidic biochip platform for cell imprinting, it has a wide application in SCA which is also another popular research topic. Advantages of using vertical cell trapping when compared to lateral trapping are that the cell analytes can be treated or measured individually without clump analyte measurement. In a vertical well, single cell analytes are preserved separately for analysis as an analogy to the conventional 6 well or 96 well plate. This technique enables the real-time observation of single cell measurements for analysis as well.

### **5.3 Fabricated carbon polymer composite (CPC)**

The surface topography results of fabricated CPC are described below in detail.

#### **5.3.1 Fabricated plain carbon polymer composite**

Results from surface topography of plain CPC revealed that the CPC can be peeled off without any distortions or damages at the bottom surface. If damages were caused while peeling, it would affect the cell replica morphology imaging. Figure 5.12 shows the plain and smooth bottom surface after peeling off from the polymer composites.

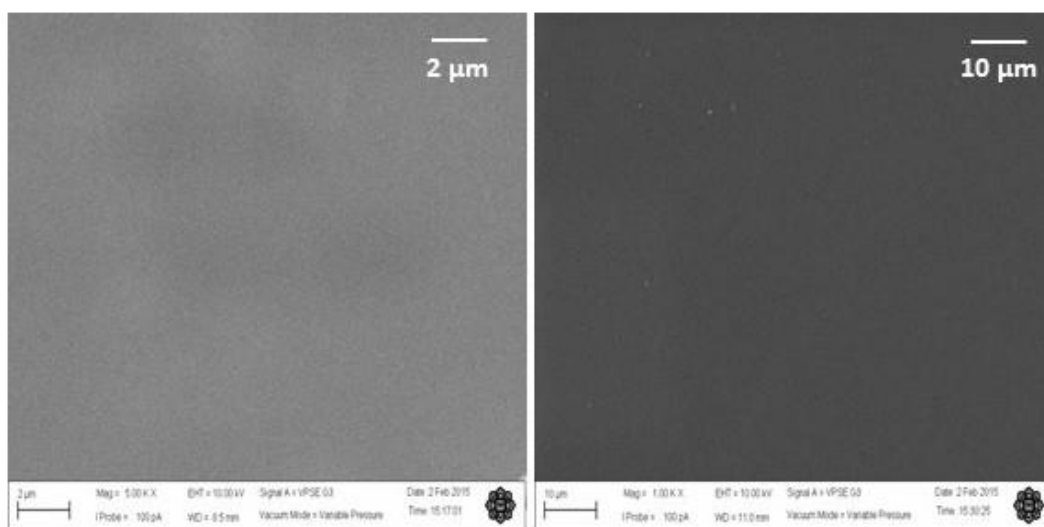


**Figure 5.12 CPC showing plain and smooth bottom surface after peeling off**

This image shows that the CPC were peeled off without causing any distortions at the bottom surface. Two images show bottom surface at various resolution scales.

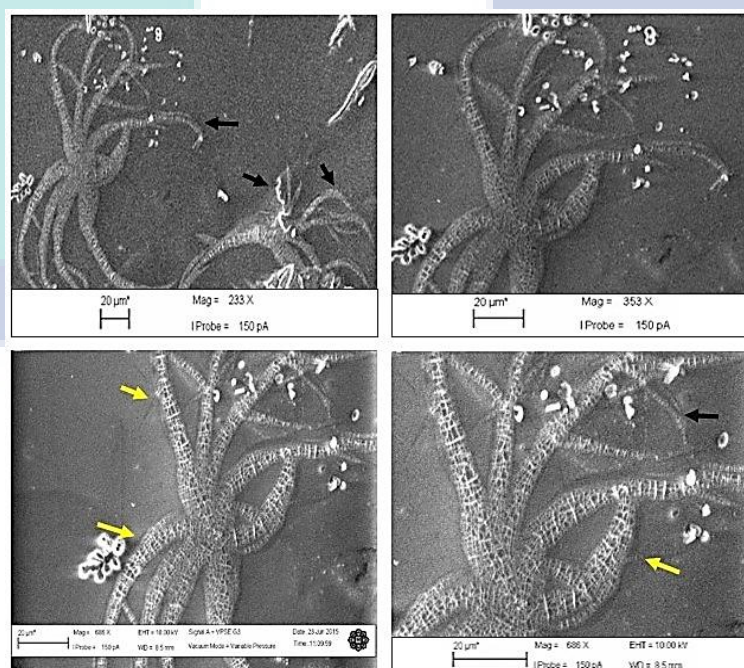


**Figure 5.13 CPC replica of fungi**

This image shows that the CPC was capable of replicating fine details of fungal morphology. Yellow arrow points to the hypha and black arrow points to the conidiophore. The obtained replica correlates with the drawing reported in (Ryley and Pereira-Smith, 2006).

### 5.3.2 Fabricated cell imprinted carbon polymer composite (CI-CPC)

CI-CPC replica was obtained with morphology features imprinted on it. Surface topography imaging from SEM showed that the cell morphology features were transferred to polymer. Cell surface topographies were clearly visible in the image. Subtle features like filopodia, lamellopodia, fusion pores and extrusions were successfully transferred and visible are shown in Figure 5.14, Figure 5.15 and Figure 5.16.

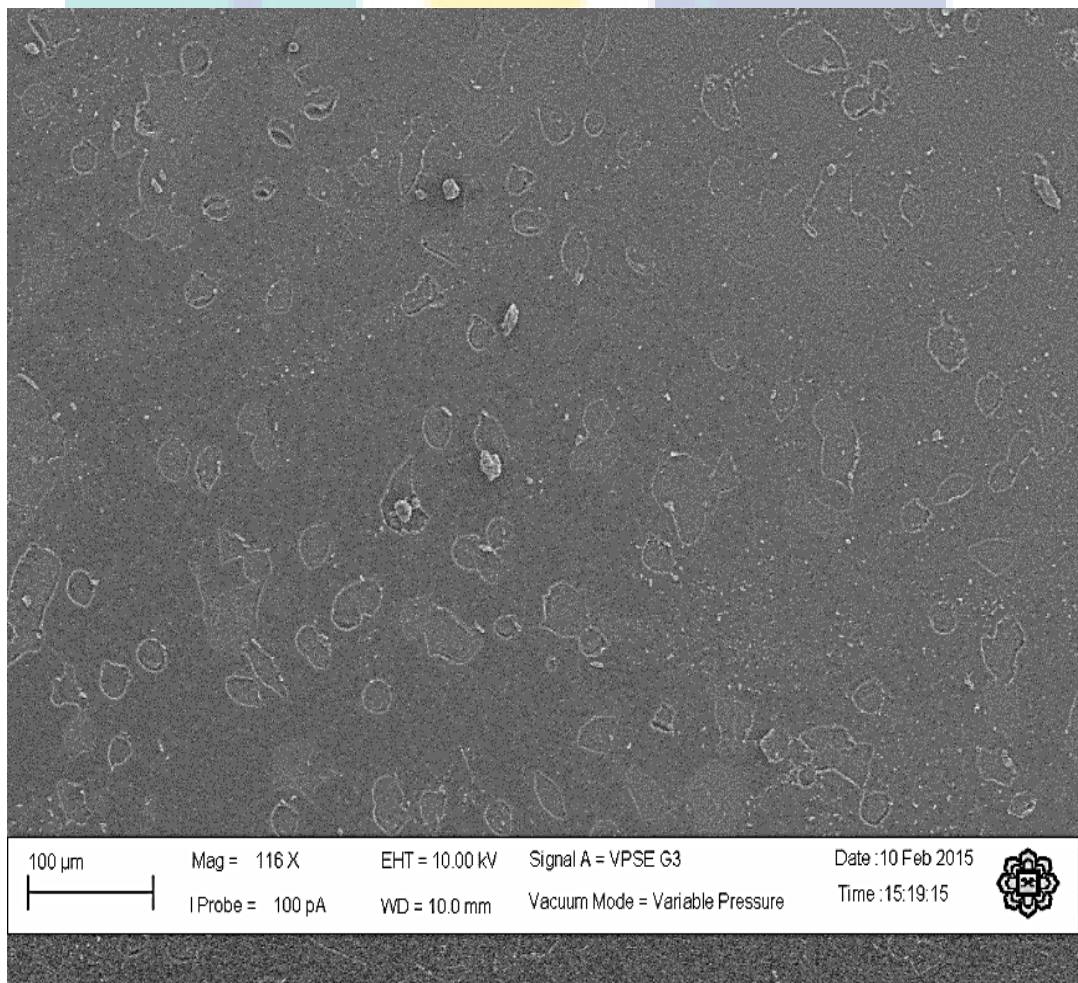


**Figure 5.14 HeLa CI-CPC replica**

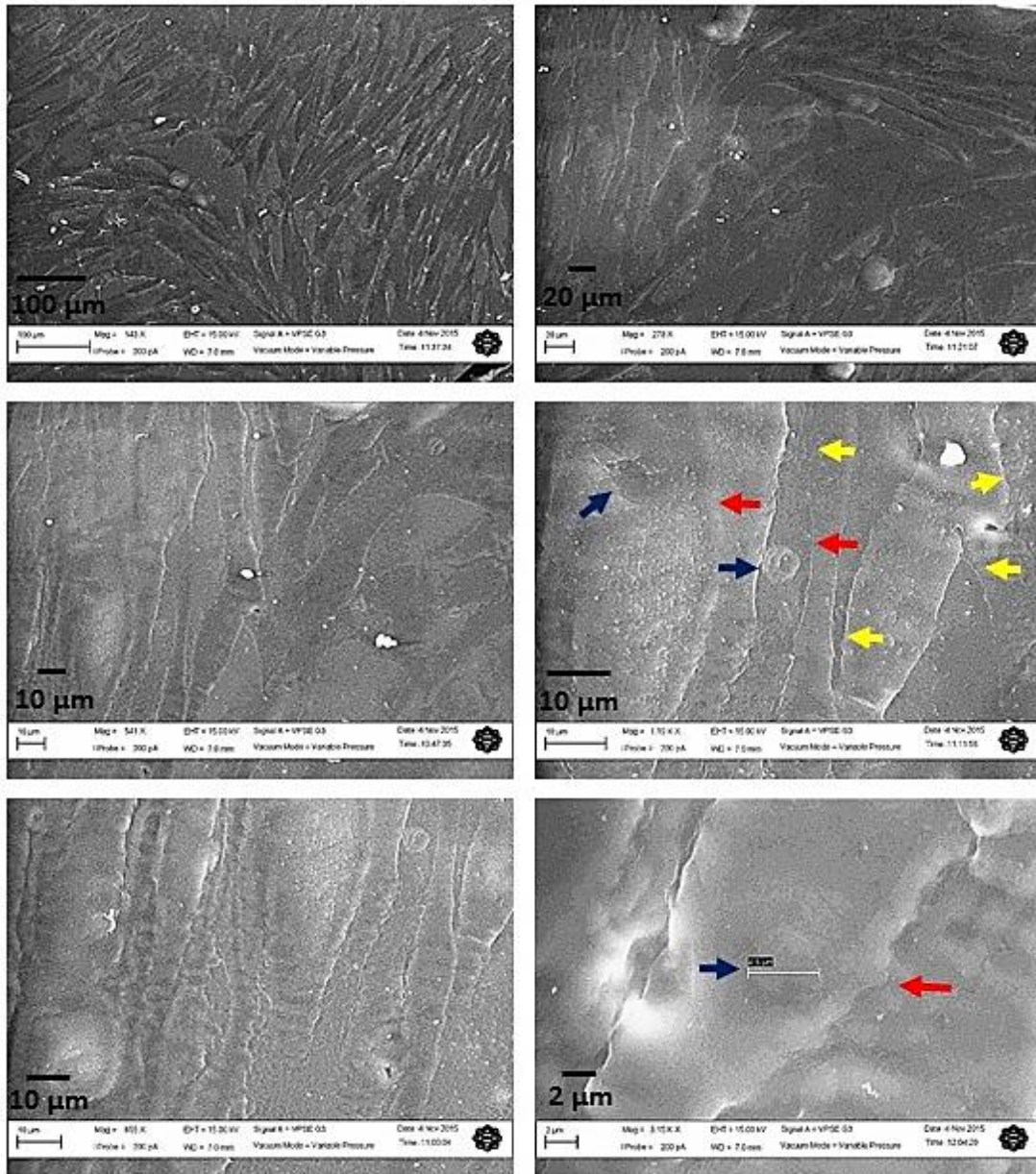


**Figure 5.15 HGF-1 CI-CPC replica**

This image shows the surface topography of HGF-1 CI-CPC at various magnifications. Fine details of cell morphology were transferred to the CI-CPC imprint. Red arrow pointing to each individual cell. Blue arrow pointing to cell nucleus. Yellow arrow pointing to the subtle cell features like filopodia and lamellopodia.

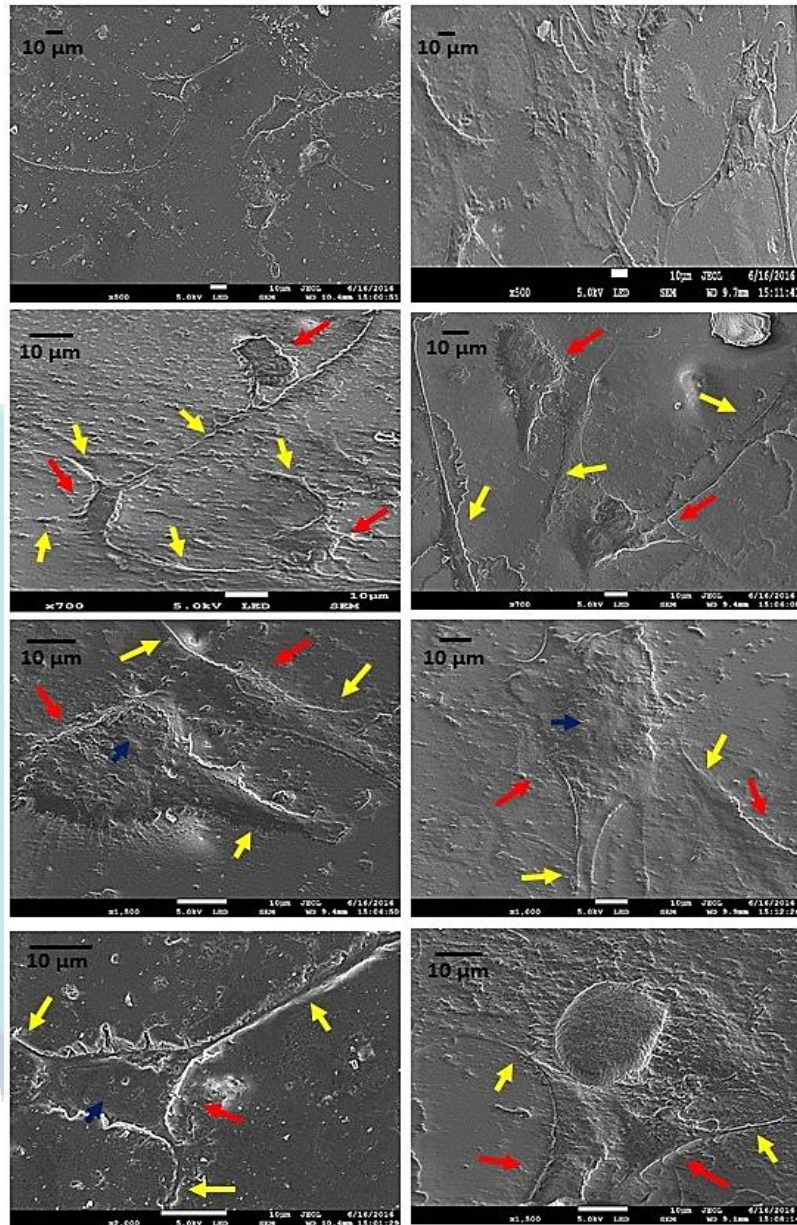


**Figure 5.16 HT-29 CI-CPC replica**

This image shows the fine details of cellular features which were transferred to the CI-CPC imprint. Red arrow pointing to each individual cell. Blue arrow pointing to cell nucleus. Yellow arrow pointing to the subtle cell features like filopodia and lamellopodia.

### 5.3.3 Cell morphology resolution comparison

Comparisons were made between cells and CI-CPC. The comparison in Figure 5.17 shows the potential capabilities of the CI-CPC in cell pattern transferring.

Comparison of feature resolution of cells and CI-CPC show that the cell morphology with fine details was imprinted.

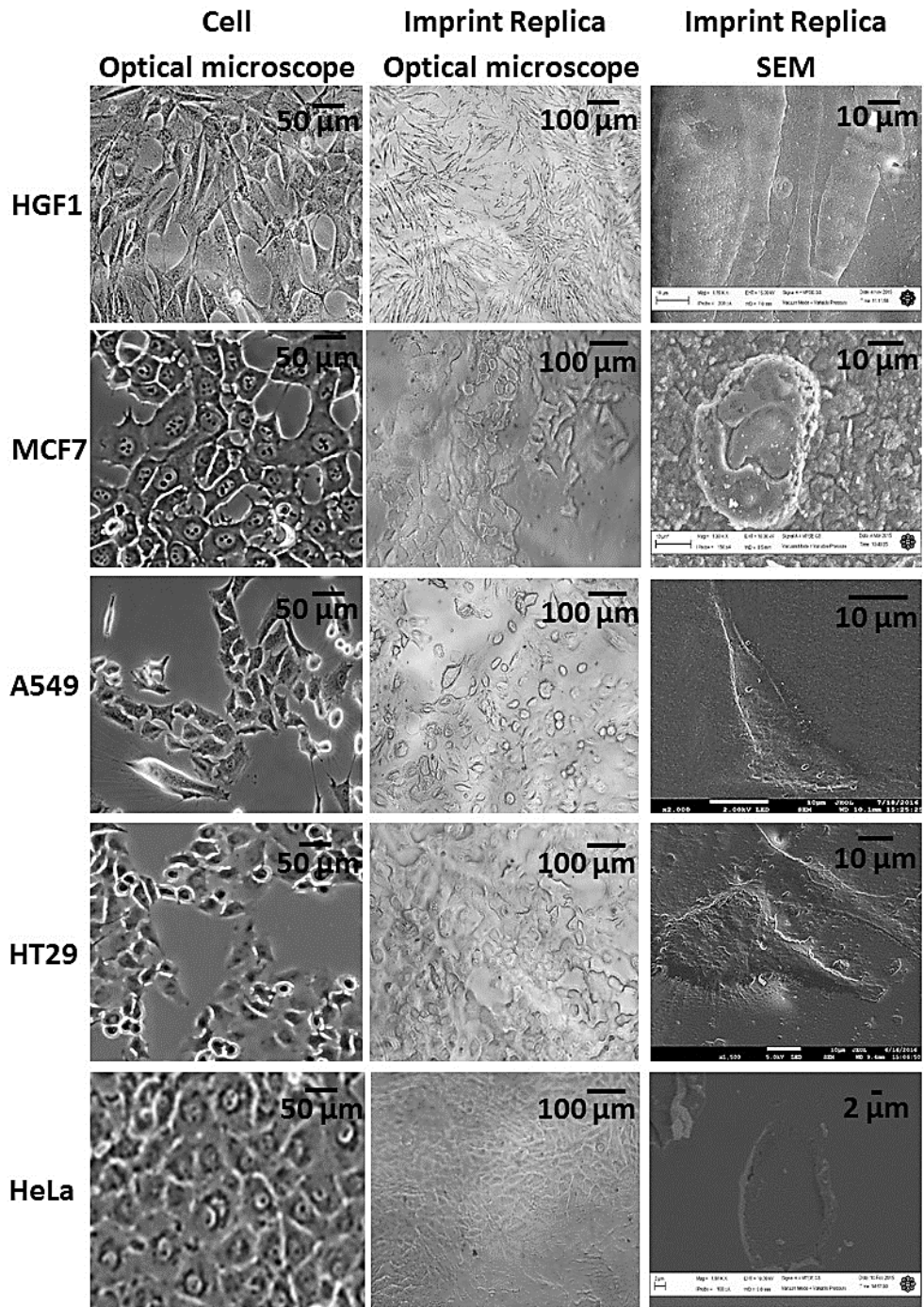


**Figure 5.17 Cell morphology resolution comparison**

This image shows resolution boundaries of various imaging modalities. Comparison of feature resolution of cell and CI-CPC in pattern transfer can be seen clearly.

## 5.4 Cell imprinted carbon polymer composite (CI-CPC) for cell diagnosis

Evaluated results of the imprinting capabilities of CPC for cell morphology based diagnosis are presented in this section. In this study A549 and MCF-7 were treated with a known cell death inducer termed VC and a potential cell death inducer extract known as the bezoar. Hence the morphology diagnosis was conducted to investigate CI-CPC technique in imprinting morphological changes of cell following VC and BZ exposure for 72 hours.

### 5.4.1 A549 cell replica morphology analysis

Presented here is the bioimprint results of untreated A549 with comparison to A549 cell exposed to VC for 72 hours in Figure 5.18. It was evidenced that the CI-CPC technique imprinted untreated cells with intact morphology as well as the budding of new cells. Untreated cells exhibited polygonal of epithelial like shape, and the yellow arrow shows the imprint capture details of cell membrane extension trying to reach out to neighboring cells (the filipodia).

VC treated A549 displayed different patterns of morphology. Results demonstrated shrinkage of cell's membrane and rounding up, and detaching itself from the next cells, as indicated by the white arrows. Moreover, cells treated with VC displayed forming apoptotic bodies as indicated by black arrows. Comparably, BZ treated cells in Figure 5.19 appeared to exhibit similar feature of morphological changes same as those treated with VC. It can be seen that the cells exhibited shrinking of cells membrane, rounding up and detached from its neighbor cells as shown by white arrows.



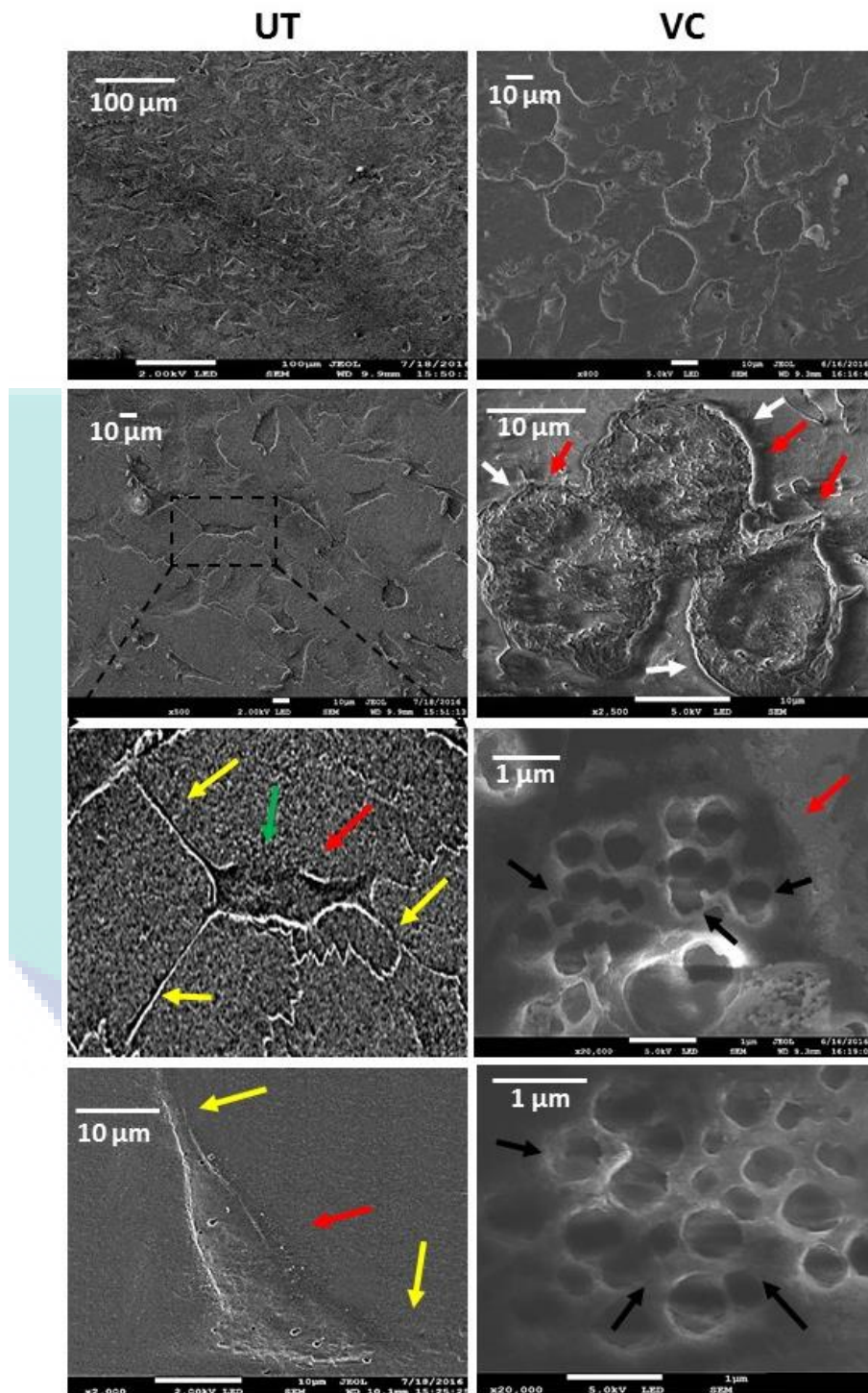


**Figure 5.18 A549 VC treated CI-CPC replica**

This image shows A549 cell morphology for untreated and VC treated. Red arrow points to each cell, white arrow points to condensed cell, yellow arrow points to the lamellopodia and filopodia, green arrow points to the nucleus and black arrow points to the micro vesicles, pores and apoptotic bodies.

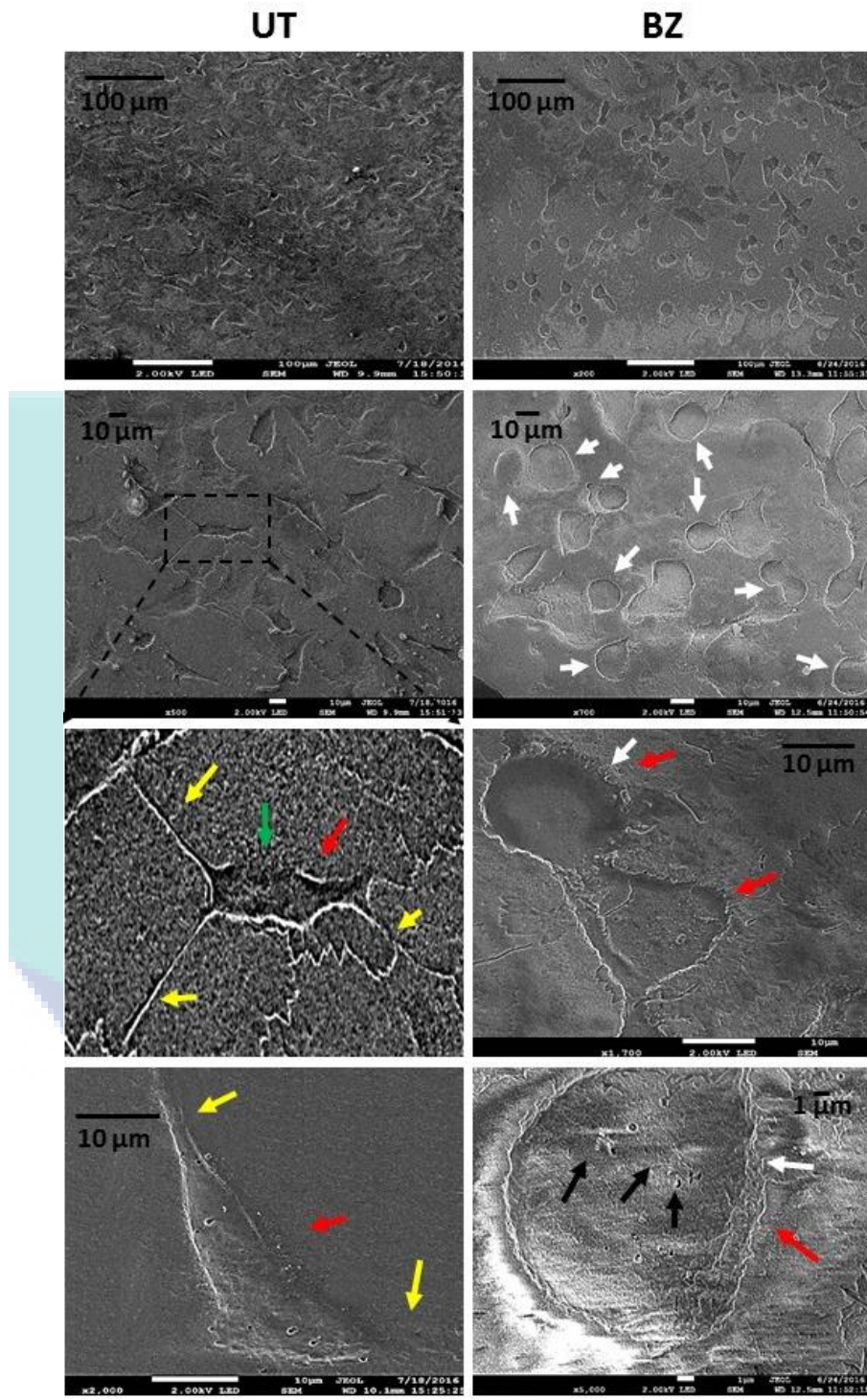


**Figure 5.19 A549 BZ treated CI-CPC replica**

This image shows A549 cell morphology for untreated and BZ treated. Red arrow points to each cell, white arrow points to condensed cell, yellow arrow points to the lamellopodia and filopodia, green arrow points to the nucleus and black arrow points to the micro vesicles and fusion pores.

Figure 5.20 shows cell imprints of A549 cells treated with BZ for 72 hours. Figure 5.20 (a and b) show the cell membrane shrunk and forming rounded morphology instead of polygonal epithelial. At higher scale, Figure 5.20 (c, d, e and f) evidently show the CI-CPC was able to capture fine details of cell's membrane that was compromised, where the cells shown to exhibit irregular pattern of cells membrane, suggesting that the BZ has affected the cells morphology.

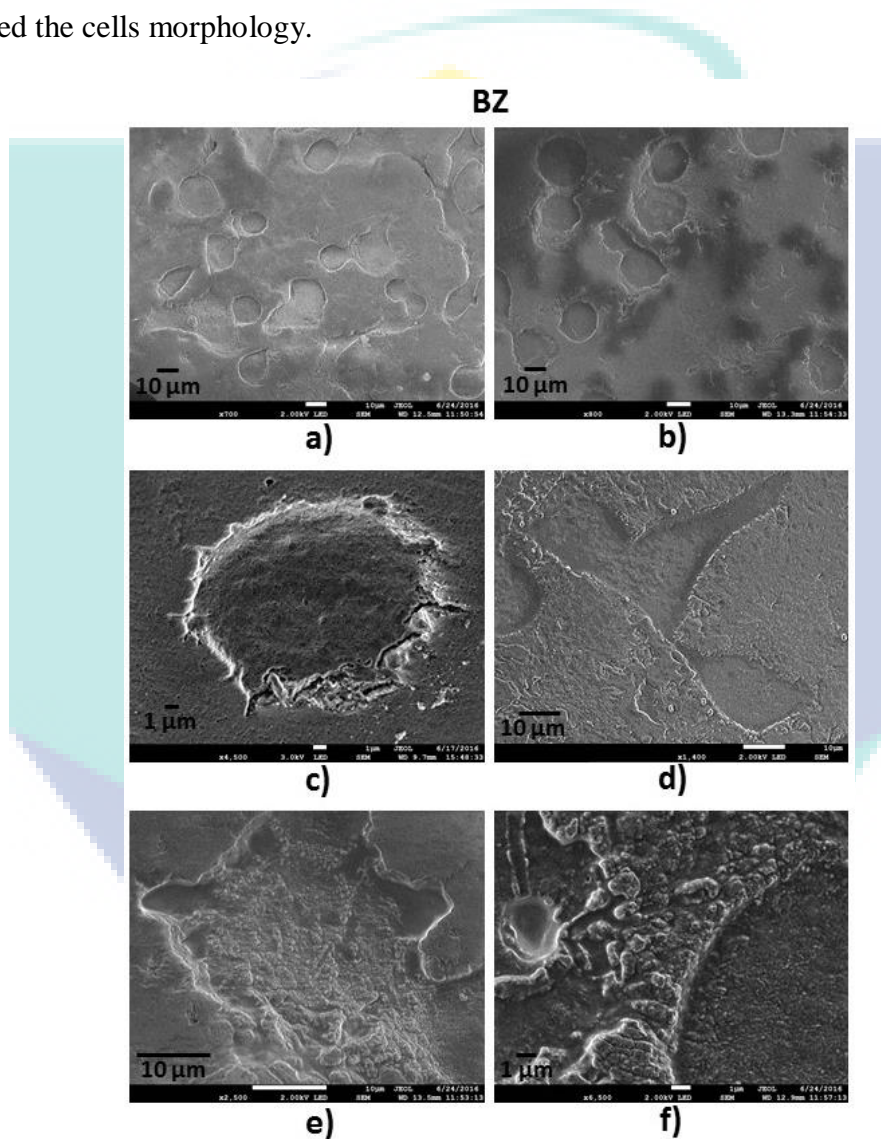


**Figure 5.20 A549 BZ treated CI-CPC replica (higher magnification)**

(a-b) the cells rounding up and detached from next cells. (c-d) has shown in details the morphological changes of cells membrane indicating rearrangement of cytoskeleton. (e-f) has shown the cell membrane variations which was in early apoptosis with vesicles and apoptotic bodies.

Further analysis on BZ treated A549 cell membrane with higher magnification was reported in Figure 5.21. Demonstrated here were the irregular cell membrane shapes that were imprinted. The surface of cell membrane seems to have release micro-vesicle as well as pore formation and malformation of the cytoskeleton. The morphology of the cell membrane suggested that the cell reorganized its own cytoskeleton due to the effect from BZ extract which resulted in shrinkage of cell membrane and formation of apoptotic bodies.

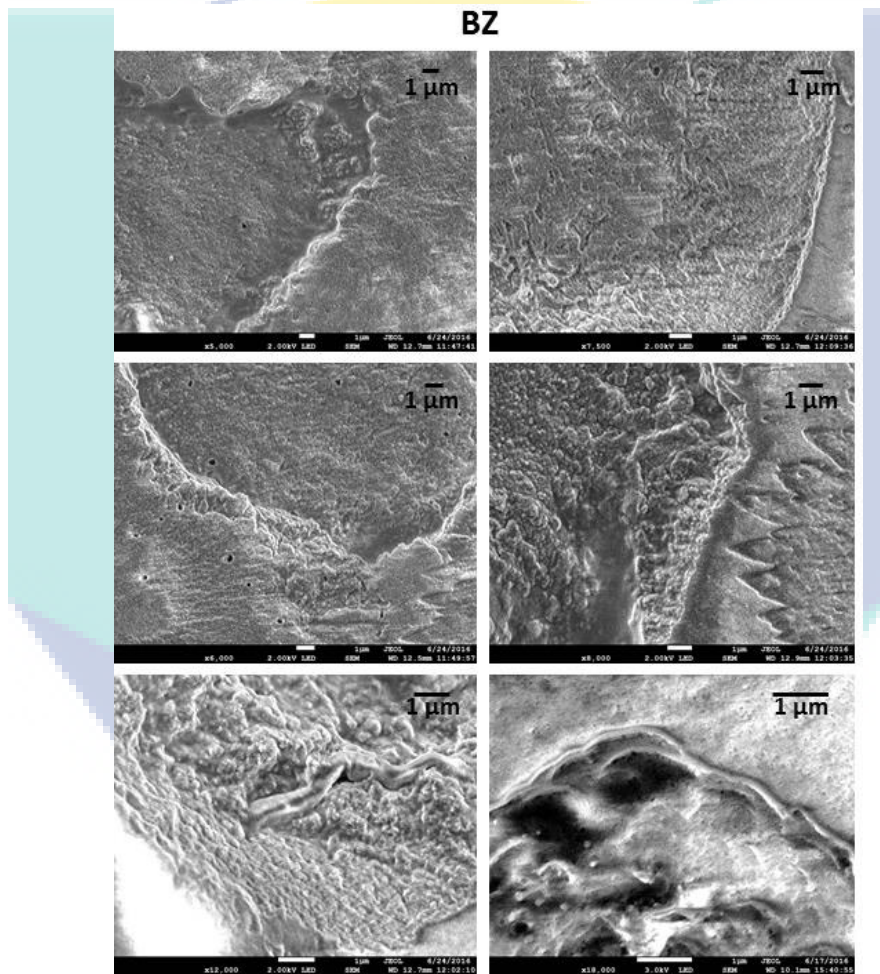


**Figure 5.21 A549 BZ treated CI-CPC cell membrane closer look**

The figure shows fine details of imprinted cells membrane surface of A549 BZ treated. Features such as micro vesicles and cell blebs can be seen clearly.

#### **5.4.2 MCF-7 cell replica morphology analysis**

Imprinting on MCF-7 cells replica was done post BZ treatment for 72 hours and untreated cells of MCF-7 were used as a control for comparison. The imprinting

technique reported that the untreated cells grown had attached to neighboring cells in monolayer formation, proliferated as incubation time increased and the morphology of the cells showed no abnormalities. One interesting finding of Figure 5.22 was the imprinting technique successfully imprinted the cytokinesis from mitosis phase where clearly the cell was dividing its nucleus and cytoplasm into two daughter cells. However, it can be seen clearly that the BZ treated cells were detached from each other and the nucleus as pointed out by the green arrows that showed the nucleus had condensed. Furthermore, cell membrane seemed to be bulgy, indicating cell membrane were compromised and had undergone the formation of apoptotic bodies (black arrows).

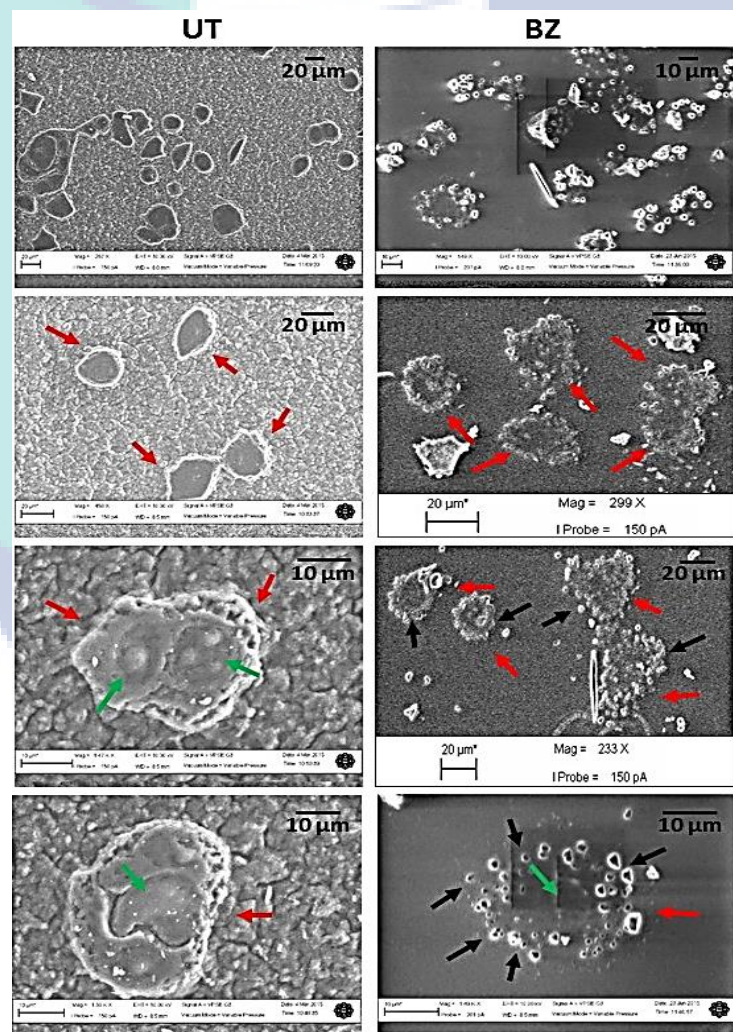


**Figure 5.22 MCF-7 BZ treated CI-CPC replica**

Red arrow points to each cell. Green arrow points to the nucleus. Black arrow points to the apoptotic bodies and micro-vesicles.

The findings of A549 and MCF-7 cells suggested that treated cells with VC and BZ, had undergone apoptosis which also known as programme cell death. Apoptosis is a normal process which occurs to maintain homeostasis from cell proliferating and occurred due to various stimuli (Häcker, 2000). Apoptosis is distinguished from other form of cell death through their hallmarks morphology, which are pkynosis (nucleus and cytoplasm condensed) and appearance of apoptotic bodies which will be engulfed by macrophage in in-vivo model (Häcker, 2000, Taatjes et al., 2008). Elmore et al., (Elmore, 2007) reported that during initial progress of apoptosis, the cells will start to lose the cell-to-cell adhesions by rounding up its cytoplasm, hence separated from neighboring cells. Same author also explained that in late phase of apoptosis, the cell will fragment into apoptotic bodies with intact cell membranes that contain cytoplasmic organelles which will become debris in in-vitro models. Additionally, apoptosis features that was highlighted are nucleus shrinkage and nuclear fragmentation. These features as highlighted by (Häcker, 2000, Saraste and Pulkki, 2000) indicates cell was in late apoptosis phase. As shown earlier (in literature review), Figure 2.13 (Neuman, 2003) shows phases of apoptosis from early to late apoptosis. Study from (Lauand et al., 2015, White et al., 2001) reported fluorecence analysis on VC treated A549 showed that the cells exhibited similar result and this supports the results obtained through this study. Based on the investigation it is evident that the CI-CPC imprinting technique was successful in replicating the subtle morphology details related to the apoptosis phase which occurred for both cells in this study. CI-CPC successfully imprinted the cells membrane surface and its morphology when undergone early and late apoptosis.

#### **5.4.3 Interpretation on various imaging techniques**

Figure 5.23 shows the correlated imaging analysis by various imaging approaches. Interpretation for accurate diagnosis was made by correlating the images obtained from optical microscope, fluorescent microscope and imprinted replica.

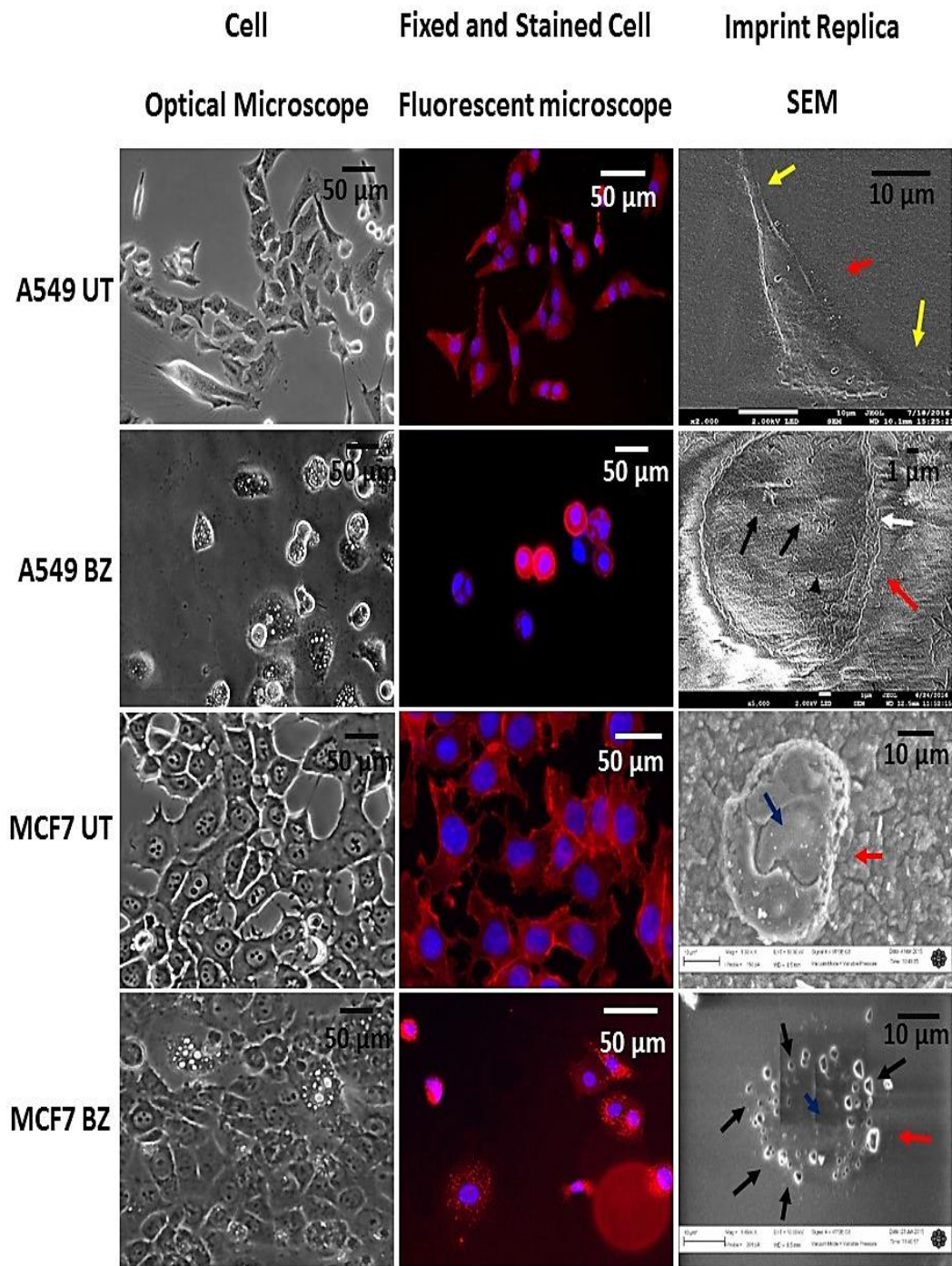


**Figure 5.23 Interpretation with different imaging techniques**

This image shows the cell morphology details obtained from different imaging techniques with correlation of extracted information. It can be seen that fine details of cell which cannot be viewed at high resolution in other two techniques can be viewed by CI-CPC replica technique. Red arrow pointing to each cell. Yellow arrow pointing to fine features like filopodia. White arrow pointing to condensed cell. Black arrow pointing to the apoptotic bodies and micro-vesicles.

It can be seen that the fine cell morphology features associated with cell signaling like micro-vesicles, fusion pores, cell blebs and apoptotic bodies can be better imaged at high resolution using imprinted replica technique.

### **5.5 Cell morphology feature detection**

Imprinted replica images were autonomously processed using National Instruments LabVIEW 2014 Vision Assistant for extracellular morphology based feature detection. Figure 5.24 (a) shows the imprint replica, and Figure 5.24 (b) presents the final feature detected images. Several images were used to test the reliability of the program and the result was positive and impressive. It shows the varied scope of cell measurement starting from cluster cell level to single cell sub organelle level. Fine extracellular features that can be detected include cell shape and size, nucleus shape and size, micro vesicles, exosomes, filopodia and lamellopodia.

Currently the morphology imaging can be done using optical methods where the resolution is limited thus much detailed information were not possible and mostly only initial screening were done. Though molecular probe based methods provide complete detailed insights but mostly involve complicated preparations, expensive reagents and experienced handling. Other conventional process for high resolution imaging like SEM or TEM involves fixation, processing (dehydration, clearing, and infiltration), embedding, sectioning and staining, where the process alters the cell morphology details. However it provides complete and much detailed insights.



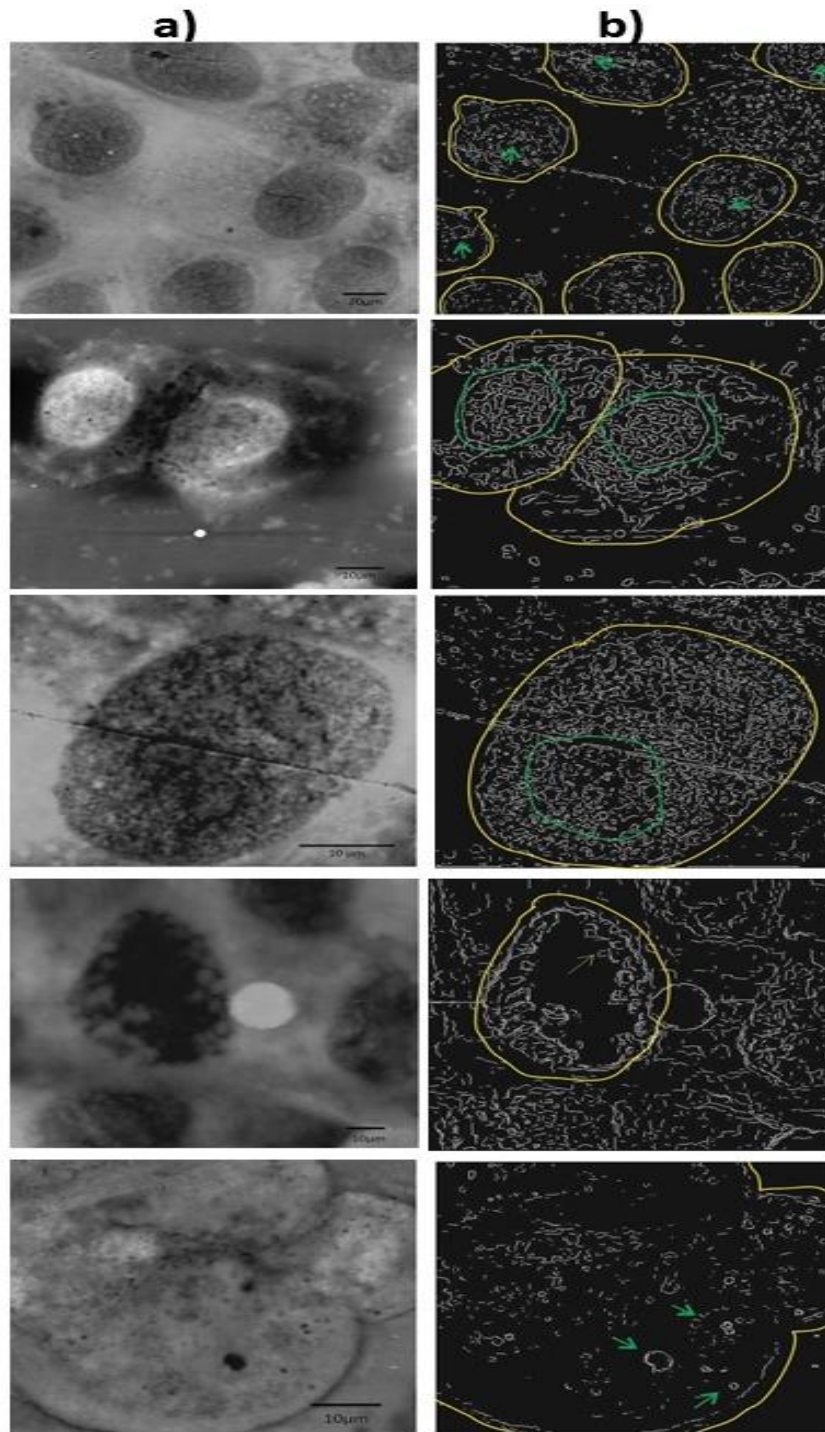


**Figure 5.24 Cell morphology feature detection**

(a) Imprinted replica and (b) features detected. Above images show the detected cell shape which is highlighted in yellow with the cell morphology grooves and pores inside it. The green highlighted region shows the detected cell nucleus size, shapes with grooves and pores clearly.

Cell imprint replica can provide high resolution morphology details keeping cells morphology and cytoskeleton unaltered. This work reports the imprinting by rapid curing at room temperature which is very essential when it comes to handling cells. Thus the replica is created in the cells natural state. As the technique provides only morphology details, the diagnosis and study can be based only on morphology. Nevertheless most of the abnormalities results in morphology change and predominantly the diagnosis are based on morphology change in abnormalities. Correlating the changes in cell morphology to its physiology can open many doors for this research.

Although the bioimprint technique cannot be a complete alternative as its operation is limited due to its morphology details alone, yet it can be a fair alternative for morphology based diagnosis. This technique facilitates imaging of morphology changes at various stages for studying the molecular pathways and also cell based research investigations at morphology level. This technique can be coupled with varying imaging modalities for various resolutions.

The molding of living cells is expected to have an expanding market than the routinely used more detailed morphological analysis of intracellular structures, including enzymatic techniques that are used in majority of the cases, as there is significant change in morphology for most of the abnormalities. In addition to that, the technique has several merits like no tedious process involved, does not require high end equipment for process, reduction in consumables, less processing time and is compatible with current conventional high end imaging modalities like AFM/SEM.

A novel method of extracting features autonomously from imprint replica rapidly has been reported where cells morphology and cytoskeleton were unaltered after the replication process. Thus this method helps visualizing the single cell sub organelle scale without damaging the cell morphology. Morphologies features were detected using image processing techniques. Shape of grooves, pores, blebs or microvillus on the cellular surface was detected clearly. Features and information related to morphology were obtained more clearly. This technique is automated and helps in performing fast and accurate diagnosis. Furthermore, this technique can be enhanced and efficiency can be increased, when neural network is coupled along with it for decision making applications. Knowledge on changes occurring in the morphological features between the normal and the abnormal cells plays a prominent role in the analysis of imprint replicas. The prerequisite for any other further processing such as the classification and testing using

neural network in the image processing is the feature extraction. This research also paves way for it. Table 5.2 shows the comparative summarization of conventional and CIL approach.

**Table 5.2 Comparative summarization of conventional and CIL approach**

S.No.	Factors	Conventional approaches	CIL based approach
1	Cell morphology	Low resolution	High resolution
2	Micro vesicles	Not clear / Low resolution	High resolution
3	Apoptotic bodies	Not clear / Low resolution	High resolution
4	Nucleus	Low resolution	High resolution
5	Fusion pores	No	High resolution
6	3D	No	Yes

### 5.6 *In-vitro* study of polymer composites for biomedical applications

In order to use the replicated composites as biomaterial scaffold for various biomedical applications, its cytotoxicity and cytocompatibility studies are required, which are presented below. Figure 5.25 shows the use of polymer composites in tissue engineering applications.

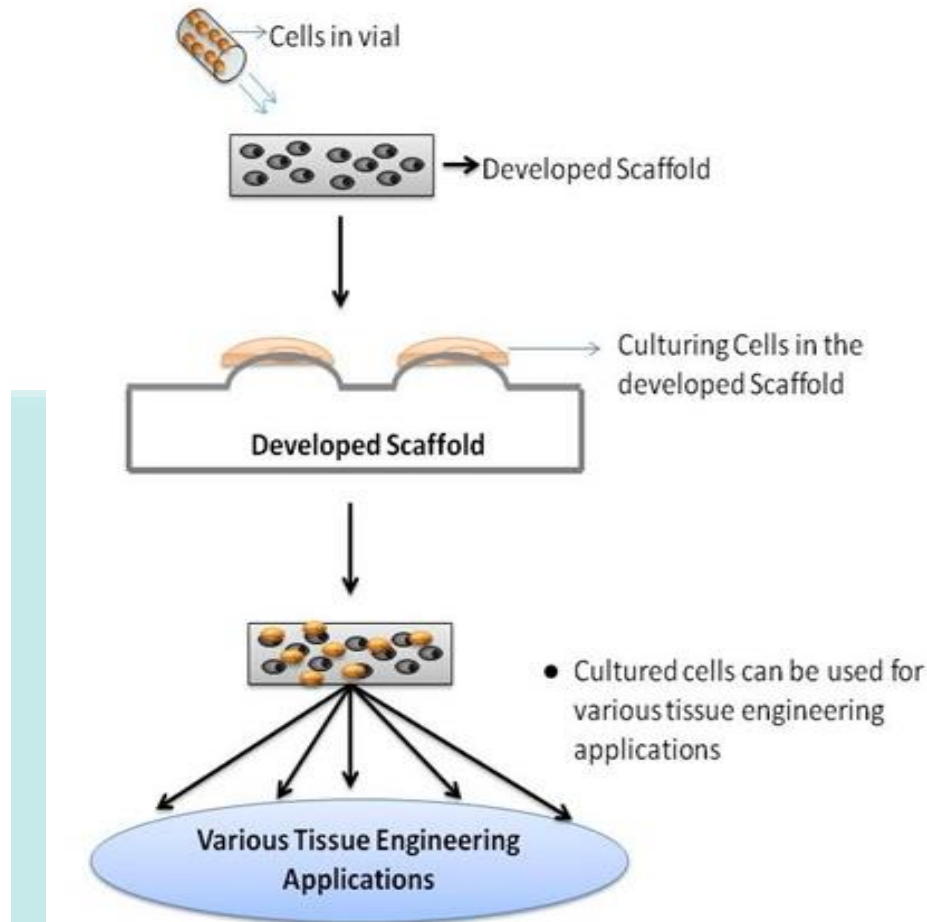


**Figure 5.25 Imprint replica for tissue engineering applications**

Image shows how positive imprint replica fabricated from negative imprint replica can be used for cell culture substrates and tissue engineering applications.

### 5.6.1 Cytotoxicity studies

Cytotoxicity study results of polymer samples by direct contact and test on extract assays are provided below.

#### 5.6.1.1 Direct contact

Results from direct contact method showed that the polymer sample was nontoxic for biomedical applications. Direct contact method of cytotoxicity evaluation which was graded as per ISO 10993-5 standard depicted the non-cytotoxic nature of the polymer by the intracellular uptake of neutral red stain compared to HDPE and PVC disc. L929 cells after 24 hours contact with polymer sample, HDPE and PVC disc (before and after staining with neutral red solution) are shown in Figure 5.26.

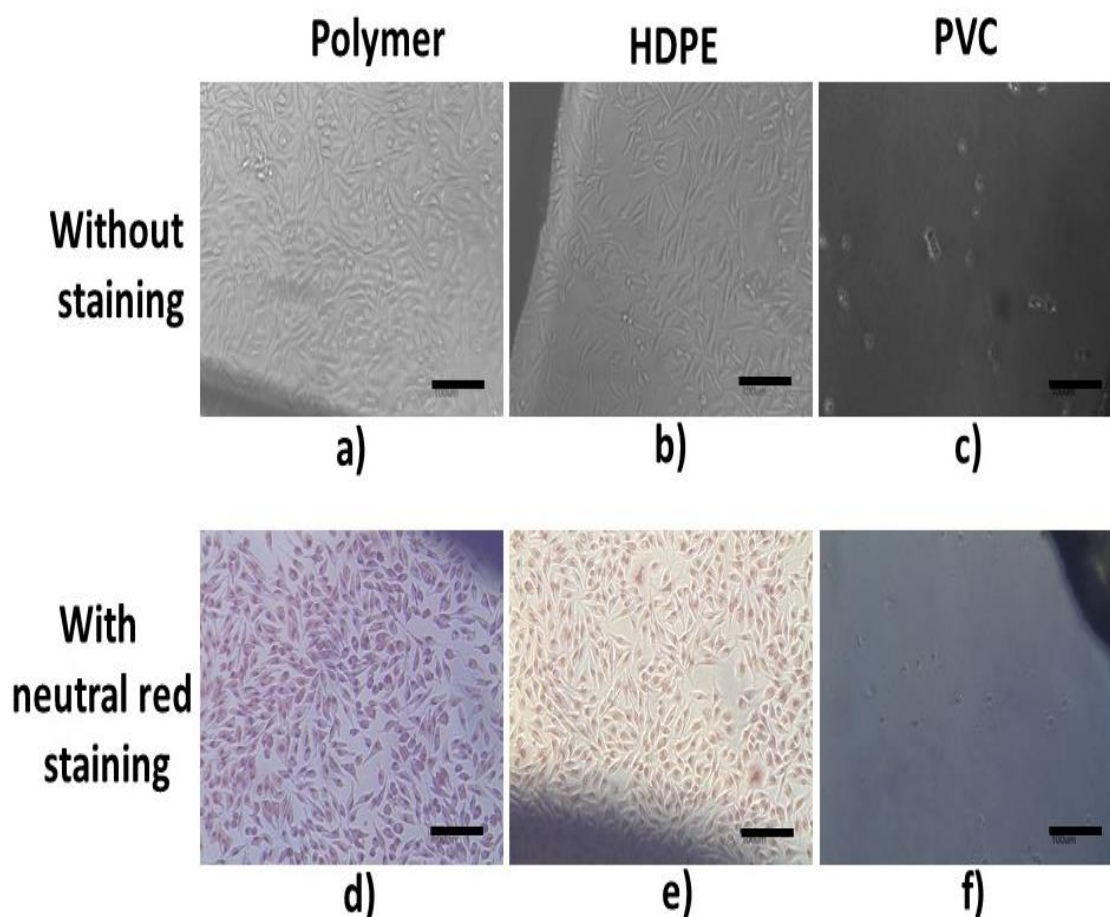


**Figure 5.26 Cell response to direct contact study**

L929 cells after 24h contact with (a) polymer sample, (b) HDPE and (c) PVC disc. L929 cells after 24h contact with (d) polymer sample, (e) HDPE and (f) PVC disc (after staining with neutral red solution). All scale bars show 100 µm.

#### 5.6.1.2 Test on extract

In order to measure the leachants that caused cell death even in small quantities, test on extract study was performed. Polymer sample was extracted at 37°C in culture medium for 24 hours and different dilutions of extract was added to cells that showed non-cytotoxic at 100%, 50%, 25% and 12.5%. Positive and negative control under similar condition of extraction showed severe cytotoxic and non-cytotoxic responses respectively. MTT assay after test on extract confirmed the non-cytotoxicity as it showed more than 80% metabolic activity. Results are shown in Figure 5.27 and Figure 5.28.

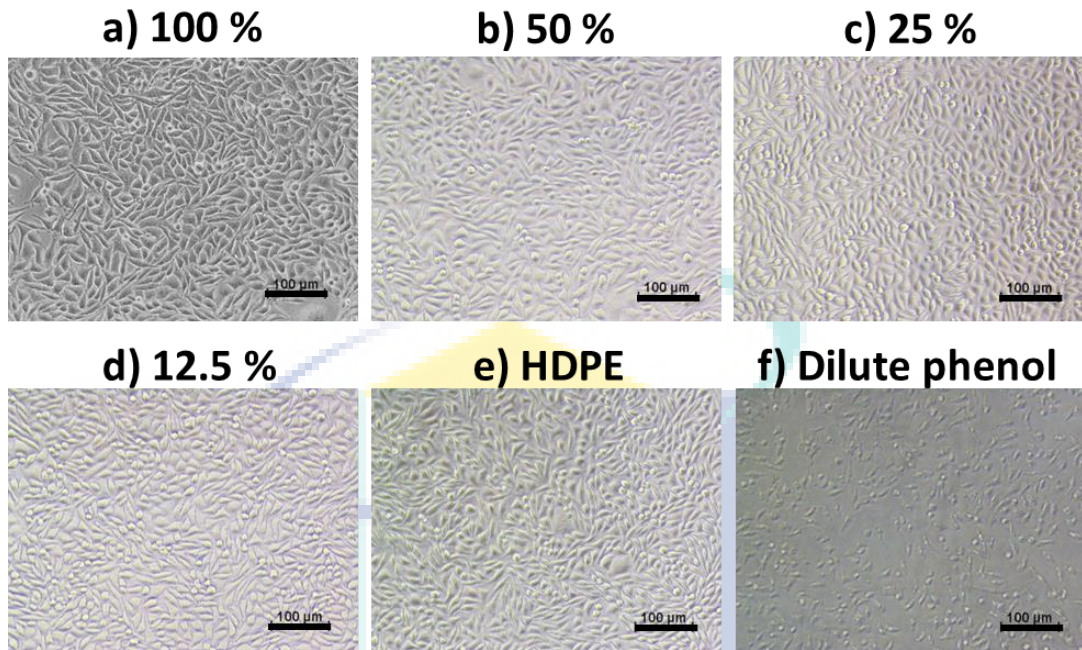


**Figure 5.27 Cell responses for test on extract study**

L929 cells after contact with 100%, 50%, 25% and 12.5% extract of polymer sample (a, b, c, d); HDPE (e) and dilute phenol (f). All scale bars show 100 µm.

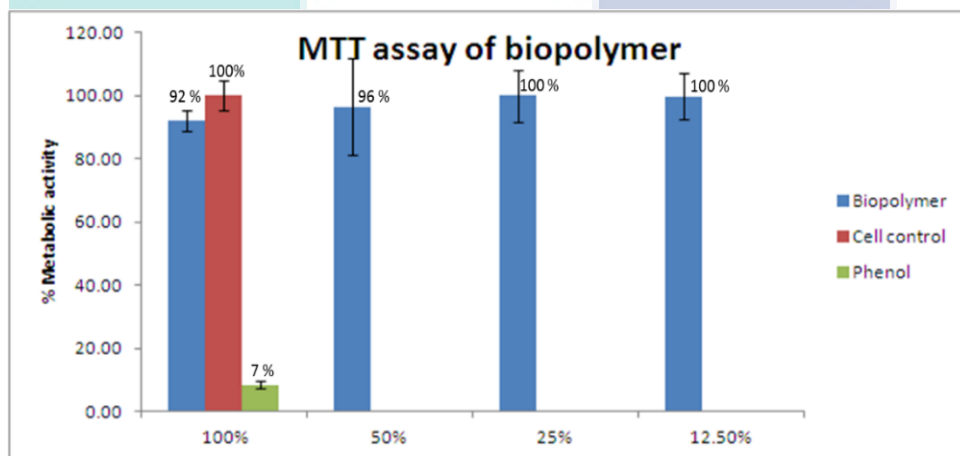


**Figure 5.28 MTT assay for test on extract**

### 5.6.2 Cytocompatibility studies

Cytocompatibility studies were evaluated using MTT assay, live dead analysis, and actin-phalloidin staining.

### 5.6.2.1 Live dead analysis

Cell viability plays an important role in cytocompatibility studies of biomaterials. Live cells shows distinct intracellular esterase activity with intact cell membrane and dead cell lack intracellular esterase activity. L929 cells cultured on polymer sample showed green fluorescence of live cells compared to cell control and only few cells dead cells were observed, indicating the viability of using polymer sample in biomedical applications. Obtained images are shown in Figure 5.29.

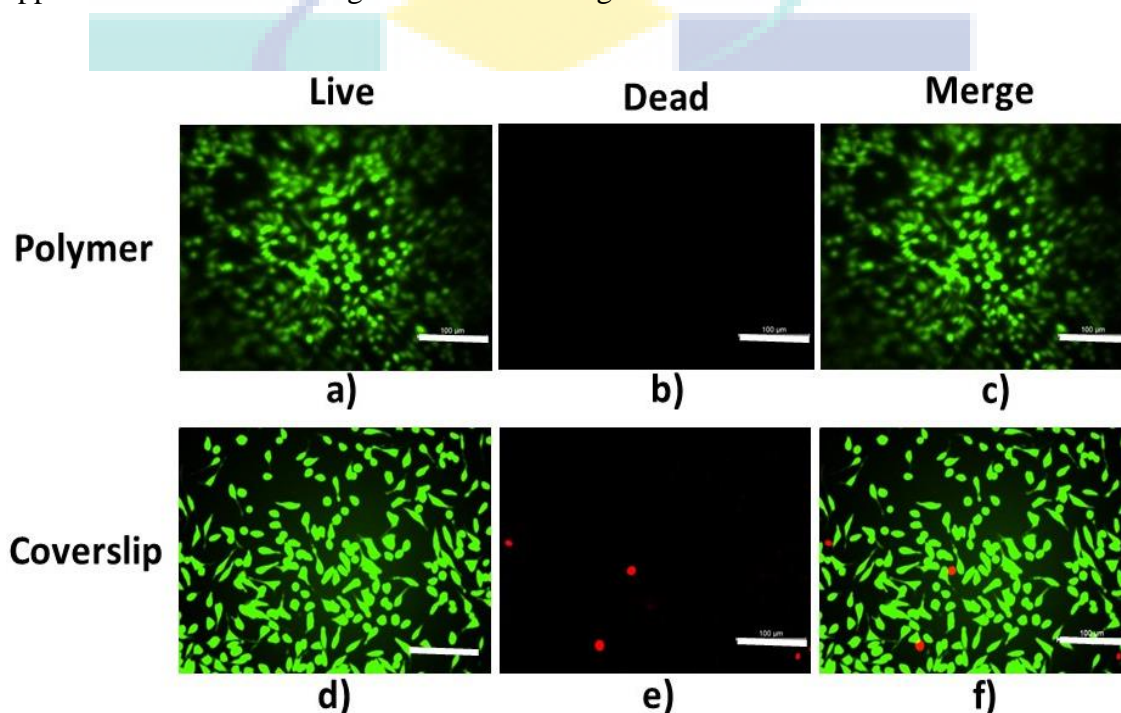


**Figure 5.29 Live dead Imaging**

Polymer - (a) Fluorescence from sample, (b) signal from PI and (c) merge of first and second image. Coverslip - (d) Fluorescence from sample, (e) signal from PI and (f) merge of first and second image. All scale bars show 100  $\mu\text{m}$ .

### 5.6.2.2 Cytoskeleton analysis

Cytoskeletal staining plays an important role in organelle transport, cell division and cell signaling. Cytoskeletal staining renders idea of colocalisation and orientation of actin filaments. Actin phalloidin staining of cells in polymer revealed that the material supported adhesion, proliferation of L929 cells and this was further confirmed by MTT assay. Results are shown in Figure 5.30.

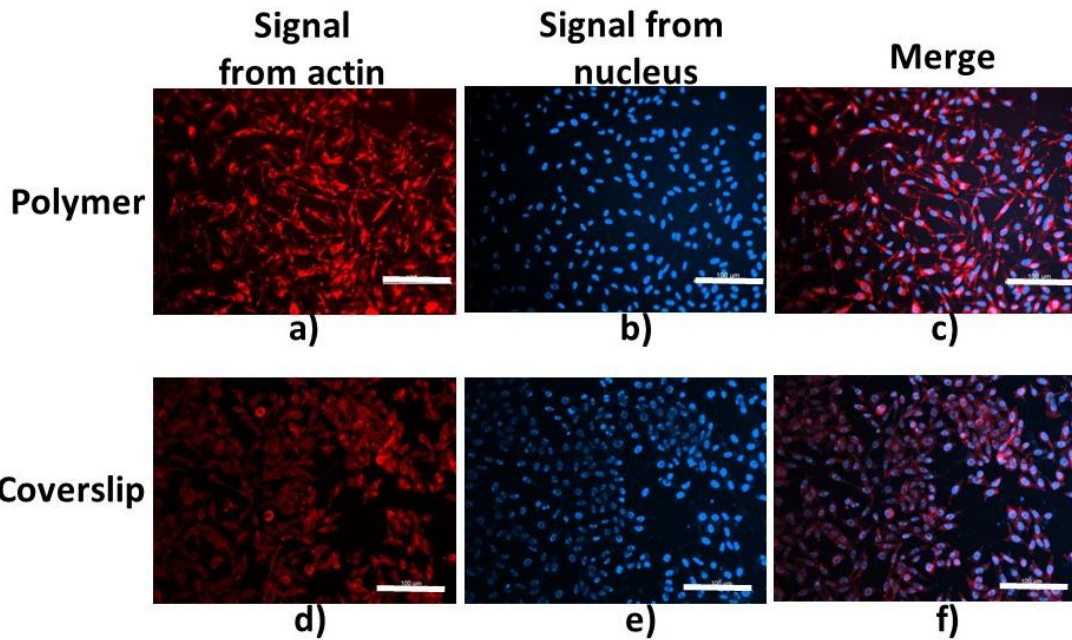


**Figure 5.30 Cytoskeleton analysis (Actin –phalloidin imaging)**

Polymer sample - (a) Fluorescence from actin, (b) signal from nucleus and (c) merge of first and second image. Coverslip - (d) Fluorescence from actin, (e) signal from nucleus and (f) merge of first and second image. All scale bars show 100  $\mu\text{m}$ .

### 5.6.2.3 Cell adhesion with MTT assay

MTT assay of polymer sample after cell adhesion reveals good biocompatibility of material similar to control. MTT assay depicted the mitochondrial enzyme activity of viable cells on the surface of the polymer sample. Metabolic activity revealed that cells were able to proliferate and moreover the surface topography of the polymer sample was comparable to control and this was unaffected after 48 hours of culture on material. Result is shown in Figure 5.31.

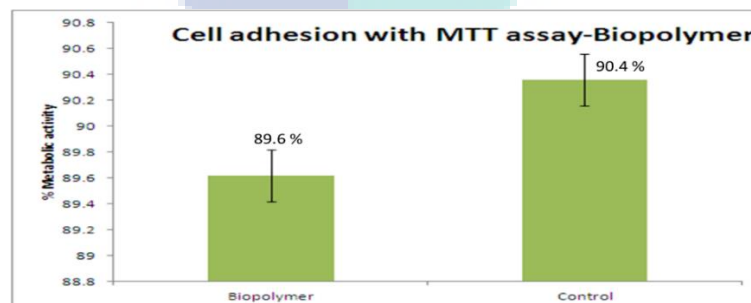


**Figure 5.31 MTT assay for cell adhesion**



Cytotoxicity analysis by direct contact and test on extract showed the material was non-cytotoxic to cells. Cell adhesion data support this as evident by good cell adhesion and proliferation.

Further cell imprint lithography paves way for many biomedical and tissue engineering applications which are shown in Figure 5.32.

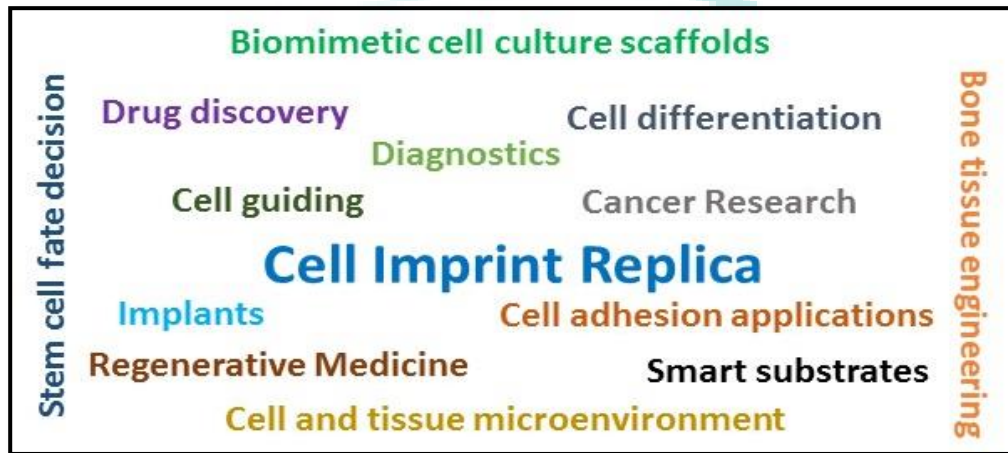


**Figure 5.32 Cell imprint replica applications**

Word crowd shows some of the applications of cell imprint replica.

Thus by CI-CPC technique, nanoparticle can be used to modify the properties of the polymer composite. Factors and properties of cell culture substrates can be varied by doping of CNP in polymer composites. This can pave way for its various biomimetic biomedical applications.

## 5.7 Chapter summary

This chapter describes the details and discussions of experimental results conducted. This chapter provides the results of the optimized CIL using CPC. CIL was captured with and without stimulations for further more analysis. CPC electrical property was modified based on the method described. Results showed that the CI-CPC were able to imprint cell features significantly. Toxicity evaluation reveals that the composites were not toxic to cells. Also discussed the evaluated single cell trapping results for designed microfluidic platforms. Single cell trapping was significantly improved based on the channel design.

## CHAPTER 6

### CONCLUSION AND FUTURE RECOMMENDATIONS

#### 6.1 Summary of the research

A novel approach for cell-imprint replica fabrication using CPC has been demonstrated. From the study, it was observed that 0.3 wt. % of load CNP in CPM were optimal for cell-imprint replica fabrication. From the electrical resistance study of fabricated CPC, it can be seen that the resistance of the 3-CPC were reduced by 68 % when compared to N-CPC.

Extracting features from cell imprint replica has been reported where cells morphology and cytoskeleton were unaltered after the replication process. Thus this method helps visualizing the single cell sub organelle scale without damaging the cell morphology. Morphologies features were detected using image processing techniques. Shape of micro-vesicles, grooves, pores, blebs or microvillus on the cellular surface was detected clearly. Features and information related to morphology were obtained more clearly in comparison to other conventional methods. These subtle morphology features play a major role and can be correlated in better understanding of cell signaling for many applications like cell diagnosis, therapy, drug delivery and many other biological applications.

This technique is automated and helps in performing fast and accurate diagnosis. Furthermore, this technique can be enhanced and efficiency can be increased when neural network is coupled along with it for decision making applications. Knowledge on changes occurring in the morphological features between the normal and the abnormal cells plays a prominent role in the cell diagnosis. The prerequisite for any other further processing such as the classification and testing using neural network in the image processing is the feature extraction. This research paves way for it.

For the fabrication of single cells imprinted replica, demonstrated by the design, fabrication, and analysis of micro-fluid dynamic based biochip for single cell trapping. Characterization of three fluid channel shapes for improving SCC was performed. Observations revealed that SCC rates can be improved based on channel shape and orientation of microwell array. This acts as a design guideline for designing non-auxiliary hydrodynamic-based microfluidics for high SCC with no or minimal MCC. Biochip investigated also has wide applications in the field of single cells microfluidic-omics technologies such as genomics, proteomics, secretomics and metabolomics.

Demonstrated cell imprint replica fabrication approach using nanoparticle polymer composite can pave way for tailoring many other associated applications like biomimetic smart culture substrates, bone tissue engineering, cell guiding, cell adhesion, tissue engineering, cell microenvironment, tissue micro environment etc.

## **6.2 Research contributions**

A novel approach for cell-imprint lithography fabrication using CPC has been demonstrated. It was observed that 0.3 wt. % of load CNP in CPM were optimal for cell-imprint replica fabrication. The resistance of the 3-CPC were reduced by 68 % when compared to N-CPC.

CIL based cell diagnosis for cancer research and drug therapy has been reported. Comparative interpretation has been done for the correlation of cell signaling to the respective features in the cell morphology.

Passive hydrodynamic based microfluidic biochip has been studied and reported for significant increase in single cell capture. Relative SCC efficiency can be improved by modification of the fluid channel design and orientation.

Autonomous vision based feature detection for cell diagnosis using CIL has been reported. It has demonstrated fine extracellular feature detection using CIL technique.

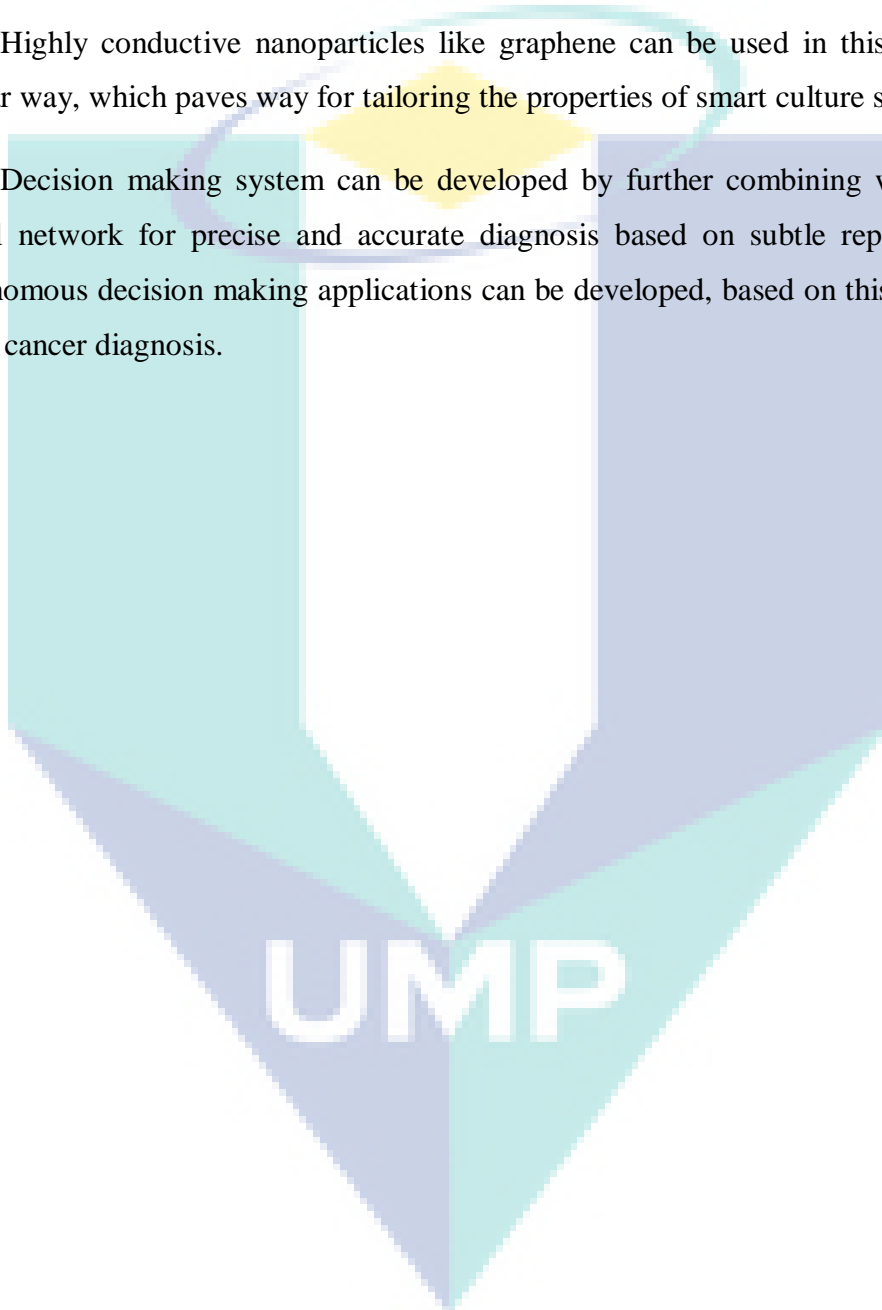
Toxicity study was concluded and that the fabricated polymer composites were biocompatible. Thus the fabricated composites can be used in biomedical applications.

### 6.3 Future recommendations

This approach can be used to correlate the minute morphological features associated with cell signaling for better understanding of the insights, thus helps in better cell diagnosis applications

Highly conductive nanoparticles like graphene can be used in this approach in similar way, which paves way for tailoring the properties of smart culture substrates.

Decision making system can be developed by further combining with artificial neural network for precise and accurate diagnosis based on subtle replica features. Autonomous decision making applications can be developed, based on this research for better cancer diagnosis.



## REFERENCES

- AGEING, C. C. M. F. H. A. 2003. Computer-Assisted Image Analysis for Cervical Screening: Assessment Report. *Medical Services Advisory Committee*.
- ALKAISI, M., MUYS, J. & EVANS, J. Bioimprint replication of single cells on a biochip. *Microelectronics, MEMS, and Nanotechnology*, 2007. International Society for Optics and Photonics, 67990V-67990V-10.
- ANDRION, A., MAGNANI, C., BETTA, P., DONNA, A., MOLLO, F., SCELISI, M., BERNARDI, P., BOTTA, M. & TERRACINI, B. 1995. Malignant mesothelioma of the pleura: interobserver variability. *Journal of clinical pathology*, 48, 856-860.
- ARAKAWA, T., NOGUCHI, M., SUMITOMO, K., YAMAGUCHI, Y. & SHOJI, S. 2011. High-throughput single-cell manipulation system for a large number of target cells. *Biomicrofluidics*, 5, 014114.
- ATLAMAZOGLU, V., YOVA, D., KAVANTZAS, N. & LOUKAS, S. 2001. Texture analysis of fluorescence microscopic images of colonic tissue sections. *Medical and Biological Engineering and Computing*, 39, 145-151.
- BAHEERATHAN, S., ALBREGTSEN, F. & DANIELSEN, H. E. 1999. New texture features based on the complexity curve. *Pattern Recognition*, 32, 605-618.
- BAILEY, T., JOHNSON, S., SREENIVASAN, S., EKERDT, J., WILLSON, C. & RESNICK, D. 2002. Step and flash imprint lithography: an efficient nanoscale printing technology. *Journal of photopolymer science and Technology*, 15, 481-486.
- BAILEY, T., SMITH, B., CHOI, B., COLBURN, M., MEISSL, M., SREENIVASAN, S., EKERDT, J. & WILLSON, C. 2001. Step and flash imprint lithography: Defect analysis. *Journal of Vacuum Science & Technology B*, 19, 2806-2810.

- BANAEIYAN, A. A., AHMADPOUR, D., ADIELS, C. B. & GOKSÖR, M. 2013. Hydrodynamic cell trapping for high throughput single-cell applications. *Micromachines*, 4, 414-430.
- BECKER, W. M., KLEINSMITH, L. J., HARDIN, J. & RAASCH, J. 2003. *The world of the cell*, Benjamin Cummings San Francisco.
- BELL, L., SESHIA, A., LANDO, D., LAUE, E., PALAYRET, M., LEE, S. F. & KLENERMAN, D. 2014. A microfluidic device for the hydrodynamic immobilisation of living fission yeast cells for super-resolution imaging. *Sensors and Actuators B: Chemical*, 192, 36-41.
- BELL, L. L., SESHIA, A. A., LAUE, E. D. & LANDO, D. A microfluidic device for high density hydrodynamic cell trapping, growth and Super-Resolution imaging. *Sensors*, 2011 IEEE, 2011. IEEE, 304-307.
- BENAVENTE-BABACE, A., GALLEGO-PÉREZ, D., HANSFORD, D. J., ARANA, S., PÉREZ-LORENZO, E. & MUJICA, M. 2014. Single-cell trapping and selective treatment via co-flow within a microfluidic platform. *Biosensors and Bioelectronics*, 61, 298-305.
- BHAGAT, A. A. S., BOW, H., HOU, H. W., TAN, S. J., HAN, J. & LIM, C. T. 2010. Microfluidics for cell separation. *Medical & biological engineering & computing*, 48, 999-1014.
- BOZZOLA, J. J. & RUSSELL, L. D. 1999. *Electron microscopy: principles and techniques for biologists*, Jones & Bartlett Learning.
- BRAFMAN, D. A. 2013. Constructing stem cell microenvironments using bioengineering approaches. *Physiological genomics*, 45, 1123-1135.

- BRAY, F., REN, J. S., MASUYER, E. & FERLAY, J. 2013. Global estimates of cancer prevalence for 27 sites in the adult population in 2008. *International Journal of Cancer*, 132, 1133-1145.
- BURGER, R. & DUCRÉE, J. 2012. Handling and analysis of cells and bioparticles on centrifugal microfluidic platforms. *Expert review of molecular diagnostics*, 12, 407-421.
- BYRNE, G. I. & OJCIUS, D. M. 2004. Chlamydia and apoptosis: life and death decisions of an intracellular pathogen. *Nature Reviews Microbiology*, 2, 802-808.
- CANNY, J. F. 1983. Finding Edges and Lines in Images. DTIC Document.
- CARPENTER, A. E., JONES, T. R., LAMPRECHT, M. R., CLARKE, C., KANG, I. H., FRIMAN, O., GUERTIN, D. A., CHANG, J. H., LINDQUIST, R. A. & MOFFAT, J. 2006. CellProfiler: image analysis software for identifying and quantifying cell phenotypes. *Genome biology*, 7, R100.
- CETIN, B., ÖZER, M. B. & SOLMAZ, M. E. 2014. Microfluidic bio-particle manipulation for biotechnology. *Biochemical Engineering Journal*, 92, 63-82.
- CHEN, H., SUN, J., WOLVETANG, E. & COOPER-WHITE, J. 2015. High-throughput, deterministic single cell trapping and long-term clonal cell culture in microfluidic devices. *Lab on a Chip*, 15, 1072-1083.
- CHOU, S. Y., KEIMEL, C. & GU, J. 2002. Ultrafast and direct imprint of nanostructures in silicon. *Nature*, 417, 835-7.
- CHUNG, K., RIVET, C., LU, H. & KEMP, M. 2013. Deterministic High-Density Single-Cell Trap Array. Google Patents.
- DARMANIS, S., GALLANT, C. J., MARINESCU, V. D., NIKLASSON, M., SEGERMAN, A., FLAMOURAKIS, G., FREDRIKSSON, S., ASSARSSON, E.,

- LUNDBERG, M. & NELANDER, S. 2016. Simultaneous multiplexed measurement of RNA and proteins in single cells. *Cell reports*, 14, 380-389.
- DENG, B., LI, X., CHEN, D., YOU, L., WANG, J. & CHEN, J. 2014. Parameter Screening in Microfluidics Based Hydrodynamic Single-Cell Trapping. *The Scientific World Journal*, 2014.
- DI CARLO, D., AGHDAM, N. & LEE, L. P. 2006. Single-cell enzyme concentrations, kinetics, and inhibition analysis using high-density hydrodynamic cell isolation arrays. *Analytical chemistry*, 78, 4925-4930.
- DITTRICH, P. & JAKUBOWSKI, N. 2014. Current trends in single cell analysis. *Analytical and bioanalytical chemistry*, 406, 6957-6961.
- DITTRICH, P. S., TACHIKAWA, K. & MANZ, A. 2006. Micro total analysis systems. Latest advancements and trends. *Analytical chemistry*, 78, 3887-3908.
- EL-ALI, J., SORGER, P. K. & JENSEN, K. F. 2006. Cells on chips. *Nature*, 442, 403-411.
- ELMORE, S. 2007. Apoptosis: a review of programmed cell death. *Toxicologic pathology*, 35, 495-516.
- EYER, K., KUHN, P., HANKE, C. & DITTRICH, P. S. 2012. A microchamber array for single cell isolation and analysis of intracellular biomolecules. *Lab on a chip*, 12, 765-772.
- FAN, Y. B., YE, L., WANG, T. Y. & WU, G. P. 2010. Correlation between morphology and human telomerase gene amplification in bronchial brushing cells for the diagnosis of lung cancer. *Diagnostic cytopathology*, 38, 402-406.
- FERLAY, J., SOERJOMATARAM, I., ERVIK, M., DIKSHIT, R., ESER, S., MATHERS, C., REBELO, M., PARKIN, D., FORMAN, D. & BRAY, F. 2015. Cancer Incidence and Mortality Worldwide: IARC CancerBase No. 11 [Internet].



- Lyon, France: International Agency for Research on Cancer. GLOBOCAN. 2013; 2012 v1. 0, [http p. globocan. iarc. fr](http://globocan.iarc.fr). Accessed, 30.
- FITZKE, F., MASTERS, B., BUCKLEY, R. & SPEEDWELL, L. 1997. Fourier transform analysis of human corneal endothelial specular photomicrographs. *Experimental eye research*, 65, 205-214.
- FUJITA, H., ESAKI, T., MASUJIMA, T., HOTTA, A., KIM, S. H., NOJI, H. & WATANABE, T. M. 2015. Comprehensive chemical secretory measurement of single cells trapped in a micro-droplet array with mass spectrometry. *RSC Advances*, 5, 16968-16971.
- GADEGAARD, N. & MCCLOY, D. 2007. Direct stamp fabrication for NIL and hot embossing using HSQ. *Microelectronic Engineering*, 84, 2785-2789.
- GAO, C., SUN, X. & GILLIS, K. D. 2013. Fabrication of two-layer poly (dimethyl siloxane) devices for hydrodynamic cell trapping and exocytosis measurement with integrated indium tin oxide microelectrodes arrays. *Biomedical microdevices*, 15, 445-451.
- GHANBARI, M., NEZHAD, A. S., AGUDELO, C. G., PACKIRISAMY, M. & GEITMANN, A. 2014. Microfluidic positioning of pollen grains in lab-on-a-chip for single cell analysis. *Journal of bioscience and bioengineering*, 117, 504-511.
- GUAN, A., SHENOY, A., SMITH, R. & LI, Z. 2015. Streamline based design guideline for deterministic microfluidic hydrodynamic single cell traps. *Biomicrofluidics*, 9, 024103.
- GYÖRGY, B., SZABÓ, T. G., PÁSZTÓI, M., PÁL, Z., MISJÁK, P., ARADI, B., LÁSZLÓ, V., PÁLLINGER, E., PAP, E. & KITTEL, A. 2011. Membrane vesicles, current state-of-the-art: emerging role of extracellular vesicles. *Cellular and molecular life sciences*, 68, 2667-2688.

- HÄCKER, G. 2000. The morphology of apoptosis. *Cell and tissue research*, 301, 5-17.
- HEATH, J. R., RIBAS, A. & MISCHEL, P. S. 2016. Single-cell analysis tools for drug discovery and development. *Nature Reviews Drug Discovery*, 15, 204-216.
- HOLADE, Y., MORAIS, C., SERVAT, K., NAPPORN, T. W. & KOKOH, K. B. 2014. Enhancing the available specific surface area of carbon supports to boost the electroactivity of nanostructured Pt catalysts. *Physical Chemistry Chemical Physics*, 16, 25609-25620.
- HU, W., YIM, E. K., REANO, R. M., LEONG, K. W. & PANG, S. W. 2005. Effects of nanoimprinted patterns in tissue-culture polystyrene on cell behavior. *J Vac Sci Technol A*, 23, 2984-2989.
- HUANG, L., CHEN, Y., CHEN, Y. & WU, H. 2015. Centrifugation-Assisted Single-Cell Trapping in a Truncated Cone-Shaped Microwell Array Chip for the Real-Time Observation of Cellular Apoptosis. *Analytical chemistry*, 87, 12169-12176.
- ISMAIL, S. M., COLCLOUGH, A. B., DINNEN, J. S., EAKINS, D., EVANS, D., GRADWELL, E., O'SULLIVAN, J. P., SUMMERELL, J. M. & NEWCOMBE, R. G. 1989. Observer variation in histopathological diagnosis and grading of cervical intraepithelial neoplasia. *BMJ*, 298, 707-710.
- JANES, D. W., KATZENSTEIN, J. M., SHANMUGANATHAN, K. & ELLISON, C. J. 2013. Directing convection to pattern thin polymer films. *Journal of Polymer Science Part B: Polymer Physics*, 51, 535-545.
- JEON, W. B., PARK, B. H., WEI, J. & PARK, R. W. 2011. Stimulation of fibroblasts and neuroblasts on a biomimetic extracellular matrix consisting of tandem repeats of the elastic VGVPG domain and RGD motif. *Journal Of Biomedical Materials Research Part A*, 97, 152-157.

- JIN, D., DENG, B., LI, J., CAI, W., TU, L., CHEN, J., WU, Q. & WANG, W. 2015. A microfluidic device enabling high-efficiency single cell trapping. *Biomicrofluidics*, 9, 014101.
- JOHANN, R. M. 2006. Cell trapping in microfluidic chips. *Analytical and bioanalytical chemistry*, 385, 408-412.
- KARIMI, A., YAZDI, S. & ARDEKANI, A. 2013. Hydrodynamic mechanisms of cell and particle trapping in microfluidics. *Biomicrofluidics*, 7, 021501.
- KELLENBERGER, E., JOHANSEN, R., MAEDER, M., BOHRMANN, B., STAUFFER, E. & VILLIGER, W. 1992. Artefacts and morphological changes during chemical fixation. *Journal of microscopy*, 168, 181-201.
- KHALILI, A. A. & AHMAD, M. R. 2015. Numerical Analysis of Hydrodynamic Flow in Microfluidic Biochip for Single-Cell Trapping Application. *International journal of molecular sciences*, 16, 26770-26785.
- KHALILI, A. A., BASRI, M. A. M. & AHMAD, M. R. 2014. Simulation of single cell trapping via hydrodynamic manipulation. *Jurnal Teknologi*, 69.
- KHOSLA, A. 2012. Nanoparticle-doped electrically-conducting polymers for flexible nano-micro Systems. *Electrochemical Society Interface*, 21, 67-70.
- KIM, C.-S., AHN, S.-H. & JANG, D.-Y. 2012a. Review: Developments in micro/nanoscale fabrication by focused ion beams. *Vacuum*, 86, 1014-1035.
- KIM, H., LEE, S. & KIM, J. 2012b. Hydrodynamic trap-and-release of single particles using dual-function elastomeric valves: design, fabrication, and characterization. *Microfluidics and nanofluidics*, 13, 835-844.
- KIM, J., ERATH, J., RODRIGUEZ, A. & YANG, C. 2014. A high-efficiency microfluidic device for size-selective trapping and sorting. *Lab on a Chip*, 14, 2480-2490.

- KIM, S. M., LEE, S. H. & SUH, K. Y. 2008. Cell research with physically modified microfluidic channels: a review. *Lab on a Chip*, 8, 1015-1023.
- KOBEL, S., VALERO, A., LATT, J., RENAUD, P. & LUTOLF, M. 2010. Optimization of microfluidic single cell trapping for long-term on-chip culture. *Lab on a Chip*, 10, 857-863.
- KOPPE, A. N., KAMATH, M., PFLUGER, C. A., BURKEY, D. D., DOKMECI, M., WANG, L. & CARRIER, R. L. 2016. Complex, multi-scale small intestinal topography replicated in cellular growth substrates fabricated via chemical vapor deposition of Parylene C. *Biofabrication*, 8, 035011.
- KOZLOWSKI, M. & KOZLOWSKA, A. Comparison of electrically conductive fillers in polymer systems. *Macromolecular Symposia*, 1996. Wiley Online Library, 261-268.
- KUKHTEVICH, I., BELOUSOV, K., BUKATIN, A., DUBINA, M. & EVSTRAPOV, A. 2015. A microfluidic chip with hydrodynamic traps for in vitro microscopic investigations of single cells. *Technical Physics Letters*, 41, 255-258.
- KUMANO, I., HOSODA, K., SUZUKI, H., HIRATA, K. & YOMO, T. 2012. Hydrodynamic trapping of *Tetrahymena thermophila* for the long-term monitoring of cell behaviors. *Lab on a Chip*, 12, 3451-3457.
- KWON, D., KIM, J., CHUNG, S. & PARK, I. A nanowire-integrated microfluidic device for hydrodynamic trapping and anchoring of bacterial cells. *Micro Electro Mechanical Systems (MEMS), 2014 IEEE 27th International Conference on*, 2014. IEEE, 246-249.
- LAN, H. & DING, Y. 2010. Nanoimprint lithography. *Lithography Rijeka: InTech*, 2010457494.

- LAUAND, C., NIERO, E., DIAS, V. & MACHADO-SANTELLI, G. 2015. Cell cycle synchronization and BrdU incorporation as a tool to study the possible selective elimination of ErbB1 gene in the micronuclei in A549 cells. *Brazilian Journal of Medical and Biological Research*, 48, 382-391.
- LAWRENZ, A., NASON, F. & COOPER-WHITE, J. J. 2012. Geometrical effects in microfluidic-based microarrays for rapid, efficient single-cell capture of mammalian stem cells and plant cells. *Biomicrofluidics*, 6, 024112.
- LEE, D., PAN, H., SHERRY, A., KO, S. H., LEE, M.-T., KIM, E. & GRIGOROPOULOS, C. P. 2012. Large-area nanoimprinting on various substrates by reconfigurable maskless laser direct writing. *Nanotechnology*, 23, 344012.
- LEE, E. A., IM, S. G. & HWANG, N. S. 2014. Efficient myogenic commitment of human mesenchymal stem cells on biomimetic materials replicating myoblast topography. *Biotechnology journal*, 9, 1604-1612.
- LEE, T. P. & MOHAMED, K. 3D Microfabrication Using Emulsion Mask Grayscale Photolithography Technique. IOP Conference Series: Materials Science and Engineering, 2016. IOP Publishing, 012032.
- LI, K., MORTON, K., VERES, T., CUI, B. & MURRAY, M. 2011. 5.11 Nanoimprint Lithography and Its Application in Tissue Engineering and Biosensing. *Comprehensive Biotechnology*, 125-139.
- LIM, G. C. C. 2002. Overview of cancer in Malaysia. *Japanese Journal of Clinical Oncology*, 32, S37-S42.
- LO, S.-J. & YAO, D.-J. 2015. Get to Understand More from Single-Cells: Current Studies of Microfluidic-Based Techniques for Single-Cell Analysis. *International journal of molecular sciences*, 16, 16763-16777.

- LOQMAN, M. Y., BUSH, P., FARQUHARSON, C. & HALL, A. C. 2010. A cell shrinkage artefact in growth plate chondrocytes with common fixative solutions: importance of fixative osmolarity for maintaining morphology. *European Cells and Materials*, 14, 214-227.
- LUTZ, B. R., CHEN, J. & SCHWARTZ, D. T. 2006. Hydrodynamic tweezers: 1. Noncontact trapping of single cells using steady streaming microeddies. *Analytical chemistry*, 78, 5429-5435.
- MARINHO, B., GHISLANDI, M., TKALYA, E., KONING, C. E. & DE WITH, G. 2012. Electrical conductivity of compacts of graphene, multi-wall carbon nanotubes, carbon black, and graphite powder. *Powder technology*, 221, 351-358.
- MARTINO, S., D'ANGELO, F., ARMENTANO, I., KENNY, J. M. & ORLACCHIO, A. 2012. Stem cell-biomaterial interactions for regenerative medicine. *Biotechnology advances*, 30, 338-351.
- MATON, A., LAHART, D., HOPKINS, J., WARNER, M. Q., JOHNSON, S. & WRIGHT, J. D. 1997. *Cells: Building blocks of life*, Pearson Prentice Hall.
- MENDES, P. M., YEUNG, C. L. & PREECE, J. A. 2007. Bio-nanopatterning of Surfaces. *Nanoscale Res Lett*, 2, 373-84.
- MOLAIRE, M. F. 2012. Static dissipative polymeric composition having controlled conductivity. Google Patents.
- MOSS, B. M., MYCOCK, I. R. & DAVIES, A. M. 2011. Antistatic or semi-conductive polyurethane elastomers. Google Patents.
- MÜLLER, C., MÜLLER, A. & POMPE, T. 2013. Dissipative interactions in cell–matrix adhesion. *Soft Matter*, 9, 6207-6216.

- MUYS, J., ALKAISI, M. & EVANS, J. 2006a. Bioimprint: nanoscale analysis by replication of cellular topography using soft lithography. *Journal of Biomedical Nanotechnology*, 2, 11-15.
- MUYS, J., ALKAISI, M. M. & EVANS, J. Bioimprint. Nanoscience and Nanotechnology, 2006. ICONN'06. International Conference on, 2006b. IEEE.
- NEUMAN, M. G. 2003. Cytokines-central factors in alcoholic liver disease. *Alcohol Research and Health*, 27, 307-316.
- NILSSON, J., EVANDER, M., HAMMARSTRÖM, B. & LAURELL, T. 2009. Review of cell and particle trapping in microfluidic systems. *Analytica chimica acta*, 649, 141-157.
- NOCK, V., MURRAY, L., SAMSURI, F., ALKAISI, M. & EVANS, J. 2010. Microfluidics-assisted photo nanoimprint lithography for the formation of cellular bioimprints. *Journal of Vacuum Science & Technology B*, 28, C6K17-C6K22.
- NOCK, V., MURRAY, L., SAMSURI, F., ALKAISI, M. M. & EVANS, J. J. 2011. Microfluidic arrays for bioimprint of cancer cells. *Microelectronic Engineering*, 88, 1828-1831.
- OKI, Y., FUKUZAWA, S. & ITO, D. 2013. Electrically conductive polyethylene resin composition, electrically conductive polyethylene resin molding, sliding bearing, and sliding sheet. Google Patents.
- ORGEL, L. E. 1998. The origin of life—a review of facts and speculations. *Trends in biochemical sciences*, 23, 491-495.
- PARK, J. Y., MORGAN, M., SACHS, A. N., SAMOREZOV, J., TELLER, R., SHEN, Y., PIENTA, K. J. & TAKAYAMA, S. 2010. Single cell trapping in larger microwells capable of supporting cell spreading and proliferation. *Microfluidics and nanofluidics*, 8, 263-268.

- PARK, M. C., HUR, J. Y., CHO, H. S., PARK, S.-H. & SUH, K. Y. 2011. High-throughput single-cell quantification using simple microwell-based cell docking and programmable time-course live-cell imaging. *Lab on a Chip*, 11, 79-86.
- PFLUGER, C. A., MCMAHON, B. J., CARRIER, R. L. & BURKEY, D. D. 2012. Precise, biomimetic replication of the multiscale structure of intestinal basement membrane using chemical vapor deposition. *Tissue Engineering Part A*, 19, 649-656.
- RELLO, S., STOCKERT, J., MORENO, V., GAMEZ, A., PACHECO, M., JUARRANZ, A., CANETE, M. & VILLANUEVA, A. 2005. Morphological criteria to distinguish cell death induced by apoptotic and necrotic treatments. *Apoptosis*, 10, 201-208.
- RETTIG, J. R. & FOLCH, A. 2005. Large-scale single-cell trapping and imaging using microwell arrays. *Analytical chemistry*, 77, 5628-5634.
- RISS, T. L. & MORAVEC, R. A. 2004. Use of multiple assay endpoints to investigate the effects of incubation time, dose of toxin, and plating density in cell-based cytotoxicity assays. *Assay and drug development technologies*, 2, 51-62.
- RODENACKER, K. & BENGTTSSON, E. 2003. A feature set for cytometry on digitized microscopic images. *Analytical Cellular Pathology*, 25, 1-36.
- ROMANUIK, S. F., GRIST, S. M., HAQ, M., GRAY, B. L., GULZAR, N. & SCOTT, J. K. The microfluidic trapping of antibody-secreting cells. ASME 2010 8th International Conference on Nanochannels, Microchannels, and Minichannels collocated with 3rd Joint US-European Fluids Engineering Summer Meeting, 2010. American Society of Mechanical Engineers, 1465-1474.
- ROSS, A. M., JIANG, Z., BASTMEYER, M. & LAHANN, J. 2012. Physical aspects of cell culture substrates: topography, roughness, and elasticity. *Small*, 8, 336-355.



- RYLEY, J. & PEREIRA-SMITH, O. M. 2006. Microfluidics device for single cell gene expression analysis in *Saccharomyces cerevisiae*. *Yeast*, 23, 1065-1073.
- SAMSURI, F., ALKAISI, M. M., EVANS, J. J., CHITCHOLTAN, K. & MITCHELL, J. S. 2011. Detection of changes in cell membrane structures using the Bioimprint technique. *Microelectronic Engineering*, 88, 1871-1874.
- SAMSURI, F., MITCHELL, J. S., ALKAISI, M. M. & EVANS, J. J. 2010. Formation of nanoscale bioimprints of muscle cells using UV-cured spin-coated polymers. *Journal of Nanotechnology*, 2009.
- SARASTE, A. & PULKKI, K. 2000. Morphologic and biochemical hallmarks of apoptosis. *Cardiovascular research*, 45, 528-537.
- SHRIVAKSHAN, G. & CHANDRASEKAR, C. 2012. A comparison of various edge detection techniques used in image processing. *IJCSI International Journal of Computer Science Issues*, 9, 272-276.
- SIEGEL, R. L., MILLER, K. D. & JEMAL, A. 2015. Cancer statistics, 2015. *CA: a cancer journal for clinicians*, 65, 5-29.
- SIEGEL, R. L., MILLER, K. D. & JEMAL, A. 2016. Cancer statistics, 2016. *CA: a cancer journal for clinicians*, 66, 7-30.
- SOCIETY, A. C. Available: [www.cancer.org/cancer/adrenalcorticalcancer/index](http://www.cancer.org/cancer/adrenalcorticalcancer/index). 2015].
- STEWART, B. & WILD, C. P. 2016. World cancer report 2014. *World*.
- STREET, W. N., WOLBERG, W. H. & MANGASARIAN, O. L. Nuclear feature extraction for breast tumor diagnosis. IS&T/SPIE's Symposium on Electronic Imaging: Science and Technology, 1993. International Society for Optics and Photonics, 861-870.

- SUBASHINI, M. M., SAHOO, S. K. & SAGAR, S. Cancer cell diagnostics based on tissue morphology using image processing. *Sustainable Energy and Intelligent Systems (SEISCON 2012)*, IET Chennai 3rd International on, 2012. IET, 1-5.
- TAATJES, D. J., SOBEL, B. E. & BUDD, R. C. 2008. Morphological and cytochemical determination of cell death by apoptosis. *Histochemistry and cell biology*, 129, 33-43.
- TANYERI, M., JOHNSON-CHAVARRIA, E. M. & SCHROEDER, C. M. 2010. Hydrodynamic trap for single particles and cells. *Applied physics letters*, 96, 224101.
- TANYERI, M., RANKA, M., SITTIPOLKUL, N. & SCHROEDER, C. M. 2011. A microfluidic-based hydrodynamic trap: design and implementation. *Lab on a Chip*, 11, 1786-1794.
- TANYERI, M. & SCHROEDER, C. M. 2013. Manipulation and confinement of single particles using fluid flow. *Nano letters*, 13, 2357-2364.
- THIRAN, J. P. & MACQ, B. 1996. Morphological feature extraction for the classification of digital images of cancerous tissues. *Biomedical Engineering, IEEE Transactions on*, 43, 1011-1020.
- TORRE, L. A., BRAY, F., SIEGEL, R. L., FERLAY, J., LORTET-TIEULENT, J. & JEMAL, A. 2015. Global cancer statistics, 2012. *CA: a cancer journal for clinicians*, 65, 87-108.
- TORRES, C. S. 2003. *Alternative lithography: unleashing the potentials of nanotechnology*, Springer.
- TRUSKETT, V. N. & WATTS, M. P. 2006. Trends in imprint lithography for biological applications. *Trends Biotechnol*, 24, 312-7.

- VALIZADEH, A. & KHOSROUSHAHI, A. Y. 2015. Single-cell analysis based on lab on a chip fluidic system. *Analytical Methods*, 7, 8524-8533.
- VAN LOO, P. & VOET, T. 2014. Single cell analysis of cancer genomes. *Current opinion in genetics & development*, 24, 82-91.
- VRATZOV, B., FUCHS, A., LEMME, M., HENSCHER, W. & KURZ, H. 2003. Large scale ultraviolet-based nanoimprint lithography. *Journal of Vacuum Science & Technology B*, 21, 2760-2764.
- WALLIN, R. F. & ARSCOTT, E. 1998. A practical guide to ISO 10993-5: Cytotoxicity. *Medical Device and Diagnostic Industry*, 20, 96-98.
- WANG, D. & BODOVITZ, S. 2010. Single cell analysis: the new frontier in 'omics'. *Trends in biotechnology*, 28, 281-290.
- WANG, Y., SHAH, P., PHILLIPS, C., SIMS, C. E. & ALLBRITTON, N. L. 2012. Trapping cells on a stretchable microwell array for single-cell analysis. *Analytical and bioanalytical chemistry*, 402, 1065-1072.
- WENDEL, M., KÜHN, S., LORENZ, H., KOTTHAUS, J. & HOLLAND, M. 1994. Nanolithography with an atomic force microscope for integrated fabrication of quantum electronic devices. *Applied physics letters*, 65, 1775-1777.
- WHITE, S. R., WILLIAMS, P., WOJCIK, K. R., SUN, S., HIEMSTRA, P. S., RABE, K. F. & DORSCHIED, D. R. 2001. Initiation of apoptosis by actin cytoskeletal derangement in human airway epithelial cells. *American Journal of Respiratory Cell and Molecular Biology*, 24, 282-294.
- WHITESIDES, G. M. 2006. The origins and the future of microfluidics. *Nature*, 442, 368-373.
- WILLIAMS, D. B. & CARTER, C. B. 1996. The transmission electron microscope. *Transmission electron microscopy*. Springer.

- WLODKOWIC, D., FALEY, S., ZAGNONI, M., WIKSWO, J. P. & COOPER, J. M. 2009. Microfluidic single-cell array cytometry for the analysis of tumor apoptosis. *Analytical chemistry*, 81, 5517-5523.
- WOLBERG, W. H., STREET, W. N., HEISEY, D. M. & MANGASARIAN, O. L. 1995. Computer-derived nuclear features distinguish malignant from benign breast cytology. *Human Pathology*, 26, 792-796.
- WOOD, D. K., WEINGEIST, D. M., BHATIA, S. N. & ENGELWARD, B. P. 2010. Single cell trapping and DNA damage analysis using microwell arrays. *Proceedings of the National Academy of Sciences*, 107, 10008-10013.
- XU, X., LI, Z., KOTAGIRI, N., SARDER, P., ACHILEFU, S. & NEHORAI, A. Microfluidic microsphere-trap arrays for simultaneous detection of multiple targets. SPIE MOEMS-MEMS, 2013. International Society for Optics and Photonics, 86151E-86151E-11.
- ZAINAL ARIFFIN, O. & NOR SALEHA, I. 2011. National cancer registry report: Malaysia cancer statistics-data and figure 2007. *Putrajaya, Ministry of Health Malaysia*.

The logo of Universiti Malaysia Perlis (Ump) is a large, stylized letter 'U' composed of four overlapping triangles in shades of teal and light blue. The letters 'UMP' are printed in white, bold, sans-serif font across the center of the 'U' shape.

UMP

## APPENDIX A

### CELL CULTURE PROTOCOLS

Cells culture protocols for this study are described in this section below.

#### 7.1 Cell culture techniques

All procedures of cell culture were carried out in a sterile environment using a Biological Safety Cabinet Class II. Alcohol (70% v/v in water) was used to wipe the area in the cabinet and all the apparatus. Sterile glassware, plastic ware and micropipette tips were used during the cell culture work. All solutions were prewarmed in a 37°C water bath before they can be used in cell culture. Gloves were worn throughout the experiments. The experiment was performed as fast as possible to minimize contamination.

#### 7.2 Complete growth media preparation

Dulbecco's modified Eagle's medium (DMEM) (Gibco,USA), Penicillin Streptomycin (Gibco,USA), and Fetal bovine serum (FBS) (Gibco,USA) were prewarmed before mix according to ratio, proportion of DMEM: 89%, FBS: 10%, and PenStrep: 1% to form complete growth media (CGM). The CGM was kept in the 4°C chiller for storage.

#### 7.3 Thawing cells

Cryovials (Thermo Scientific, USA) were taken out of -80°C freezer (Samsung, Korea) was thawed by either immersing in a 37°C water bath (Memmert, Germany) or rubbing the vials between palms. Before the content fully melted, entire content of cryovials was transferred into 15 ml centrifuge tubes (Thermo Scientific, USA) containing 7 ml prewarmed CGM. The cell suspension was centrifuged at 180 g for 5 min to remove Dimethyl Sulphoxide (Sigma-Aldrich, USA). Supernatant was removed and the pellet was resuspended in 1 ml of CGM. Cells slowly transferred into T75 tissue culture flask (Thermo Scientific, USA) and incubated at 37°C, 5 % CO<sub>2</sub>.

#### **7.4 Changing media**

Every time before the media was to be changed, the cells were observed under an inverted microscope to check for cell confluency, morphological changes and contamination. Media were removed from the flask (Nunc, USA), and washed at least 3 times with PBS (Gibco, USA). Prewarmed media was added to cells before incubating at 37°C, 5 % CO<sub>2</sub>.

#### **7.5 Subculturing cells**

Cells confluency, morphological changes and contamination were checked under an inverted microscope (Thermo Scientific, USA). Media were removed, cells were washed with PBS at least 3 times. Trypsin-EDTA (0.25 %) (Sigma Aldrich, USA) was added (1 or 2 ml depend on flask size) to trypsinize adherent cells. The flask was incubated for 1 to 2 min, then the flasks were gently tapped to detach the cells from the flasks. Once all cells were detached, CGM was added directly to neutralize trypsin. All content of the flask was transferred into 15 ml centrifuge tube (Greiner, USA) and centrifuged at 180 g. The supernatant was removed and 2 ml of complete growth medium was added to the pellet. Depending on pallet size, the cells were split and transferred into flasks (25 cm<sup>2</sup> or 75 cm<sup>2</sup>) containing 5 or 10 ml of culture media respectively. The flasks were then further incubated at 37 °C, 5% CO<sub>2</sub> and 95% air. After 24 hours of incubation, cell confluence was observed under the inverted microscope. The growth media were replaced every three days.

#### **7.6 Cryopreservation of cells**

Cells that reached 80% confluency in the flask were trypsinize, collected, centrifuged at 180 g for 5 min, then supernatant was removed. After that, the cell pellet was resuspended in freezing media consisting of 10% DMSO and 90% CGM. Obtained cell suspension was further aliquoted in 1 ml of the labelled cryotube and sealed. The cryotubes were kept in freezing container (Nalgene, USA) in -80°C at least for 24 hours before kept in other boxes in -80°C freezer or liquid nitrogen storage tank for prolonged storage. As in the beginning, the cryotube were kept in freezing container the cooling rate during the freezing process is estimated at ± 1°C /min. The cell that were cryopreserved can be thawed to continue culture or kept frozen in liquid nitrogen for prolonged storing.

## 7.7 Measuring cell density using trypan blue exclusion assay method

Briefly, trypsinized cells that had been neutralized were collected in 15 ml centrifuge tubes and centrifuged at 180 g, for 5 min. Supernatant was discarded, 1 ml of CGM was added to cell pallet and resuspended until pallet not visible. 10 µl of CGM with the media was mixed with 10 µl of trypan blue (Sigma-Aldrich, USA), and if needed can dilute more with another of 10 µl of trypan blue. 10 µl of cell suspension diluted in trypan blue solution was placed in the hemocytometer chamber. Then, the cells under hemocytometer chamber (GmbH, Germany) were observed and counted under microscope at 100X magnification. Only viable cells, which were not stained within the square of the grid, were counted and all the blue stained cells (dead cells) were excluded.

## 7.8 Seeding of cells

Cells were trypsinized, measured the cell density and from that the volume of cell density to take for specified cell density calculated by using below formulas.

$$\frac{\text{Cells}}{\text{ml}} = \text{Number of cells counted} \times \frac{\text{Dilution factor}}{\text{Number of chamber}} \times 10000 \quad (7.1)$$

$$\frac{\text{Total cell density (available)}}{\text{Cell density (required)}} = \frac{\text{Volume of cells (available)}}{\text{Volume of cell density, X (required)}} \quad (7.2)$$

2 ml of prewarmed media was filled in each 6 well plate. From calculation, (x) volume of cell density from measured was filled in each well of 6 well plate to get specified cell density. The 6 well plates, then incubated at 37°C, 5% CO<sub>2</sub> and 95 % air for determined assay.

## APPENDIX B

### INTELLECTUAL PROPERTIES

#### Patents

1. A Microfluidic Biochip (*Patent Filed*).

#### Publications

1. N.Vigneswaran, Fahmi Bin Samsuri, Balu Ranganathan 2014. "Bioimprint Replication For Cancer Research Investigations and Its Analysis Using Artificial Neural Network" **International Journal of Artificial Intelligence and Neural Networks**, Volume 4: Issue 4 [ISSN 2250–3749] 2014.
2. N.Vigneswaran, Fahmi Bin Samsuri, Nithya Kalyani 2014. "Development of Scaffold for Tissue Engineering Applications using Imprinting" **IEEE Xplorer**, **978-1-4799-7614-0** 2014.
3. N.Vigneswaran, Fahmi Bin Samsuri, Nithya Kalyani 2015. "Bioimprinting based Scaffold Development for Tissue Engineering Applications" **Biomedical and Pharmacology Journal**, Volume-08 No: 1, 2015.
4. N.Vigneswaran, Fahmi Bin Samsuri, Balu Ranganathan, Padmapriya 2014. "Recent Advances in Nano Patterning and Nano Imprint Lithography for Biological Applications", **Elsevier - Journal of Procedia Engineering** **97(2014) 1387 – 1398**.
5. Nithya Kalyani.K, R.Kalpana, N.Vigneswaran 2014. "Volumetric Assessment of Human Brain Morphology using Pixel counting technique" **IEEE** 2014.



6. Nithya Kalyani.K, R.Kalpana, N.Vigneswaran 2014. "A novel Pixel counting technique to assess the volumetric changes in human brain morphology"  
**Biomedical and Pharmacology Journal**, Volume-08 No: 1, 2015.
7. Vigneswaran Narayanamurthy, Fahmi Samsuri 2016. "Perspectives of a Farmer Digital Expert Assistant System" **Engineering, Technology & Applied Science Research** Volume-06, No. 2, 2016, 972-975.
8. Vigneswaran Narayanamurthy, Sujatha, Fahmi Samsuri 2017. "Design optimization and analysis of proof mass actuation for MEMS accelerometer: A simulation study" **Journal of circuits, systems, and computers**, Volume 26, Issue 6, June 2017.
9. Narayanamurthy, Vigneswaran, et al. 2017. "Microfluidic hydrodynamic trapping for single cell analysis: Mechanisms, Methods and Applications."  
**Analytical Methods-RSC** 2017.

#### Conferences and Exhibitions

10. N Vigneswaran, Fahmi Bin Samsuri and Balu Ranganathan "Solar Energy Powered Farmer Digital Assistant" CREATION, INNOVATION, TECHNOLOGY & RESEARCH EXPOSITION - **CITREx 2014**, Kuantan, Malaysia. (Poster Presentation and secured Bronze Medal)
11. N.Vigneswaran, Fahmi Bin Samsuri, Balu Ranganathan "Bioimprint Replication for Cancer Research Investigations and Its Analysis Using Artificial Neural Network". International Conference on Advances in Applied Science and Environmental Engineering - **ASEE 2014**, Kuala Lumpur, Malaysia. (Oral Presentation)

12. N.Vigneswaran, Fahmi Bin Samsuri, Nithya Kalyani "Development of Scaffold for Tissue Engineering Applications using Imprinting" International Conference on Science, Engineering, Research and Management - **ICSEMR 2014**, Chennai, India. (Oral Presentation)
13. N.Vigneswaran, Fahmi Bin Samsuri, Balu Ranganathan, Padma Priya "Recent Advances in Nano Patterning and Nano Imprint Lithography for Biological Applications" 12th GLOBAL CONGRESS ON MANUFACTURING AND MANAGEMENT, **GCOMM 2014**, Vellore, India. (Oral Presentation)
14. L.Sujatha , N.Vigneswaran , and Fahmi Bin Samsuri "Design, Optimization and Analysis of Proof Mass Actuation for MEMS Accelerometer" International Conference on MEMS and Sensors - **ICMEMSS 2014**, IIT Chennai, India. (Poster Presentation)
15. Nithya Kalyani.K, R.Kalpana, N.Vigneswaran "Volumetric Assessment of Human Brain Morphology using Pixel counting technique" International Conference on Science, Engineering, Research and Management - **ICSEMR 2014**, Chennai, India. (Oral Presentation)
16. Vigneswaran Narayanamurthy, Fahmi Samsuri, and Gopalakrishnan Narayanamurthy "Microcontroller Based Handheld Support Device for Farmers" National Postgraduate Conference - **NCON-PGR 2015**, Kuantan, Malaysia. (Oral Presentation)
17. N.Vigneswaran, Fahmi Bin Samsuri "Cell Diagnostic Equipment- Replica Fabrication and Imaging" CREATION, INNOVATION, TECHNOLOGY & RESEARCH EXPOSITION - **CITREx 2015**, Kuantan, Malaysia. (Poster Presentation and secured Bronze Medal)

18. N.Vigneswaran, Fahmi Samsuri, Sairam Nagarajan, Sridhathan.C "Study of Particles Tracing in Bio-Microfluidic Channels" International Conference on Fluids and Chemical Engineering (**FluidsChE 2015**), 25-27 November 2015, Langkawi, Malaysia. (Oral presentation)
19. N.Vigneswaran, Fahmi Bin Samsuri "Microfluidic Biochip" CREATION, INNOVATION, TECHNOLOGY & RESEARCH EXPOSITION - **CITREx 2016**, Kuantan, Malaysia. (Fluids special silver award with cash price RM 750)
20. N.Vigneswaran, Fahmi Bin Samsuri "Farmer Digital Expert Assistant System" CREATION, INNOVATION, TECHNOLOGY & RESEARCH EXPOSITION - **CITREx 2016**, Kuantan, Malaysia. (Gold Medal)
21. N.Vigneswaran, Fahmi Bin Samsuri "Farmer Digital Expert Assistant System" 27th International Invention & Innovation Exhibition - **ITEX 2016**, Kuala Lumpur Convention Centre, Malaysia. (Silver Medal)
22. N.Vigneswaran, Fahmi Bin Samsuri "Microfluidic Biochip" BioMalaysia & Asia Pacific Bioeconomy 2016, Kuala Lumpur Convention Centre, Malaysia - **BIOMALAYSIA 2016**.
23. N.Vigneswaran, Fahmi Bin Samsuri "Agrisoft" **MAHA 2016**, Putrajaya, Malaysia.

## GALLERY

